UNIVERSITÀ DI PISA

Facoltà di Ingegneria

Dipartimento di Ingegneria Civile e Industriale

Use of PLIF to investigate mixing of immiscible liquids in static mixer

Supervisors:

Prof. Elisabetta Brunazzi

Prof. Mark Simmons

Prof. Chiara Galletti

Candidate:

Giuseppe Forte

Master's Degree in Chemical Engineering

Academic Year 2014/2015

"Science is not only a disciple of reason but, also, one of romance and passion"

Stephen Hawking

"Even if I knew that tomorrow the world would go to pieces, I would still plant my apple tree"

Martin L. King

UNIVERSITY OF PISA

Abstract

Department of Civil and Industrial Engineering

Master Thesis in Chemical Engineering

Use of PLIF to investigate mixing of immiscible liquids in static mixer

Giuseppe Forte

The performance of Kenics (KM) and Sulzer (SMX+) designs of static mixer has been investigated for the mixing of immiscible fluids using *in situ* optical measurements. The fluids used are water as the continuous phase and Lytol mineral oil in the presence of a non-ionic surfactant (Span 80) as dispersed phase. The dispersed phase volume fraction was between 0.0072% and 0.028 % and the superficial velocities ranged from 0.16 to 0.91 m/s. The pipe diameter was 0.0127 m and 6 or 12 mixing elements were used for each mixer type. Planar Laser Induced Fluorescence (PLIF) has been used to obtain images of the droplets formed in a traverse section across the mixer outlet. Image analysis methods have been developed, based upon the areal distribution and individual striation methods proposed by Alberini *et al.* (2014a, 2014b) for the blending of miscible fluids. The analysis enables drop size distributions to be obtained as a function of the number of mixing elements, interfacial tension and superficial velocity. A model for the drop size distribution has been developed in order to predict mixer performance *a priori.*

Contents

List of Figures

List of Tables

Symbols

E	Energy
A	Surface area
σ	Interface tension
T	Temperature
ΔS	Entropy variation
ΔG	Gibbs Energy variation
ΔP	Pressure drop
R	Radius of a sphere
τ	External stress
Re	Reynolds number
ρ	Density
v	Superficial velocity
D	Diameter of a pipe
μ_c	Viscosity of the continuous phase
Ca	Capillary number
We	Weber number
$\dot{\gamma}$	Shear strain
ε	Energy dissipation rate (average)
Q	Volumetric flow
l	Pipe length
d	Diameter of a drop

E_{sup}	Superficial energy of the drop
f	Fanning friction factor
φ	Volume fraction of the dispersed phase
a_v	Total interfacial area per unit volume of mixed phases
$f_n(d_i)$	Number frequency
$f_v(d_i)$	Volume frequency
$F_v(d_k)$	Cumulative volume frequency
d_{32}	Sauter mean diameter

Alla mia famiglia

Chapter 1

Introduction

1.1 Objectives and aims

The purpose of the present thesis is to deepen the knowledge about mixing of immiscible fluids in static mixer. These devices are important in several industrial processes and their use has become increasingly widespread thanks to their versatility and the low running costs. These ones and other advantages, that characterize their employment, have pushed the research to investigate the events that happen while a multiphase flow crosses static mixer. Emulsions are often blended using these motionless devices and, in general, the quality of the final products are closely related to mixing performance.

Amongst the several industrial products that involve emulsions, there are valuable products like pharmaceuticals or cosmetics/body care products that require strict properties for the effectiveness of the product. In general the online control of the microstructure of the emulsion is difficult and slow, it often requires sampling and measuring offline that causes delays in correcting and handling the process. This procedure can cause losses and defects in the final results, even if many efforts are made every day for providing better measuring and control devices.

The purpose of this work is investigating another way to ascertain that the microstructure of the products is the desired one by using bulk properties within the process. Indeed, if it is intricate for example to measure the interfacial tension or the drop size distribution of the dispersed phase of an emulsion, it is much easier to detect the temperature or the pressure drop of the whole flow. Basically, the objective of the research is modelling the drop size distribution using the pressure drop data for providing to the designer and the controller a useful tool for the set-up of the process.

For achieving this purpose several experimental data have been collected using an emulsion of oil in water. The first performed experiment was the detection of pressure drop of the double-phase flow crossing the static mixer. Different models and numbers of elements of static mixer have been involved in the experiments. The second part of the work has been done in the laser laboratory, where the PLIF technique has been developed and applied successfully to the analyzed system. The Planar Laser Induced Fluorescence (PLIF) technique has been used to characterize the drop size of the emulsion after passing through the mixing elements. The dynamic of an emulsion formation and the thermodynamic of the droplet breakup have not been analyzed before using the classical PLIF; despite this, the developed method has been found to be reliable and repeatable as explained in detail in Chapter 4.

After the experimental part done in the laboratories, the processing and analysis of the data have required the use of the software MATLAB (MathWorks®). The PLIF images processing has been found to be the crucial part of the analysis as further explained in the paragraph 4.2. Once the codes have been implemented, the drop size distribution data of the dispersed phase have been related to the energy input into the system, in order to enhance the

understanding in the emulsion dynamic and proposing an energy model to predict the mixing performance.

1.2 Structure of the thesis

This dissertation consists of five chapters:

In the present chapter, the motivation and the goal of this work are discussed. The topic of the research is introduced and the outline of the experiments briefly illustrated.

Chapter 2 presents the state of the art in this field. Basic but fundamental information are provided for the development of the study. First, basic emulsion stability principles, including information about emulsification processes, surfactants, and the most important emulsion breakdown mechanisms are discussed. Then the most employed mixing equipments are presented enlightening the advantages of continuous motionless devices. Finally, the drop size characterization of the dispersed phase is addressed, explaining the most important techniques and parameters involved.

In the Chapter 3 the experimental approach is described. The techniques, instruments and materials employed in this work are presented in details.

Chapter 4 is about the experimental and analysis part of the research. In the first part the pressure drop collection is explained and the experimental data are compared with the literature models and expectations. In the second part the image processing is described and the drop size distribution data are shown and compared with the theoretical predictions. In the last part of the chapter, a model, involving the pressure drop and the drop size distribution data, is proposed.

Chapter 5 summarizes the conclusions of this study and suggests recommendations for further research.

1.3 Publication

The present work has been presented at the Chem Eng UK Conference in Sheffield. All the most important Chemical Engineering departments of the United Kingdom have taken part in this event. In the following Figure 1.1 the presented poster with the title "*Drop size distribution for the blending of immiscible fluids in static mixer using PLIF*" is illustrated.

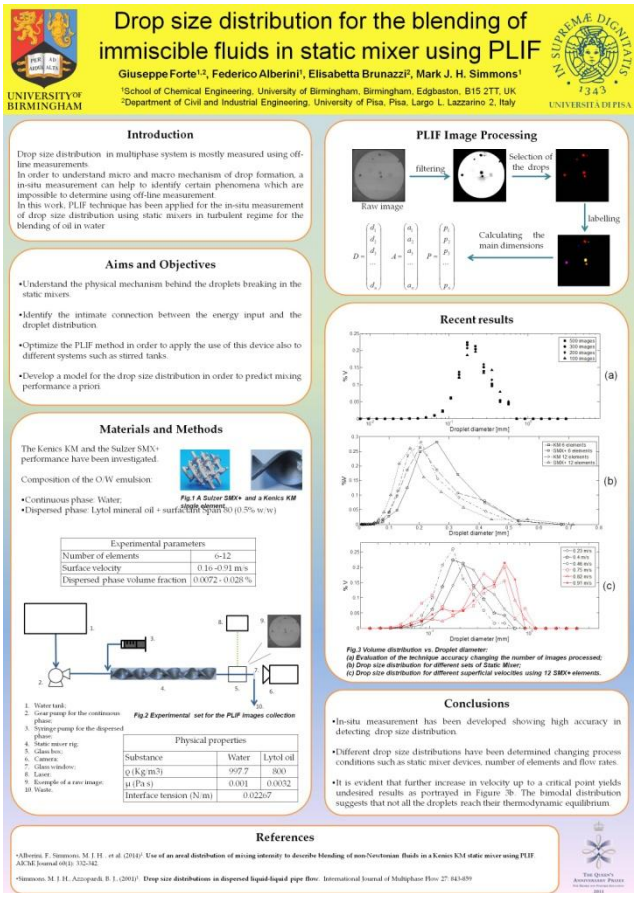

Figure 1.1 Poster presented at the Chem Eng UK 2015 Conference

Chapter 2

Literature Review

2.1 Introduction

This chapter contains a review of the current literature on the fundamentals of multiphase flow and in particular on the equipment and detection systems applied in the blending of immiscible liquids. In the first section of this chapter, the emulsion nature is analysed focusing on the droplet breakup mechanism. In the following part, two different approaches to the dispersing process are shown: the batch stirred tank and the continuous devices. Amongst the latter the static mixers are described in detail presenting the several commercial models. At last, methods to quantify the mixing performance are reviewed focusing onto the drop size distribution.

2.2 Immiscible Liquid-Liquid Systems

2.2.1 Introduction

In an immiscible system in general two or more mutually insoluble substances are present as separate phases. When the two phases are liquids, the system itself is named emulsion. In an emulsion is possible to identify a dispersed or drop phase and a continuous or matrix phase, in which the dispersed phase is

commonly smaller in volume than the continuous phase (Lemenand, Habchi et al. 2014).

Emulsions are meta-stable systems (Cramer, Fischer et al. 2004) well known in the manufacture industry. Their use ranges from the food industry through pharmaceutical, passing through personal care and cosmetics, bitumen, cleaning products and wastewater treatment. Even in the oil industry it is common to come across emulsions: many crude oils contain water droplets (for example, the North sea oil) and these must be removed by coalescence followed by separation. Unfortunately, fundamental research on emulsions is not easy because model systems are difficult to produce (Das, Legrand et al. 2005). In many cases, theories on emulsion stability are not exact and semi-empirical approaches are used.

2.2.2 Emulsions

As Tadros summarizes in his overview (Tadros 2013), several emulsion classes may be distinguished: oil-in-water (O/W), water-in-oil (W/O), and oil-in-oil (O/O). The latter class may be exemplified by an emulsion consisting of polar oil dispersed in non polar oil and vice versa. To disperse two immiscible liquids, one needs a third component, namely the emulsifier. The choice of the emulsifier is crucial in the formation of the emulsion and in its long-term stability.

The two fundamental processes occurring during emulsification are drop breakup and drop coalescence (Rueger and Calabrese 2013). These are concurrent processes, and the relative rates of the two mechanisms determine the final drop size (Tcholakova, Denkov et al. 2004). Surfactants can influence both these processes: by reducing the interfacial tension and interfacial energy, thereby promoting rupture, and by providing a barrier to coalescence via

interactions between the adsorbed layers on two colliding drops (Lobo and Svereika 2003).

Another classification that can be done is accordingly to the drop size of the dispersed phase:

- O/W and W/O macroemulsions: size range of 0.1–5 μm with an average of 1–2 μm;
- Nanoemulsions: size range of 20–100 nm. Similar to macroemulsions, they are only kinetically stable;
- Micellar emulsions or microemulsions: these usually have the size range of 5–50 nm. They are thermodynamically stable;
- Double and multiple emulsions: these are emulsions-of-emulsions, W/O/W, and O/W/O systems;
- Mixed emulsions: these are systems consisting of two different disperse droplets that do not mix in a continuous medium.

To prepare an emulsion, as well as the material, a certain amount of energy is needed (Tadros, Izquierdo et al. 2004). Energy is required to expand the interface:

$$E = \Delta A \cdot \sigma \tag{2-1}$$

where ΔA is the increase of the interfacial area when the drop with surface A_1 splits producing a large number of drops with total area A_2; noting that after the breakup $A_2 >> A_1$. The other parameter is σ, the interfacial tension. Since the interfacial tension is positive, the energy to expand the interface is positive. This energy cannot be compensated by the small entropy of dispersion $T\Delta S$ and the total Gibbs free energy of formation of an emulsion, ΔG is positive:

$$\Delta G = \Delta A \sigma - T\Delta S \tag{2-2}$$

Thus, emulsion formation is non-spontaneous and energy is required for producing the droplets (Capek 2004). The smaller are the droplets, the higher is the needed energy. Once again it is important to underline that in the absence of any stabilization mechanism, the emulsion has a high probability to break by one of the phenomena discussed later.

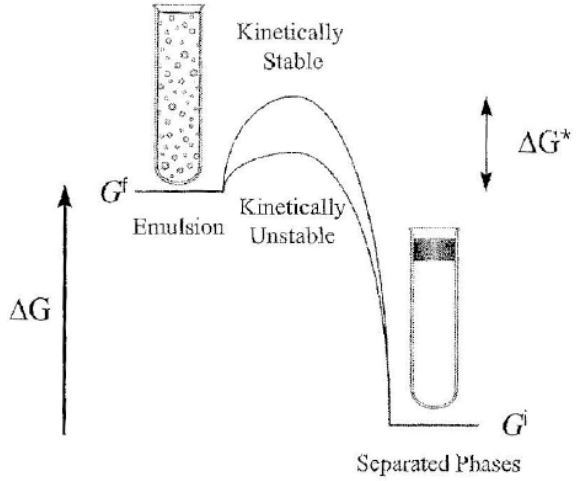

Figure 2.1 Energy gap in the emulsification process

In Figure 2.1 the energy gap between the separate phases condition and the dispersed condition is represented. In the chart, ΔG^* is the energetic barrier due to the eventual presence of the emulsifier that has the role of avoiding the return to the low energy condition.

It is a well-known phenomenon that surfactants, even at low concentration, influence strongly the droplet formation (Fischer and Erni 2007). They help to control the oil droplet size by reducing the interfacial tension and decreasing coalescence by affecting interfacial mobility. The drop formation in the actual process is due mainly to the Kelvin-Helmholtz instability (Kiss, Brenn et al. 2011), a phenomenon that takes place when two fluids, with different densities,

move in parallel flows (Thomson 1871). This mechanism was also found in spray formation by pre-filming atomizers (Dorfner et al., 1995).

In the next paragraph the droplet breakup mechanism will be deeply analyzed, but before, to have a full overview of the emulsion process it is important to understand the phenomena which affect the emulsification process causing an increasing in the final drops size:

- Creaming and Sedimentation: these processes result from external forces usually gravitational or centrifugal. A concentration gradient builds up in the system and the droplets start to move to the top or to the bottom, depending on the density ratio. In the limiting cases, the droplets may form a close-packed structure.
- Flocculation: it refers to aggregation of the droplets (without any change in primary droplet size) into larger units as a result of the van der Waals attraction that is universal with all disperse systems.
- Ostwald Ripening: it comes out from the not null solubility of the liquid phases (Taylor 1998). Liquids that are referred to as being immiscible often have mutual solubilities that are not negligible. With time, the smaller droplets disappear and their molecules diffuse to the bulk and become deposited on the larger droplets.
- Coalescence: it refers to the process of thinning and disruption of the liquid film between the droplets with the result of fusion of two or more droplets into larger ones. The limiting case for coalescence is the complete separation of the emulsion into two distinct liquid phases (Kukukova, Aubin et al. 2009).
- Phase Inversion: it results from an exchange between the disperse phase and the medium due to changed conditions in the system (Rao and McClements 2010).

The physical phenomena involved in each breakdown process are not simple, and it requires analysis of the various surface forces involved. In addition, the above-mentioned processes (shown in Figure 2.2) may take place simultaneously rather than consecutively and this complicates the analysis.

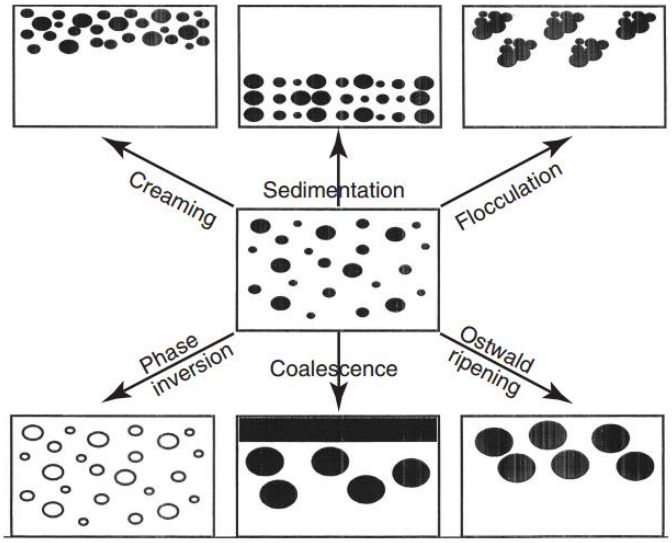

Figure 2.2 Overview of the main breakdown processes (Tadros 2013)

Preventing the occurrence of those phenomena is crucial for the long term stability of the emulsion, in this, adsorbed surfactants exert their role. The main mechanisms are two:

- steric stabilization;
- electrostatic stabilization.

Steric stabilization arises from a physical barrier to contact and coalescence. High-weight polymers molecules are widely used for this scope; essentially they adsorb to the surface of the droplet from one end and extend outwards, thus creating a physical obstruction (Hiemenz and Rajagopalan 1997,Alboudwarej et al. 2002).

Electrostatic stabilization is based on the mutual repulsive forces that are

generated when electrical charged surfaces approach each other. In an electrostatically stabilized emulsion, an ionic or ionisable surfactant forms a charged layer at the interface (Tesch, Gerhards et al. 2002, Dickinson 2003). For an oil-in-water emulsion, this layer is neutralized by counter ions in the continuous phase. The charged surface and the counter ions are termed a double layer. If the counter ions are diffuse (thick double layer), the disperse phase droplets act as charged spheres as they approach each other. If the repulsive forces are strong enough, the droplets are repelled before they can make contact and coalesce, and the emulsion is stable (Schramm 2005). In general, electrostatic stabilization is significant only for oil-in-water emulsions since the electric double-layer thickness is much greater in water than in oil.

Both electrostatic and steric forces (Figure 2.3) can prevent aggregation or coalescence and hence stabilize emulsions.

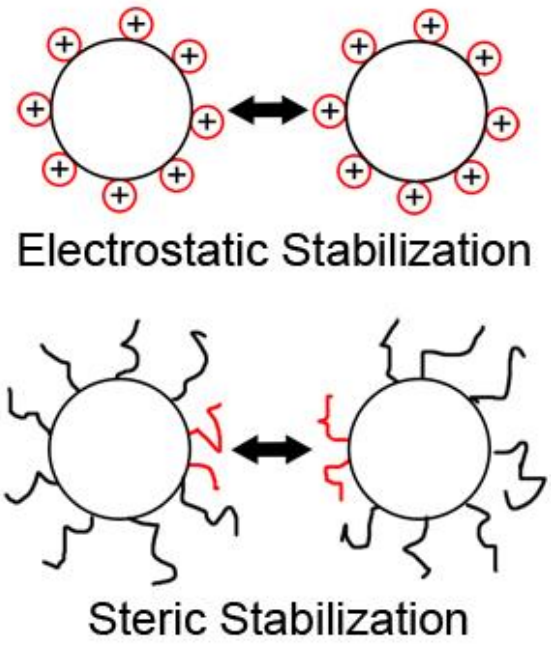

Figure 2.3 Surfactant stabilizing action

2.2.3 Droplet breakup mechanism

"It is easy to make droplets (gentle shaking suffices), but it may be difficult to make the droplets small enough" (Walstra 1993).

The prediction and the control of the final drop size of the dispersed phase require a deep analysis of the droplet breakup mechanisms.

Since this difficulty in achieving the satisfying final dimension, the processes are commonly conducted in turbulent regime. Turbulent particles breakup has been the subject of an ongoing investigation, beginning with the pioneering work of Kolmogorov (1949) and Hinze (1955). Many efforts have been done in this field for understanding the turbulent dispersions in stirred tanks and pipelines (Shinnar 1961, Sleicher 1962, Arai 1977, Calabrese 1986a, Calabrese, Wang et al. 1986b, Wang and Calabrese 1986b, Berkman and Calabrese 1988, Hesketh, Etchells et al. 1991, Cabaret, Rivera et al. 2007). Other research has focused on the study of particle breakup frequency developing models to predict the final drop size distribution (Coulaloglou and Tavlarides 1977, Konno, Matsunaga et al. 1980, Prince and Blanch 1990, Tsouris and Tavlarides 1994, Luo and Svendsen 1996, Eastwood, Armi et al. 2004).

The break up mechanism starts with the deformation of the drop; to do this, the Laplace pressure must be overcome. Laplace pressure is the difference in pressure between the convex and the concave side of the curved interface of the droplet (supposed as a sphere):

$$\Delta P = P_{inside} - P_{outside} = \frac{2\sigma}{R} \tag{2-3}$$

The deformation of the drop required a high external stress and this implies a very large pressure gradient. The stress can be due to a velocity gradient or to a

pressure difference arising from inertial effects (Walstra, 1993). Naming those external stresses as τ it is allowed to state that the droplet breaks if:

External stress > Laplace pressure ($\tau > \frac{2\sigma}{R}$).

The ratio of disruptive forces to cohesive stress $\frac{\tau}{\sigma/R}$ is known as the Capillary number (Ca) if the regime is laminar or Weber number (We) in the case of turbulent flow.

The flow regime is indicated by the value of the Reynolds number:

$$\mathrm{Re} = \frac{\rho \cdot v \cdot l}{\mu_c} \tag{2-4}$$

In a pipe when:

- Re < 2100: the regime is laminar;
- Re > 4000: the regime is turbulent.

2.2.3.1 Maximum stable drop size in laminar regime

In laminar flows two different cases can occur:

- Simple shear: when the velocity gradient and the flow direction are parallel;
- Simple extensional: when the elongation is present and the stretching is on a single axis.

The stress that deforms the drops is: $\tau = \mu_c \dot{\gamma}$; hence substituting in the Capillary number:

$$Ca = \frac{\mu_c \cdot \dot{\gamma} \cdot R}{\sigma} \tag{2-5}$$

If Ca is small, it means that the interfacial forces dominate and the drop takes a steady spherical shape. If otherwise Ca is large, the shear stress dominates and makes the drop deform causing in the end its rupture.

The value of capillary number corresponding to the maximum stable drop size is known as critical capillary number (Weber has a corresponding critical value) (Legrand, Morancais et al. 2001):

$$Ca_{cr} = \frac{\mu_c \cdot \dot{\gamma} \cdot R_{\max}}{\sigma} \tag{2-6}$$

if Ca exceeds a critical value Ca_{Cr} (of the order of one), the drop bursts. The critical capillary number is a function of the viscosity ratio of the dispersed phase to the continuous (Pacek, Man et al. 1998).

2.2.3.1 Maximum stable drop size in turbulent regime

In a turbulent regime, the kinetic energy is involved in an energy cascade in which the kinetic energy is transferred from the largest eddies (of the order of pipe diameter) to the smaller eddies and in the end dissipates below eddies of Kolmogorov's scale. This energy applies a stress to the drops causing deformation. An important distinction must be done based on the relative size of drops and the smallest eddies (Simmons 2014). If the drops are larger than Kolmogorov's length scale (inertial sub-range), they are disrupted by the pressure/velocity fluctuation across the drop; in the other case when the droplets are smaller than Kolmogorov's scale the mechanism is similar to the laminar case.

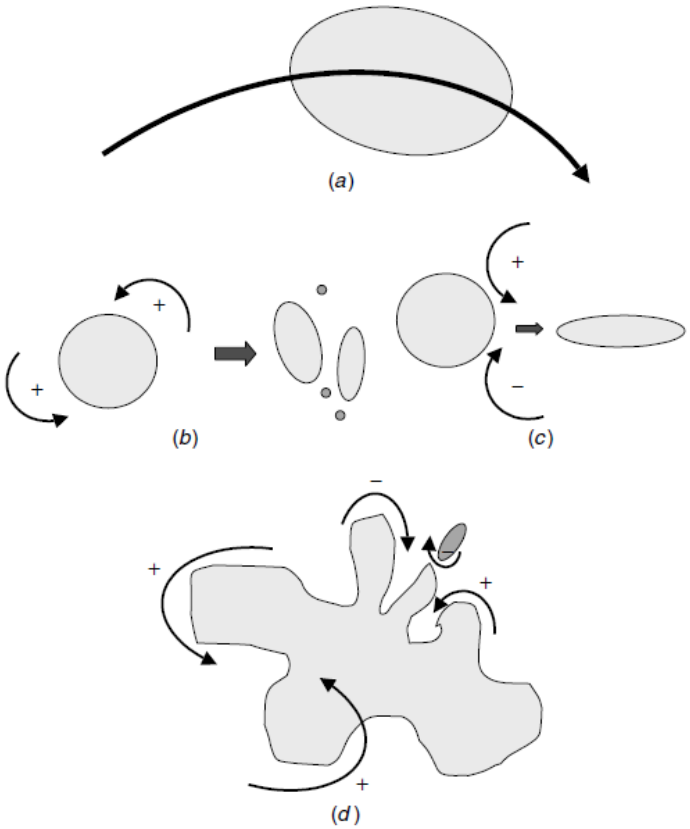

Figure 2.4 Mutual interaction between drops and eddies in a turbulent flow: convection (a), erosion by co-rotating eddies (b), elongation by counter-rotating eddies (c), multiple scales of turbulent deformation (d) (Paul 2003).

In the first case, the external stress is proportional to velocity fluctuations:

$$\tau \propto \rho_c u(d) \tag{2-7}$$

and considering Hinze's (1955) studies, the velocity fluctuations can be related to the energy dissipation rate ($\varepsilon = \frac{\Delta P \cdot Q}{\rho \cdot A \cdot l}$ (2-8) for a motionless mixer (Middleman 1979, Berkman and Calabrese 1988)):

$$u(d) \propto (\varepsilon \cdot d)^{1/3} \tag{2-9}$$

Substituting in the Weber or Capillary number definition, a critical value is found:

$$We_{cr} = \frac{\rho_c \cdot \varepsilon^{2/3} \cdot d_{\max}^{5/3}}{\sigma} \tag{2-10}$$

Reversing the formula, it is possible to find a correlation between the maximum drop size and the dissipation rate:

$$d_{\max} = C_x \left(\frac{\sigma}{\rho} \right)^{0.6} \cdot \varepsilon^{-0.4} \tag{2-11}$$

with $C_x \approx 0.725$ (Hinze, 1955).

In the other case, when the drops have a size smaller than the smallest eddies the correlation is (Davies 1985):

$$d_{\max} = C_2 \cdot \mu^{-1} \cdot \upsilon^{0.5} \cdot \varepsilon^{-0.4} \tag{2-12}$$

In each of the above-mentioned cases to achieve high shearing stress needed to deform and break up small droplets, very much energy needs to be dissipated in the liquid. The dispersed droplet diameter is also conditioned by the energy input into the system. A simple order of magnitude calculation shows that the energy spent to form an emulsion is usually much larger than the actual droplet surface energy in the final product. Most of the energy is actually lost as heat (thermal dissipation) or converted into momentum for phase contacting (hydrodynamic mixing) (Fradette, Brocart et al. 2007).

The energy consumption in the system is basically given by the pressure drops that are in general several orders bigger than the surface energy of the drops; this energy is defined for a single drop as:

$$E_{\sup} = \pi \cdot \sigma \cdot d^2 \tag{2-13}$$

The higher is the diameter, the higher is the energy available in the system for starting the breakup mechanism and it is easier for the droplets to split thus.

The viscosity of the secondary phase also plays an important role in the breakup of droplets; the higher the viscosity, the longer it will take to deform a drop. The deformation time t_{def} is given by the ratio of oil (the dispersed phase) viscosity to the external stress acting on the drop $t_{def} = \mu_D / \tau_{ext}$.

2.3 Mixing equipment

2.3.1 Introduction

The mixing of liquids is a unit operation in which two or more miscible or immiscible liquids are mixed together to reach a certain degree of homogeneity or dispersion (Paul 2003). Mixing is a common operation for the manufacture of a wide range of products such as food, personal care, home care and catalysts industry. When the mixing involves immiscible fluids the operation is called dispersion. Stirred vessels, rotor-stator mixers, static mixers, decanters, settlers, centrifuges, homogenizers, extraction columns, and electrostatic coalescers are examples of industrial process equipment used to handle liquid-liquid systems. All these operations can be classified as batch or continuous processes (Hall, Cooke et al. 2011). In batch processes, stirred tanks and similar devices are used to blend fluids, employing an impeller for generating the fluid motion. The amount of time required to reach the degree of homogeneity desired is known as the blend time or residence time, which is the time spent by the fluid inside the tank before reaching the desired level of mixing. Static mixers and similar devices are used for continuous processes where fluids are pumped through mixing elements installed inside pipes. In the following table the main

characteristics of static mixers compared with stirred tanks are reported (Thakur, Vial et al. 2003).

Table 2.1 Comparison between features of static mixer and stirred tank

Static Mixer	CSTR
Small space requirement	Large space requirement
Low equipment cost	High equipment cost
No power required except pumping	High power consumption
No moving parts except pump	Agitator drive and seals
Short residence times	Long residence times
Approaches plug flow	Exponential distribution of residence times
Self-cleaning, interchangeable mixers or disposable mixers	Large vessels to be cleaned

2.3.2 Mixing of immiscible liquids in Stirred Tank

Stirred tanks are generally used for intermixing of mutually insoluble liquids. Turbine impellers are often employed for this purpose, because they increase the interfacial area. The industrial applications are wide in reacting and non-reacting systems: extraction, alkylation, suspension polymerization, emulsification and phase transfer catalysis. Crucial is the individuation of the right energy provision, because a surplus can create undesirable process results; for example it can create highly stable emulsions and generate excessive heat, which can affect the quality of the final product. It can also cause foaming and vapour entrainment in the zone close to the turbine. Turbine impellers provide the desired mixing conditions for contacting of immiscible liquids. The turbines

are the usual choice even in the case of high viscosity liquids. Several correlations have been published in the literature for predicting average drop size and drop size distribution based on mixer design parameters and liquid physical properties. These correlations take into account the drops break up due to the sharing action near the impeller, as well as the coalescence in the zone of low circulation away from the turbine. The time required to reach an equilibrium drop size distribution depends on system properties and can sometime be longer than the process time. Even if for many common systems they have been replace by continuous devices, stirred vessels remain powerful tools in process industry and find vast applications especially for processing highly viscous products (Aubin, Naude et al. 2000, Cabaret, Rivera et al. 2007).

3.3.3 Mixing of immiscible liquids in Static Mixer

A static mixer can be a hollow tube or channel with a specific geometrical construction that influences the flow structure in a manner to promote secondary transverse flows that enhance mass and heat transfer in the cross-section. The purpose of the elements is to redistribute the fluid in the directions transverse to the main flow, giving to it not null radial and tangential components. Static mixers divide and redistribute streamlines in a sequential fashion using only the pumping energy of the flowing fluid.

The advantages offered by the use of static mixer in mixing and in heat transfer operations have insured an increasing employment of these devices in process industries. Amongst the others, their main characteristic is the absence of moving mechanical part and the possibility to set a continuous process. The small space requirement, low equipment operation and maintenance costs, sharp residence time distribution, improved selectivity through intensified mixing and isothermal operation, by-product reduction, and enhanced safety

are the remaining features that have promoted the use of these devices in chemical (Streiff 1997, Thakur, Vial et al. 2003, Ferrouillat, Tochon et al. 2006, Ghanem, Lemenand et al. 2014).

In the literature the actual first patent on a static mixer is dated 1874 (Sutherland 1874), it was a single element, multilayer, motionless mixer, used to mix air with a gaseous fuel. It is only in the early 1950's that staged elements are designed to promote heat transfer (Lynn 1958) and the first industrial application dates 1970. Nowadays, they are widely used devices in the process industry. They are used in continuous processes as an alternative to conventional agitation since equal mixing performance can be achieved with a lower energy expenditure. The flexibility of production is also another important factor which addresses the development of inline mixing. Static mixers for process industry applications were initially developed for blending of fluids in laminar flow (Grace 1982) and applications in heat transfer; the expansion towards turbulent and multiphase systems were implemented much later (Baldyga 2001). Economic and environmental needs have prompted the studies on characterizing mixing in industrial processes in the last years (Anxionnaz, Cabassud et al. 2008, Lobry, Theron et al. 2011).

Important handbooks and textbooks discuss fluid mixing and applications in process technology from a much wider perspective (Oldshue 1983, Nienow 1997, Paul 2003). Extensive blending data have been collected by Wadley (Wadley and Dawson 2005) for the Sulzer SMV, KM and HEV mixers in the transitional and turbulent flow regimes, using a laser-induced fluorescence (LIF) technique. Meijer in his work thoroughly analyzes several different motionless mixers (Meijer, Singh et al. 2012).

Different types of static mixer are shown in Figure 2.5.

Figure 2.5 Static mixer design options. From left: vortex mixer (KVM), corrugated plate (SMV), wall-mounted vans (SMF), cross-bar (SMX), helical twist (KHT), cross-bar (SMXL). (Koch-Glitsch, LP.)

Three different stages are introduced to describe the mixing mechanism: macromixing, mesomixing and micromixing (Fournier, Falk et al. 1996, Bałdyga and Bourne 1999). In all these cases, the key parameters to compare the different available static mixer at the same performance (drop size distribution) are the energy consumption or pressure drop and the number of elements necessary. In both laminar and turbulent cases the pressure drops in a static mixer are related to the pressure drops in an empty pipe, with the same length and diameter, by a K factor (K_L for laminar and K_T for turbulent flow) that is an empirically determined parameter for different geometries:

$$\Delta P_{sm} = \begin{cases} K_L \cdot \Delta P_{EmptyPipe} \\ K_T \cdot \Delta P_{EmptyPipe} \end{cases} \tag{2-14}$$

Where the standard pressure drop for an empty smooth pipe are:

$$\Delta P = 4 f \frac{L}{D} \rho \frac{v^2}{2} \tag{2-15}$$

And the Fanning friction factor is given by the Blasius equation for turbulent flow:

$$f = \frac{0.079}{\mathrm{Re}^{0.25}} \tag{2-16}$$

and in laminar flow by:

$$f = \frac{16}{\mathrm{Re}} \tag{2-17}$$

In the Table 2.2 the values of K_L and K_T for different devices. In literature the constants for the SMX+, investigated in this thesis, are not available. Though, on the website of the producer company it is declared that this static mixer has 50% lower pressure drop compared to a standard SMX (©Sulzer).

Table 2.2 Values of K_L and K_T for different static mixer (Streiff 1997)

Device	**K_L**	**K_T**
Empty pipe	1	1
KMS	6.9	150
SMX	37.5	500
SMXL	7.8	100
SMR	46.9	-
SMV	-	100-200

Drop size distribution and dynamics of the liquid-dispersions are important characteristics, because their values can affect the quality of the final products. In general, in multiphase flows the purpose of the mixing process is to achieve a precise drop size distribution. This parameter and its time evolution depend on

the relative break-up and coalescence rates. These two phenomena are functions of agitation, as well as of physical properties of the mixed phases. Narrow size distribution of liquid droplets can be achieved due to the relatively homogeneous flow yield in static mixers. However, in order to optimize and control liquid–liquid dispersion processes it is essential to understand and model the drop behaviour affected by variations of the physical properties and the mixing intensity. One important base for mathematical modelling of these systems are reliable experimental data. Different models for the prediction of the mean diameter of liquid–liquid dispersions in static mixer have been proposed in the literature. They are generally derived from models developed for batch stirred tanks.

2.4 Mixing performance for the drop size distribution

2.4.1 Particle size characterization techniques

The importance of emulsions in nature and industry has given considerable impetus to the development of analytical techniques to provide information about droplet size, e.g. light microscopy, electron microscopy, light scattering, and electrical conductivity measurements (Dickinson 1982). Most of these efforts have brought to the development of industrial instruments nowadays widely employed in analyzing emulsions. Nevertheless, each technique has its own application fields and limitations, and consequently it is important from time to time understanding which one is the most suitable in the specific case.

Amongst the several available methods, an important classification divides them in two big categories:

- Offline techniques;
- Online techniques.

Microscopic techniques belong to the first category. These methods provide the most direct information about the overall microstructure of emulsions, i.e. the size and spatial distribution of droplets (McClements 1996). The problem of this technique is the preparation of samples for analysis that it is hardworking and time consuming and can cause alteration in the properties of the measured system. Light scattering based methods are simple to operate and give quick answers over a wide range of droplet size distributions (typically 0.1-1000 μm). The limitation of these techniques is that concentrated samples must be diluted considerably before the measurement. Instruments based on electrical conductivity measurements, such as the "Coulter Counter", also require dilute samples and have the added disadvantage that an electrolyte must often be added to an emulsion before analysis to increase the conductivity of the aqueous phase. Nuclear magnetic resonance (NMR) techniques have recently been developed for measuring the droplet size distribution of concentrated and optically opaque emulsions (Soderman 1992). These techniques are based on measurements of the restricted diffusion of molecules within emulsion droplets. At present, the NMR application is limited because involves expensive equipment, requires highly skilled operators, and it has not been adapted successfully to on-line measurements. Ultrasonic spectrometry is a particle-sizing technology which has been developed recently. It has the advantages to measure the particle sizes with a non-destructive and non-invasive approach. One of the major limitations of the ultrasonic technique is that it cannot be used to study emulsions which contain small gas bubbles. This is because the gas bubbles scatter the ultrasound so effectively (even at very low concentrations) that the ultrasonic signal is completely attenuated.

Optical methods usually contemplate the addiction of external substances to the system and the presence of transparent material to make possible the

measurement (Maa and Hsu 1997, Arratia and Muzzio 2004, Alberini, Simmons et al. 2014). PLIF has been demonstrated to be effective in providing planar concentration measurements in both gaseous and liquid flows (Dahm, Southerland et al. 1991, Karasso and Mungal 1996, Unger and Muzino 1999, Pan and Meng 2001).

2.4.2 Characterization of the drop size

The following expressions describe the common drop size notation used in this thesis. The total volume fraction of dispersed phase is φ, the total interfacial area per unit volume of mixed phases is a_v, and $d_{\max}$ is the maximum drop size. The Sauter mean diameter, d_{32}, is a parameter often used for representing the average drop size averaged on the volume fraction. It is defined by:

$$d_{32} = \frac{\sum_{i=1}^{i=m} n_i d_i^3}{\sum_{i=1}^{i=m} n_i d_i^2} \tag{2-18}$$

where m is the number of size classes describing the drop size distribution (DSD), n_i the number of drops, and d_i the nominal diameter of drops in size class i. There are also other mean diameters such as d_{43}. The subscripts indicate that for instance d_{32} is formed from the ratio of the third to second moments of the DSD. The mean diameter of choice is often d_{32}, since it is directly related to φ and a_v by

$$d_{32} = \frac{6\varphi}{a_v} \tag{2-19}$$

Another common parameter is d_n; for instance d_{10} is defined as 10% by volume of all drops smaller than d_{10}, d_{50} is defined as 50% by volume of all drops smaller than d_{50} and it is the same for every other value of n in the range 0-100. To derive these values it is necessary to plot the size distribution data in terms of cumulative volume frequency, defined below.

The droplet size distribution can be sometimes bimodal or trimodal and this shows the presence of multiple breakage mechanism and unusual breakage patterns (Paul 2003).

The DSD can be represented in a discrete or histogram form in terms of number frequency, $f_n(d_i)$, given by

$$f_n = \frac{n_i}{\sum_{j=1}^{m} n_j} \tag{2-20}$$

Or volume frequency $f_v(d_i)$:

$$f_v = \frac{n_i d_i^3}{\sum_{j=1}^{m} n_j d_j^3} \tag{2-21}$$

In the present work the second definition of frequency has been employed since it is the most convenient and widely used in the industrial applications.

The DSD can also be described by a cumulative curve. The cumulative volume frequency $F_v(d_k)$ is defined by

$$F_v(d_k) = \frac{\sum_{i=1}^{k} n_i d_i^3}{\sum_{j=1}^{m} n_j d_j^3} \tag{2-22}$$

where d_k is the size of drops in the k[th] size class.

Cumulative drop size distributions can be plotted conveniently on linear or log probability curve. Accordingly to Simmons et al. (2001) to model the drop size distribution an upper-limit log-normal function can be used.

$$f_v(d) = 1 - \frac{1}{2}[1 - erf(\delta \cdot z)] \tag{2-23}$$

Where the cumulative volume fraction of particles smaller than size d is $f_v(d_i)$, and

$$z = \ln\left[\frac{a \cdot d}{d_{\max} - d}\right], \tag{2-24}$$

$$a = \frac{d_{\max} - d_{50}}{d_{50}}, \tag{2-25}$$

$$\delta = \frac{0.394}{\log_{10}\left[\frac{v_{90}}{v_{10}}\right]}, \tag{2-26}$$

where $v_i = \frac{d_i}{d_{\max} - d_i}$. The characterizing parameters are a and δ, which can be derived from the experimental data.

A theoretical model for the determination of $d_{\max}$ has been made by considering the emulsification of a dispersed phase in a turbulent flow field. Most of the formulas for maximum drop size are based on the model of Hinze (1955).

$$\frac{d_{\max}}{D} = 0.55 \cdot \left(\frac{\rho_c u_c^2 D}{\sigma} \right)^{0.6} \varepsilon^{-0.4} \tag{2-27}$$

Where u_c is the velocity of the continuous phase, ρ_c is the density of the continuous phase, σ is the interfacial tension, D is the pipe of the diameter and ε is the turbulent dissipation rate.

Chapter 3

Materials and Methods

3.1 Introduction

In this thesis different data about static mixers performance are collected and analysed and various experimental techniques have been used. In this chapter the main equipment and procedure adopted during the experimentations are listed and explained. The analyzed system is a rig of static mixer that has been tested with pressure transmitter to evaluate the energy consumption and using the PLIF technique for the evaluation of performance in dispersing an O/W emulsion.

3.2 Static Mixer rig

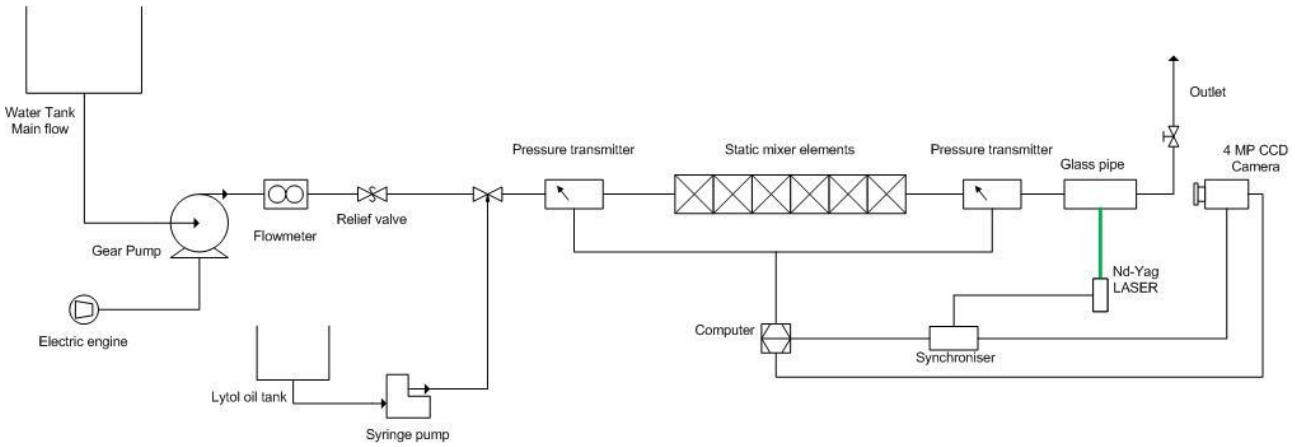

(a)

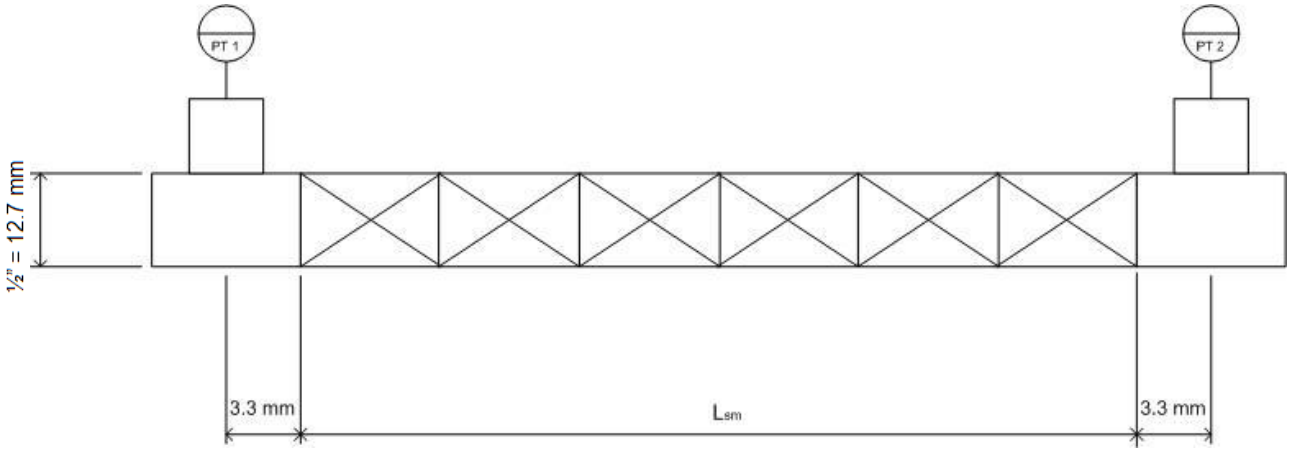

(b)

Figure 3.1 Schematics of the static mixer rig. (a) overall scheme¸(b) dimensions of static mixer test section

Figure 3.1(a) shows an overall scheme of the experimental rig which consists of a primary flow delivered by a Siemens gear pump controlled using a motor drive (Excal Meliamex Ltd.) and monitored using an electromagnetic flow meter (AC 690+ Integrator). The secondary flow is introduced using a syringe pump (Harvard PHD 2000). This pump drives the secondary flow in the mean flow through a needle having an external diameter N_{eedle}= 1.2 mm. After the junction of the two fluids, the mixture crosses the static mixer and is invested by a laser sheet before flowing out.

The main flow is water doped with a fluorescent dye and the secondary flow is Lytol oil with the addition of a surfactant. Both fluids are discussed in details in the paragraph 3.3.1. In Figure 3.1(b) the dimension of a general static mixer device is shown. At the extremities of each device two pressure sensors are attached.

Since different static mixers and different number of elements are used, in the Figure 3.1(b) the length of the static mixer elements set is not specified. In the following Table 3.1 the length in each case is reported.

Table 3.1 Static mixer length and pipe length in the different cases

Set of static mixer	SMX+ 12 el.	SMX+ 6 el.	KM 12 el.	KM 6 el.	Empty pipe
L_{sm} (m)	0.190	0.095	0.270	0.135	0.430

In the whole work the used pipe was made of glass and the only diameter of pipe used is ½″ = 0.0127 m. This value is also the distance between the needle and the first mixing element. The location of the needle (centred relative to the pipe section) has been chosen to facilitate the inlet of the oil drop on the first element. The initial diameter of the drops has been monitored using the High speed camera. Findings are discussed in the paragraph 3.5.1.

An Extech Manometer, equipped with piezoelectric sensors, has been used to collect the pressure data with a sample rate of 0.8 seconds. The operating range of the pressure transmitter was ± 2000 mbar. At the end of the rig a glass pipe cut by a laser sheet, is positioned. A camera, synchronized with the pulsating laser, takes picture of the pipe section. The whole PLIF equipment is explained in details in the paragraph 3.5.2.

A relief valve with a maximum pressure of 3 bar is also used for safety reasons.

3.3 Physical properties measurement

As specified above, the pressure drops and the drop size distributions are investigated. For the accuracy of the results and the subsequent analysis it is essential collecting some important data on the properties of the involved fluids. In particular, the rheological properties of the fluids involved in the pressure drop calculation (water and water-glycerol solutions) and the interfacial tension between the two phases of the O/W emulsion have been collected with the procedures illustrated in the following subparagraphs.

3.3.1 Fluid properties

The crucial first parameter to evaluate the efficiency of a static mixer is the energy dissipation that occurs while the fluid flows through the equipment. Turbulent, laminar and transition regimes are investigated using different fluids. The three different regimes are considered to evaluate the energy loss in a wide range of situations and to compare the results with the relations available in the literature. Three solutions are employed in this first experimentation part and their properties at 23°C are shown in the table below. In the table it is assigned a short name to each substance for simplicity.

Table 3.2 Properties of Water and Glycerol solutions at 23 °C

	Density (kg/m^3)	Viscosity (Pa s)	Regime	Abb.
Water	997.8	0.001	Turbulent	W
Glycerol (aq. solution 80% v/v)	1206	0.048	Laminar	G80
Glycerol (aq. solution 50% v/v)	1146	0.008	Transient	G50

In the PLIF experimentations two different mixtures are used as primary and secondary flow. The primary flow is a solution of water to which a dye is added, in order to give the necessary fluorescence property to the fluid, essential to the success of the PLIF measurements. Rhodamine 6g has been used as dye with a concentration of $5 \cdot 10^{-4}$ g/L. The dye gives to the solution a slightly magenta colour and, as mentioned, fluorescence properties but does not affect the rheological behaviour of water. For this reason, in the whole dissertation the density and viscosity of water are taken considering the fluid as water at 23°C reported in Table 3.3.

The secondary flow is made by Lytol oil added with a non-ionic surfactant Span80 (0.5% w/w) in order to increase the interfacial tension and to facilitate the drops formation. The presence of the surfactant enhances the interfacial tension giving to the droplet surface more stability. In Figure 3.2 the oil feed is displayed while flowing out of the needle. It is evident that in the case (a) the droplets formation is guaranteed in contrast to the case (b) in which the turbulent main flow disturbs the oil inlet impeding the droplets formation.

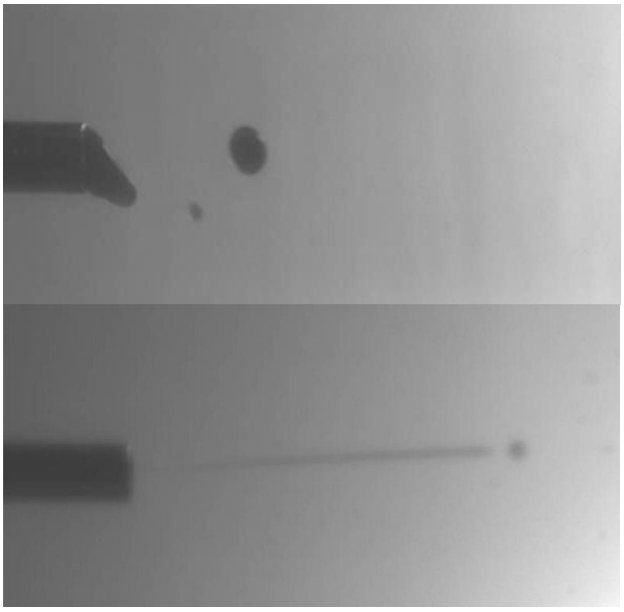

Figure 3.2 Secondary flow inlet (a) with surfactant addiction and (b) without surfactant addiction.

In every test the volumetric flow of the oil is maintained constant, because is not amongst the investigated variables. Several flow rates have been tested to find the optimal flow rate that it has been individuated to be 0.5 ml/min. This value is enough high to enable the drop formation in the whole range of the investigated main flow rate, but at the same time it keeps the frequency of drop formation considerably low allowing us to ignore the coalescence phenomenon.

In the following figure, some examples of the high speed camera captures at different oil flow rate.

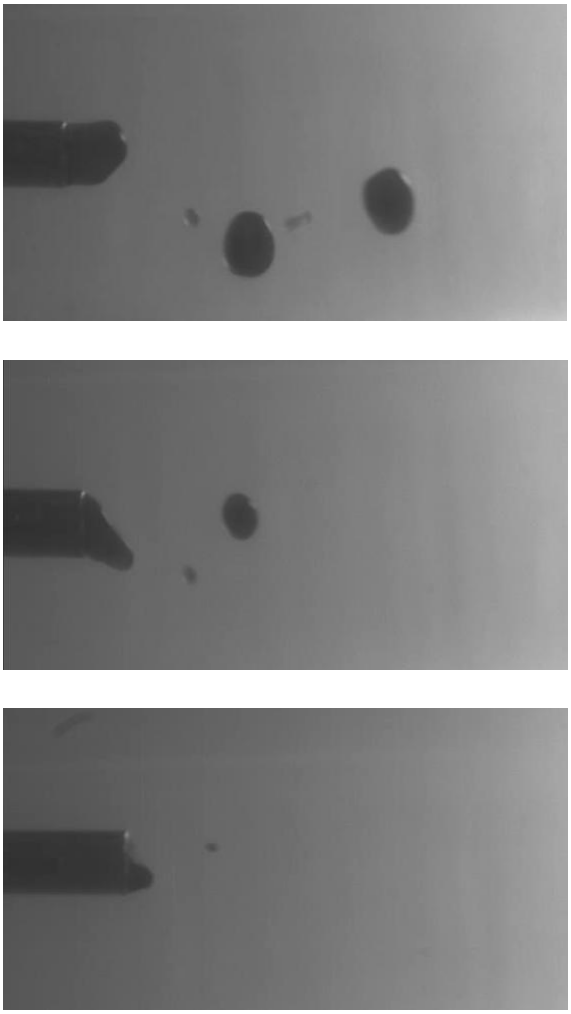

Figure 3.3 High Speed Camera images of the oil fed into the system for different flow rate: 5 ml/min (a), 0.5 ml/min (b) and 0.1 ml/min (c).

The first image, Figure 3.3 (a), has an high drops formation frequency that can also affect the PLIF measurement, in fact as discussed in the image processing an high density of drops in the system can bring to inaccurate results. In the third image (c), on the other hand, the oil flow rate is too low, and for high superficial velocity of the main flow the drops formation is not predictable; the

primary flow snatches little droplets randomly. The second image, Figure 3.3 (b) represents the chosen flow rate.

Another substance has been added in trace to Lytol oil to give to it the black colour that it allows to distinguish the two phases in the pictures above. This substance is Nigrosin powder, a mixture of black dyes.

A summary of the main properties of the involved fluids is reported in the following table.

Table 3.3 Properties of Water and Lytol oil

	Phase	Density (kg/m3)	Viscosity (Pa s)	Interface tension (N/m)
Water	Continuous	997.8	0.001	0.02267
Lytol oil	Dispersed	800	0.0032	

3.3.2 Interfacial tension

The interfacial tension between the two phases has been evaluated by using KRÜSS Force Tensiometer K100.

Figure 3.4 KRÜSS Tensiometer K100

The instrument evaluates the interfacial tension between the two phases by using a Platinum plate. This method is known as the Wilhelmy Plate tensiometer and it is widely acknowledged as one of the most accurate method for measuring the interfacial tension.

Four different measurements have been taken; they are reported in Table 3.4:

Table 3.4 Interfacial tension measurements

Measurement	Interfacial tension [mN/m]
1	22.44
2	22.74
3	22.72
4	22.76
Average value	22.67

The last value is the one used in the subsequent work.

3.3.3 Rheology

For the consideration about the pressure drops data, rheological measurements were necessary. Since the viscosity of water is a well-known data, only the viscosities of the two aqueous solutions of glycerol are evaluated by using TA AR 1000 rheometer. The Newtonian behaviour of the fluids involved in the experiments allows the use of a single coefficient characterizing the viscosity. The rheometer consists of 4 main parts: the rheometer head, draw rod, geometry and sample platform. The rheometer head is the motorized part where the drag-cup motor is located. In addition, an air bearing allows virtually friction free application of torque.

The values of the viscosity are shown in Table 3.2.

3.4 Pressure drop measurement

For the current work, the widest used static mixer in industrial application, have been investigated and evaluated. The scope of the research, in fact, is to enhance the knowledge about the mechanism inside the devices and to provide useful information about static mixer performance for industrial purposes. The models that have been under study are:

- Kenics® KM (Chemineer™);
- Sulzer™ SMX+.

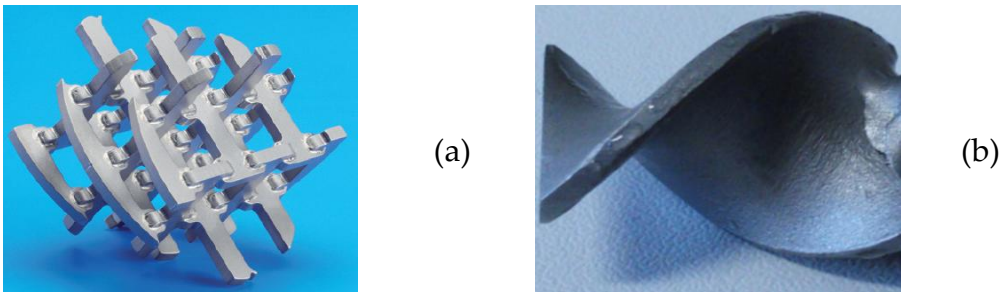

(a) (b)

Figure 3.5 A single mixing element of SMX + (a), and of KM (b)

The effect of varying the number of elements is evaluated. Each experiment has been done for the two different static mixers using 6 and 12 elements and for the empty pipe, taken as reference.

For moving the fluids in the pressure drop measurement another pump (respect to PLIF experiments) has been used: Varmeca gear pump (Leroy® Somer). Before starting the collection of the pressure drop data, a manual calibration of the pump was necessary to assess. The calibration was necessary for knowing the flow rate associated with the position of the control knob of the pump. In fact for each configuration the pump had to overcome a different

prevalence and consequently the fed flow rate changed case by case. The calibration curves are shown in the Figure 3.6.

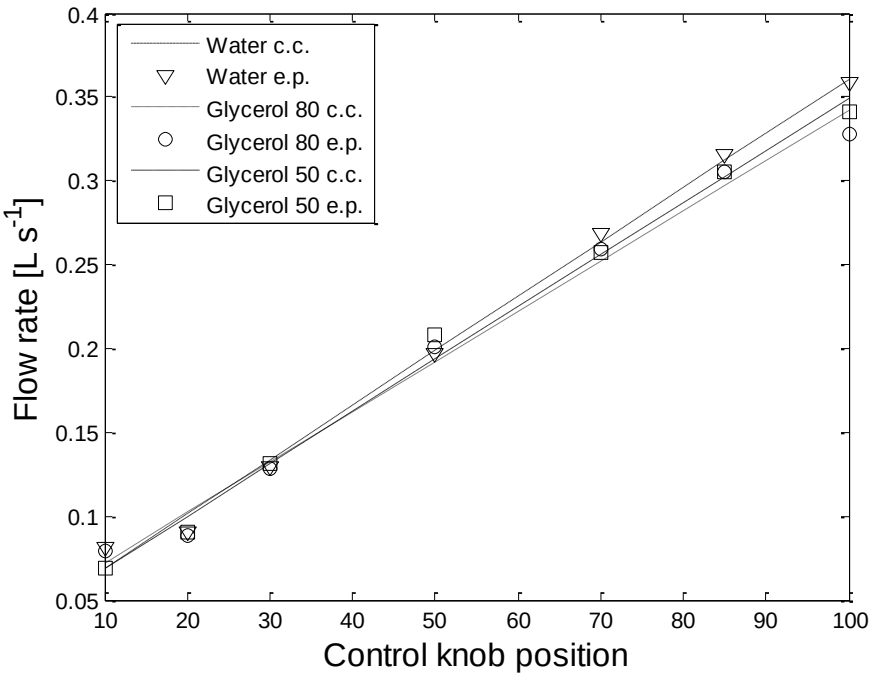

(a)

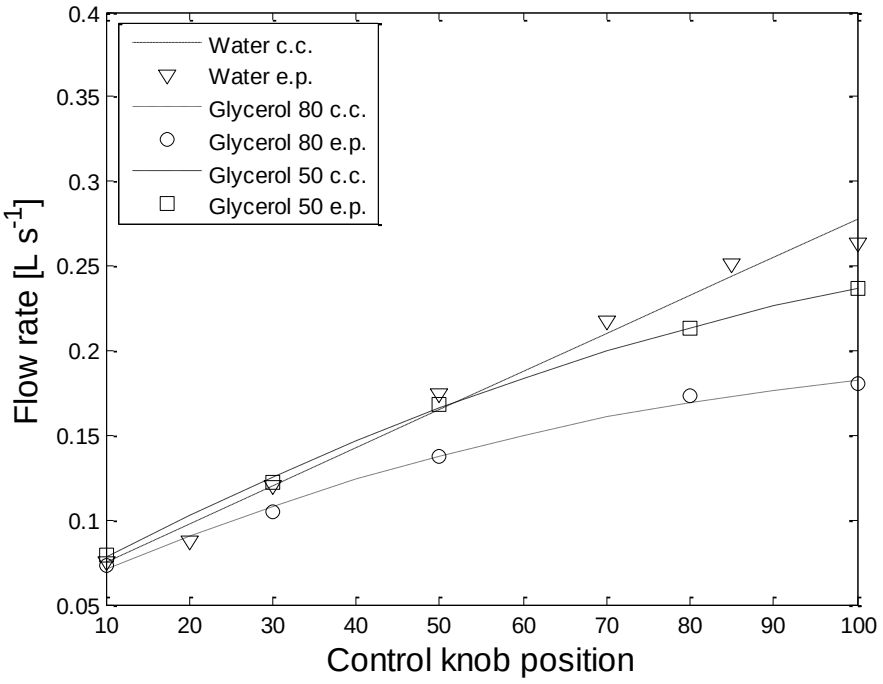

(b)

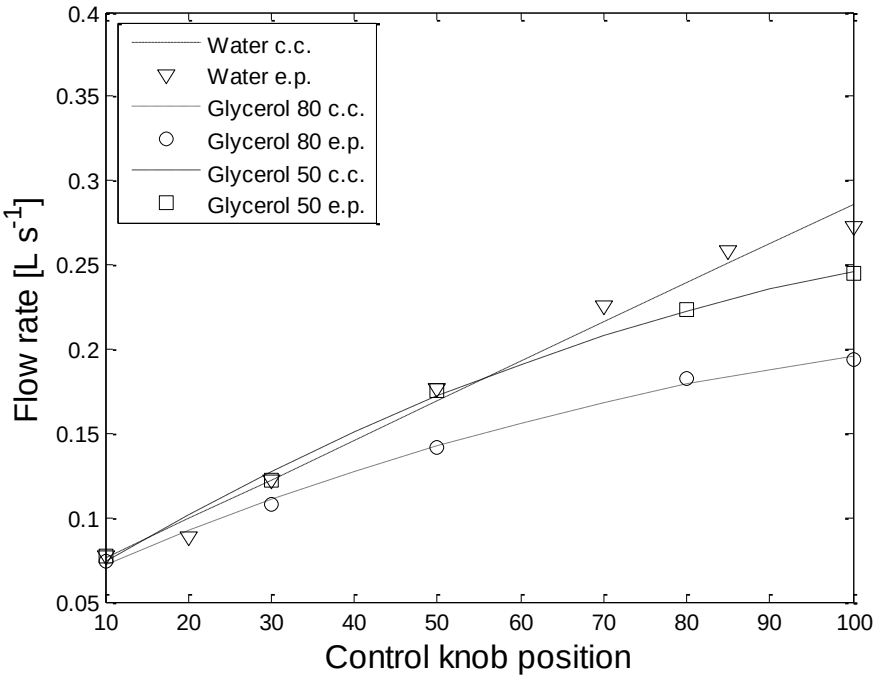

(c)

Figure 3.6 Calibration curve (c.c) and experimental points (e.p.) for W, G80 and G50 flowing across: the empty pipe (a), SMX+ 12 elements (b) and KM 12 elements (c).

It has been noticed that, for different configurations the pressure drop downstream changes and this makes the flow rate change as well. Hence, it was fundamental drawing a calibration curve for each fluid and set of static mixer.

The pressure drops are collected for a single phase flow because it has been noticed that the presence of the second phase does not have significant effects on the measurements.

3.5 Flow visualization

3.5.1 High Speed Imaging

For this work a Photron FASTCAM SA3 has been used. This camera has a CMOS sensor which provides mega pixel resolution (1K by 1K pixels) up to 2000 frames per second (fps). The sensor provides 12-bit dynamic range from its

large seventeen micron square pixels which allows an excellent resolution shout. A two microsecond global electronic shutter ensures a blur free regardless of speed.

To generate the emulsion, a Syringe pump has been used to inject oil drops in the water primary flow through a needle. The FASTCAM SA3 has been used to evaluate the initial diameter of the drops out from the needle and to set the operating flow rate of the secondary flow (Figure3.7). For every configuration four drops have been analyzed and measured; the resulting initial diameter shown in the following figure has been calculated as an average of the analyzed droplets.

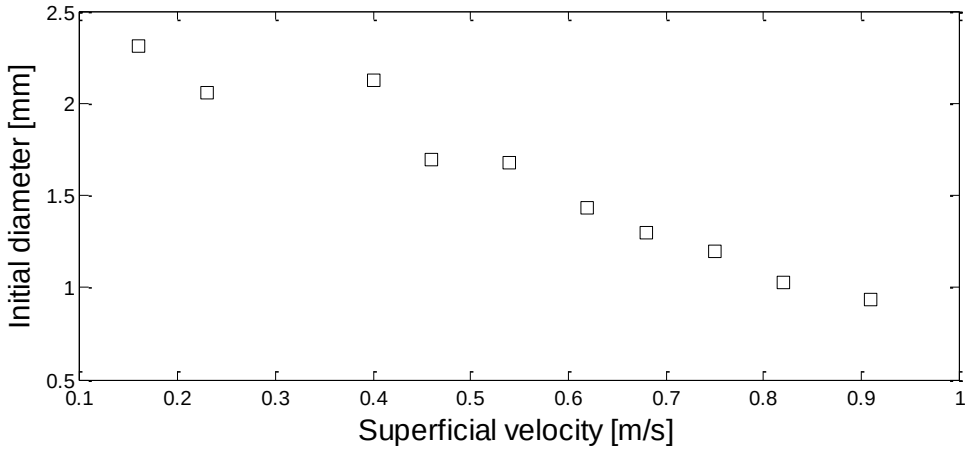

Figure 3.7 Initial droplet diameter trend raising the superficial velocity of the main flow

3.5.2 PLIF

In this work, the PLIF technique has been used as a visualization device. The output images show the section of the tube and the two phases and these data have been used for the characterization of the drop size distribution. The 2-D PLIF measurements were performed using a TSI PIV system (TSI Inc., USA). The system comprises a 532 nm (green) Nd-Yag laser (New Wave Solo III)

pulsing at 7 Hz, synchronized to a single TSI Powerview 4MP (2048 x 2048 pixels) 12 bit CCD camera using a synchronizer (TSI 610035) attached to a personal computer. The PIV system was controlled using TSI Insight 4G software. The camera was equipped with a 545 nm cut-off filter to eliminate reflected laser light so that only the fluorescent light emitted by the Rhodamine 6G dye (lambda=560, yellow) excited in the measurement plane was captured on the image. The spatial resolution of the measurement was 10 μm·pixel^{-1}. In correspondence of the incidence plane of the laser sheet, the glass pipe was surrounded by a glass cubic box filled of distilled water. The role of the box was to offer to the laser sheet a perpendicular plane to hit, reducing the aberrant effect of the curve surface of the pipe.

A tee piece has been placed at the end of the mixer section. This particular item had a glass window inserted on the corner of the tee, normal to the axis of the main pipe, in order to enable flow measurements using PLIF, that requires optically transparent materials. The design is illustrated in Figure 3.8.

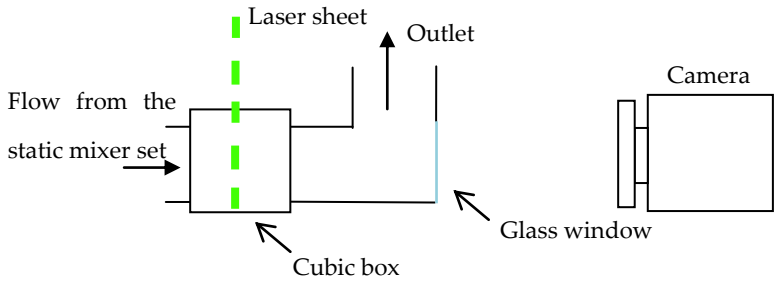

Figure 3.8 Design of the terminal part of the rig

Chapter 4

Results

4.1 Introduction

As previously described, the experimental chapters are divided essentially in three parts. In the first part pressure drops data are collected for the different setting of static mixers (presented in paragraph 4.2); in the second part, discussed in section 4.3, the drop size distribution has been characterized using the PLIF technique and the consequent image processing. The last one consists in connecting the pressure drop data with the drop size distribution in order to find out a correlation between the two.

The objective of this work is finding a connection between these two important parameters in order to facilitate the prediction of the mixing performance of static mixer and the reaching of the set point in terms of drop size. A model is proposed and discussed in the last section of this chapter, 4.4.

4.2 Energy consumption

The evaluation of the energy consumption in the static mixer rig has required the collection of pressure drop data for different sets of static mixer. First of all, to verify the accuracy of the instruments, the pressure drops for an empty pipe have been collected and compared with the well-known theoretical model,

(Equation 2-15). As specified in Chapter 3, the laminar, turbulent and transient regimes have been investigated employing different fluids.

4.2.1 Pressure drop for empty pipe

In the Figure 4.1 three plots are reported in which experimental and theoretical pressure drop are compared in the different regimes. The theoretical pressure drops are calculated from the Equation 2-15 valid for the smooth empty pipe.

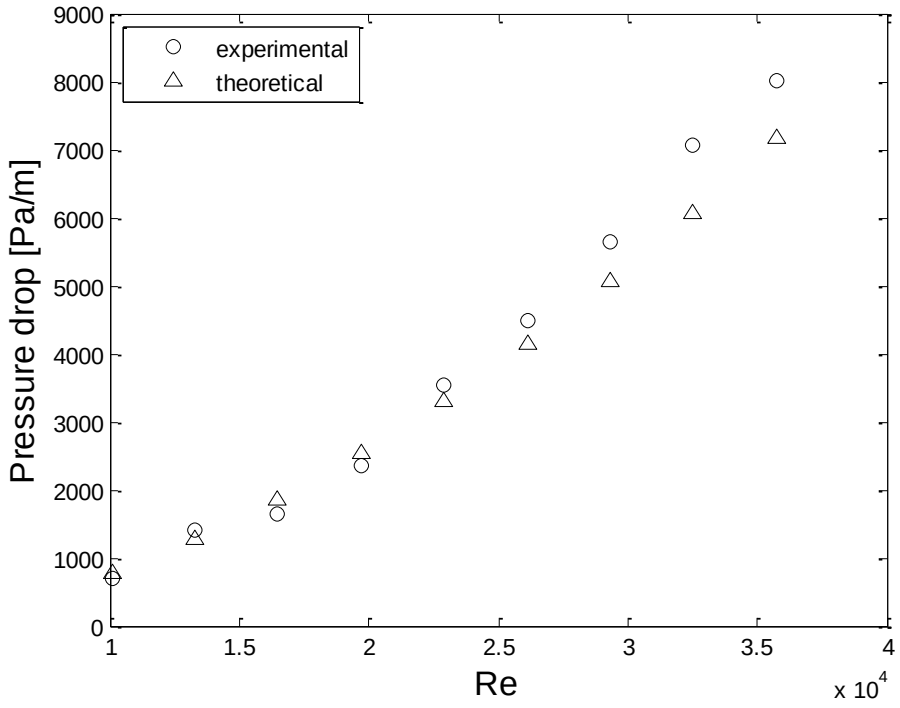

(a)

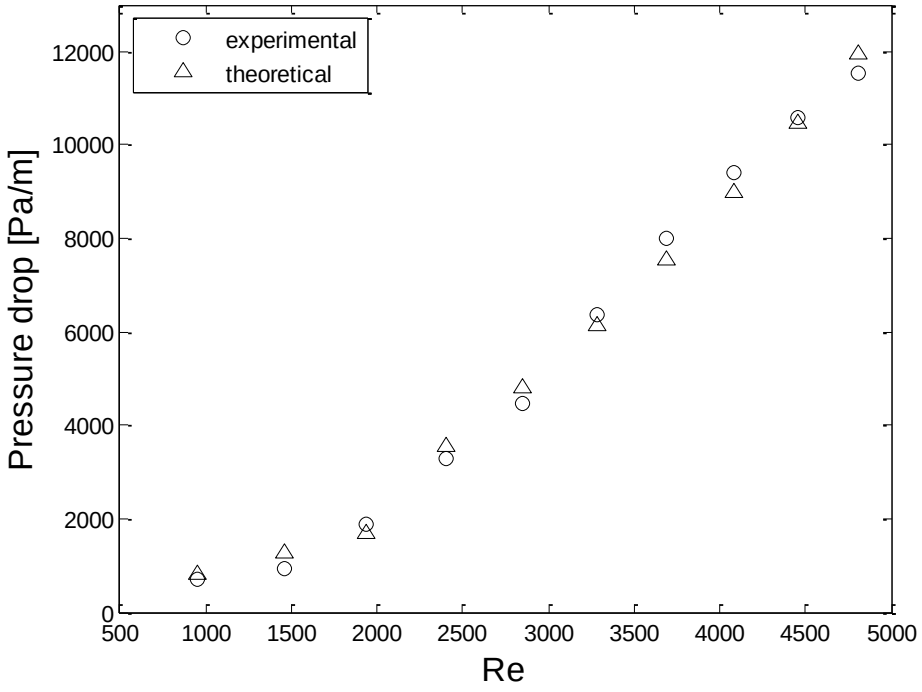

(b)

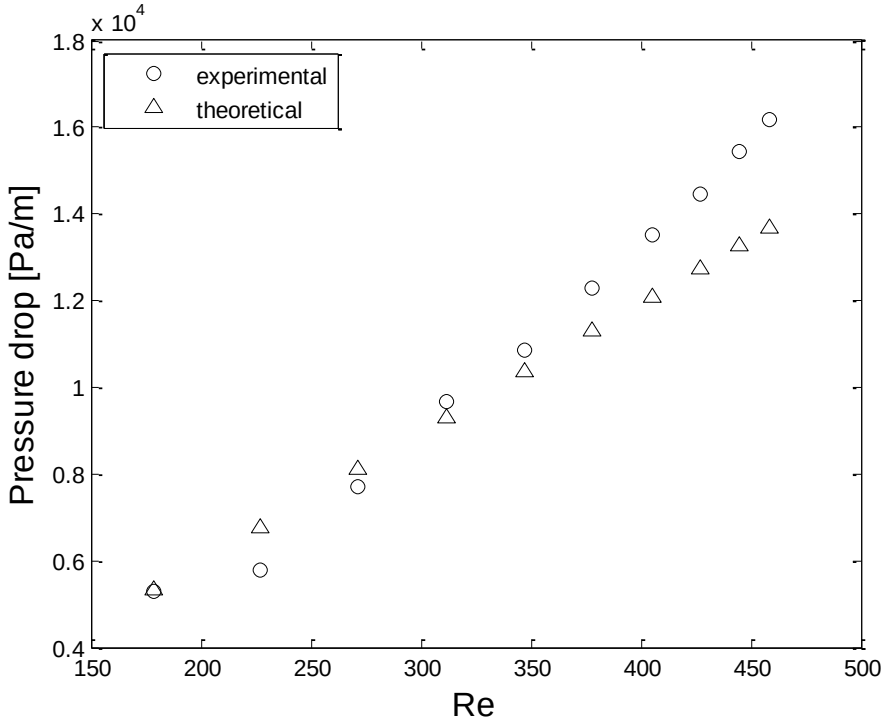

(c)

Figure 4.1 Pressure drop per unit length in empty pipe: (a) turbulent regime (W), (b) transition regime (G50) and (c) laminar regime (G80)

In Figure 4.1 the pressure drops per unit length are shown and it is easy to see that in the cases (a) and (b) in particular the experimental data are faithful to the expectation, while in the case (c) there is a slight underestimation in the range of Re = 400-460. From this comparison, the data collected can be considered reliable and can be used as reference for the static mixer pressure drop evaluation.

4.2.2 Pressure drop for Static Mixer

In evaluating the pressure drop of static mixer, the inlet Reynolds is considered using the inlet velocity and the diameter of the empty pipe. Since the pressure drop per unit length have been plotted in Figure 4.2, the expectation is to obtain similar pressure drop for 6 and 12 elements of each static mixer model.

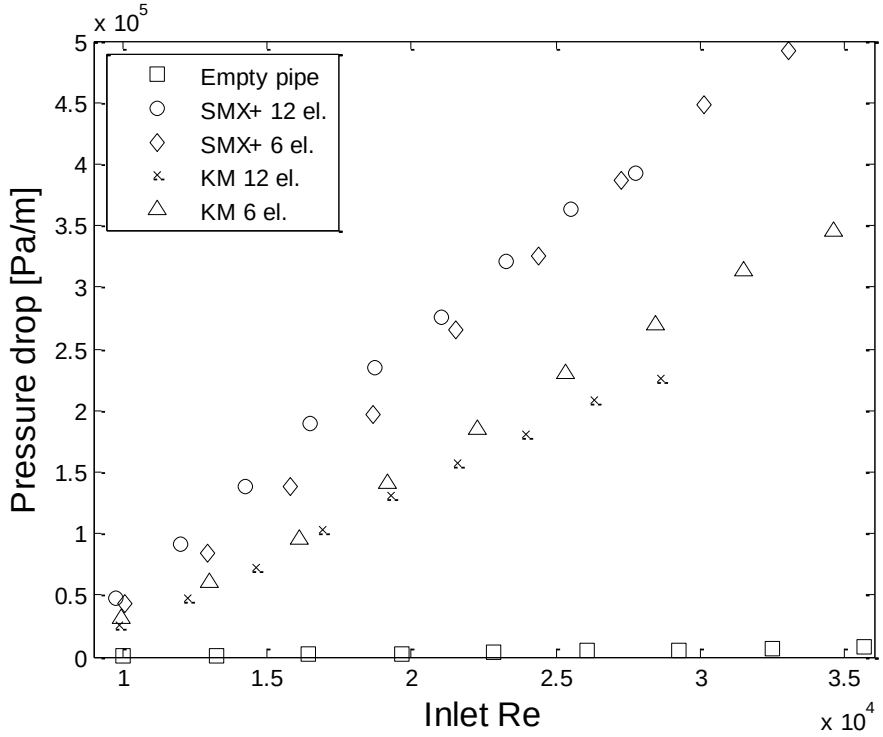

(a)

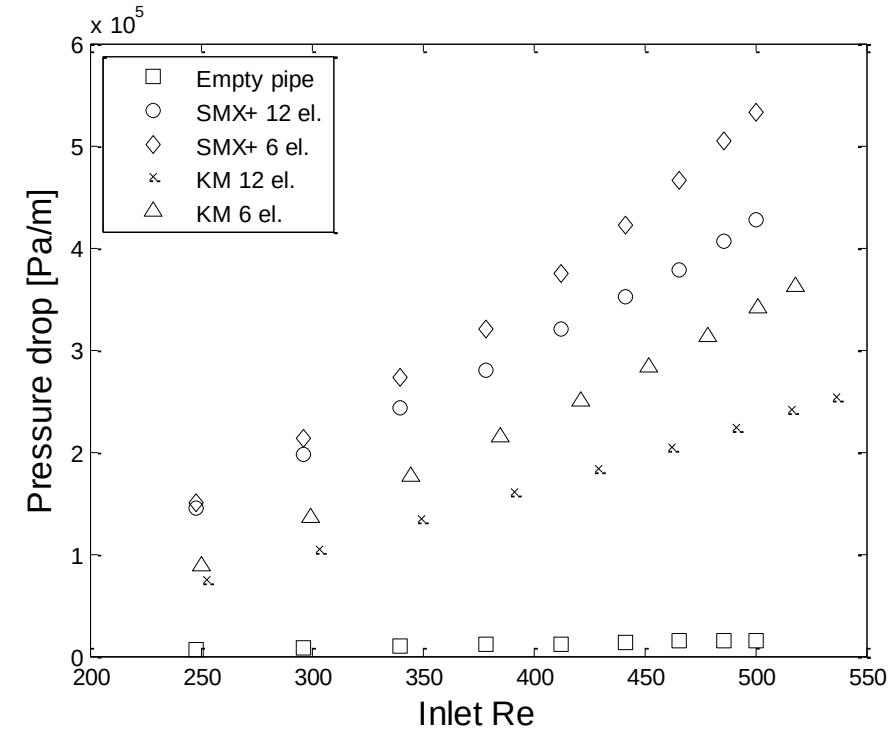

(b)

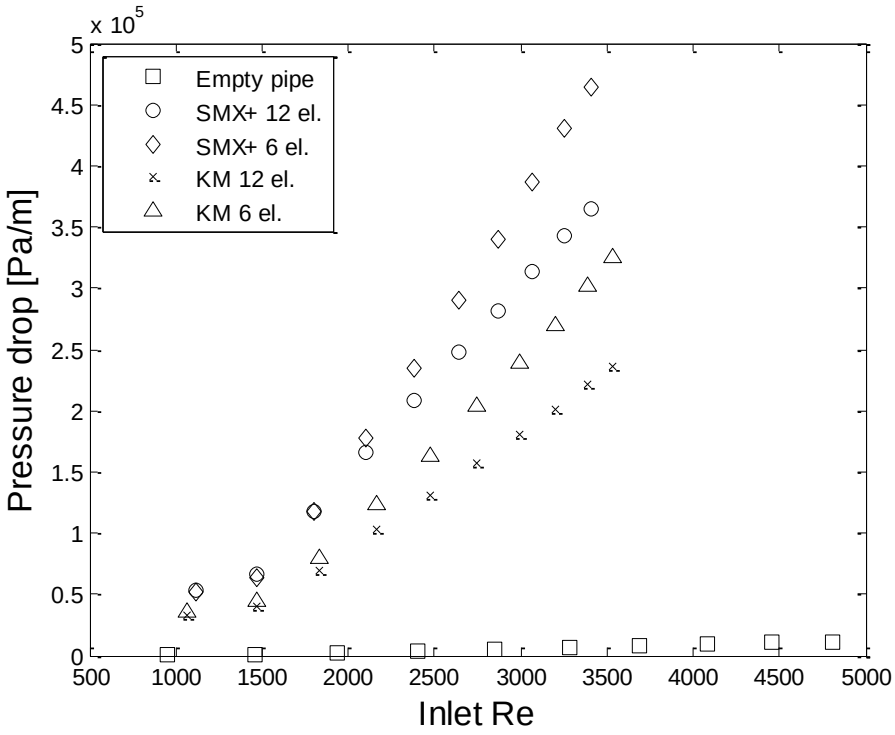

(c)

Figure 4.2 Pressure drop per unit length for the different settings of static mixers: (a)Turbulent case; (b) Laminar; (c) Transition.

In the three cases the empty tube pressure drops are always smaller than the ones in static mixers. The expectations have been met mostly in the turbulent case, while in the laminar case, in particular, there is an aberration between the values for 6 and 12 elements. This fact depends on the first element pressure drop. In fact, the first element is the one that gives the biggest energy loss because it is the one appointed to break the input flow, giving to it radial and tangential components of the velocity. Considering that, it is obvious that distributing this first big energy loss among 6 elements causes higher pressure drop than distributing it among 12 elements. This phenomenon is called entrance effect (Theron and Le Sauze 2011).

In the literature, the used model for the pressure drop is described by the equation 2-14, that basically uses as reference the pressure drop for an empty tube. In the following plots (Figure 4.3) the comparisons between the expected pressure drop and the experimental data are reported for turbulent and laminar regime and for both the static mixer models.

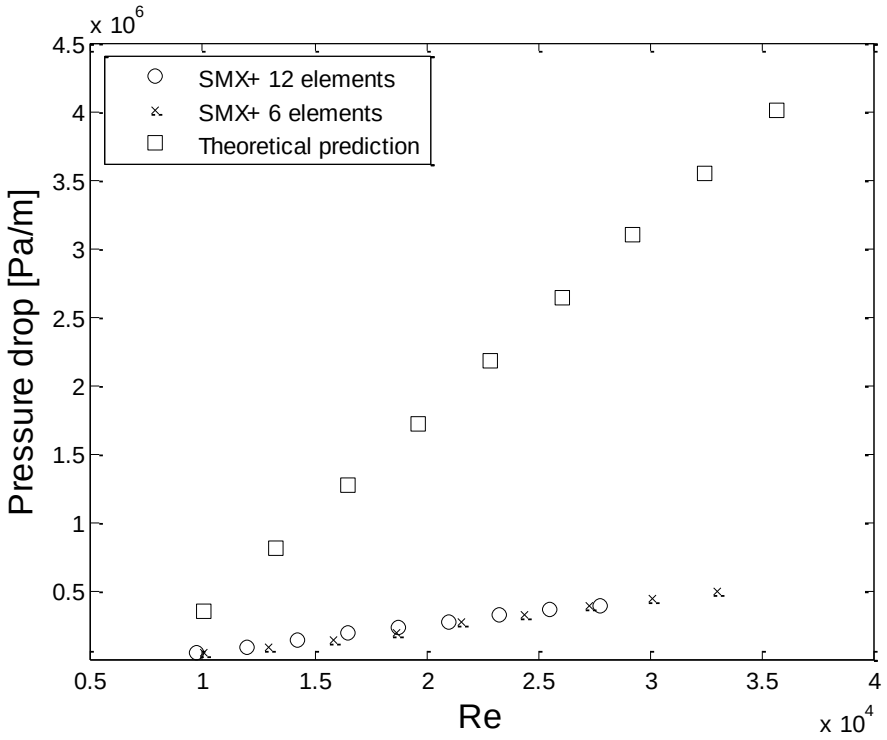

(a)

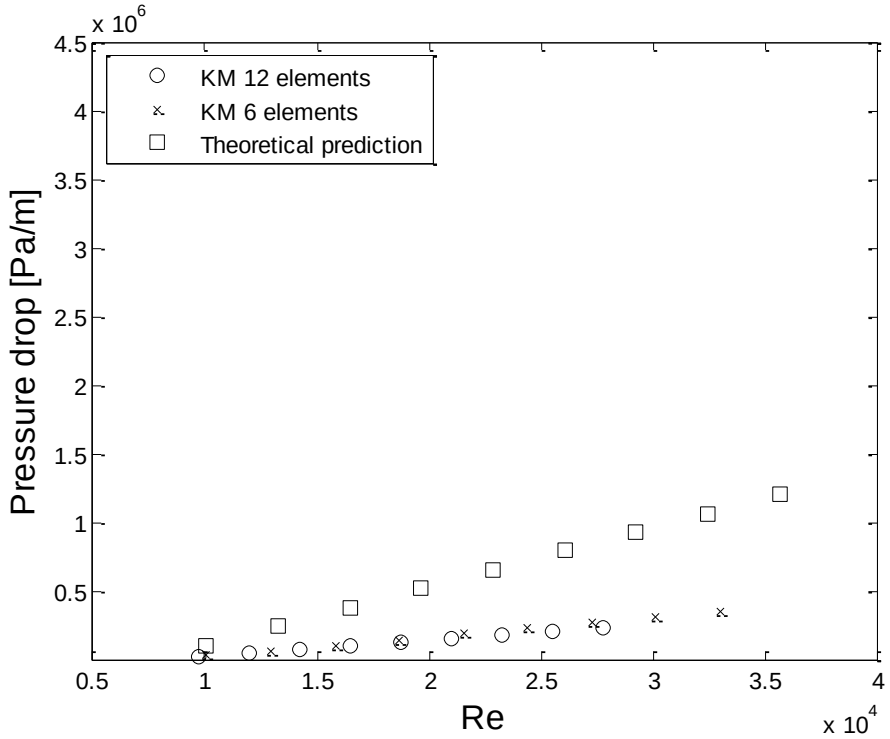
x 10^6
KM 12 elements
KM 6 elements
Theoretical prediction
Pressure drop [Pa/m]
Re
x 10^4

(b)

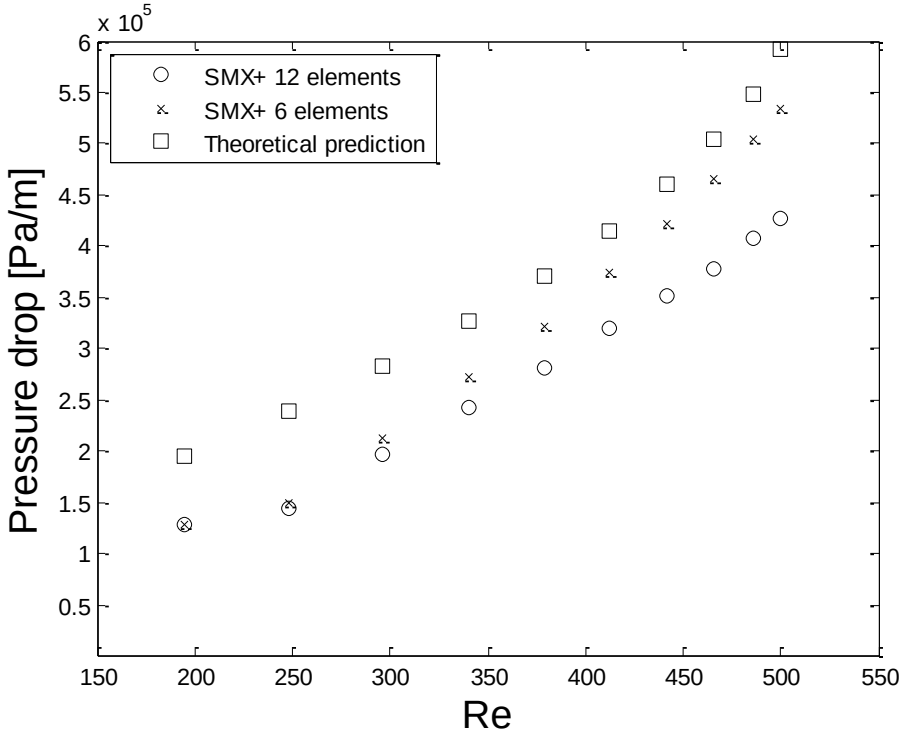
x 10^5
SMX+ 12 elements
SMX+ 6 elements
Theoretical prediction
Pressure drop [Pa/m]
Re

(c)

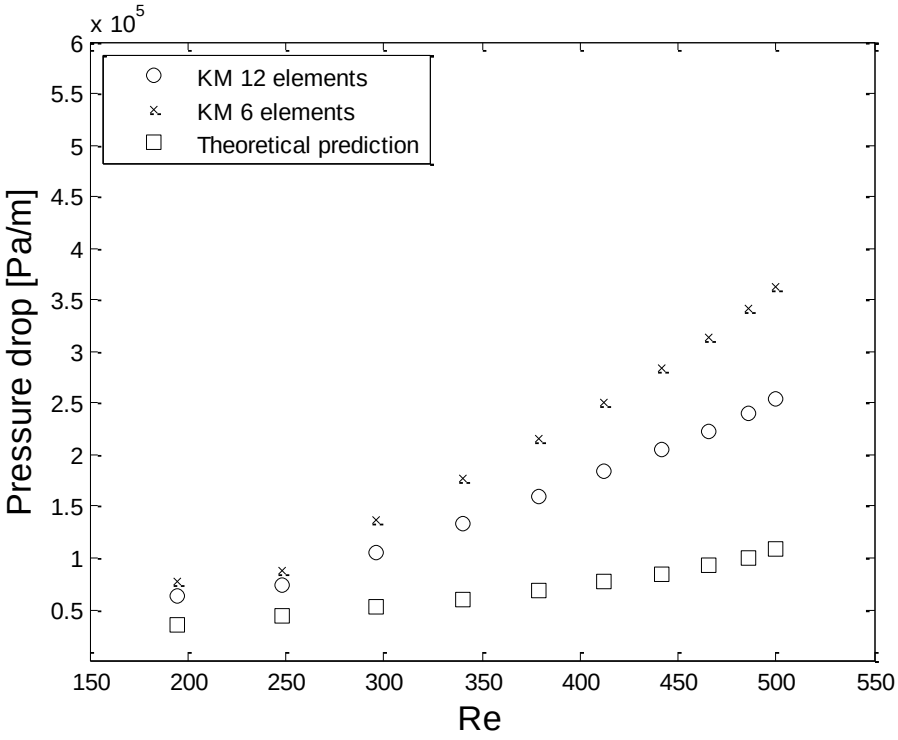

(d)

Figure 4.3 Theoretical and experimental pressure drop per unit length for the turbulent case: SMX+ (a), KM (b); and for the laminar case: SMX+ (c), KM (d).

The plots are reported in pairs with the same scale in order to show that the Sulzer static mixer has higher pressure drop at the same Reynolds number. This difference is due to the geometric shape of the two mixers, while the helical KM element divides the flow in two parts, the SMX+ has a particular grid geometry that splits the flow in more parts and gives more changes of direction.

From Figure 4.3 it can be noticed that the expectations differ greatly from the measured pressure drop, especially in the turbulent case. The reason can be found in the nature of the literature data; in fact the values of K_L and K_T in the Table 2.2 have been calculated on the basis of CFD simulations and further information about the settings and the validation are not available in the literature. Furthermore, there are not available constants for the SMX+ model, then the proposed K_L and K_T for the SMX model have been used for the

comparisons; even if the producing company states that the SMX+ model has 50% lower pressure drop than the classic SMX.

4.2.3 Evaluation of K_L and K_T

Pressure drop for empty pipe and static mixer have been collected, therefore it is possible to result from them the experimental K_L and K_T. To achieve this intent, in Figure 4.4 the empty pipe pressure drop are plotted on the horizontal axis versus the pressure drop for static mixer. Referring again to Equation 2-14, the angular coefficient of the straight line results to be the value of K. Three cases are plotted: turbulent, laminar and transient.

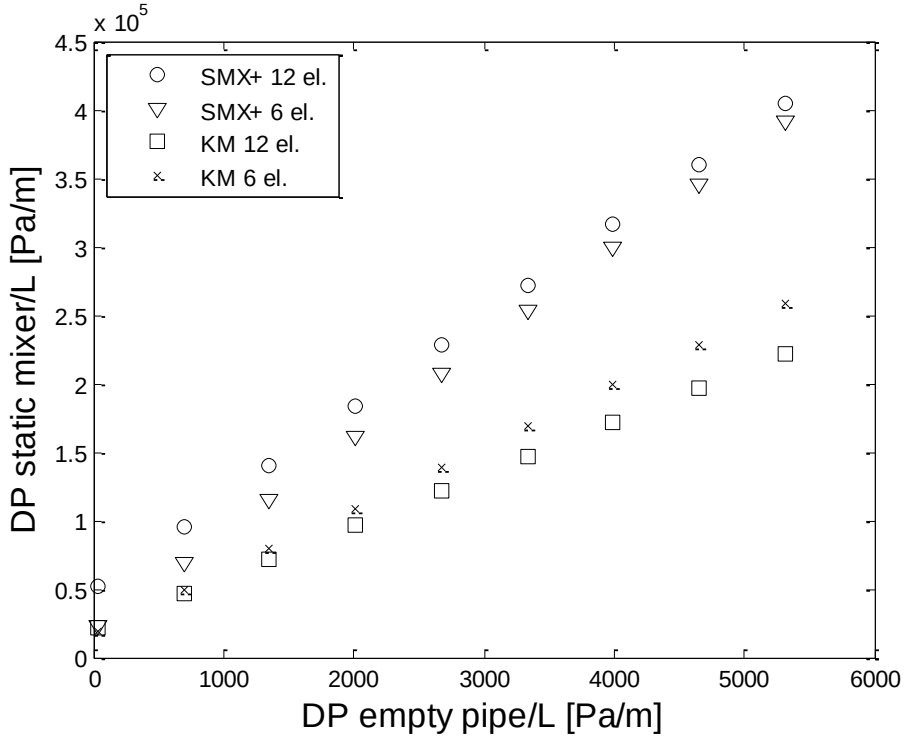

(a)

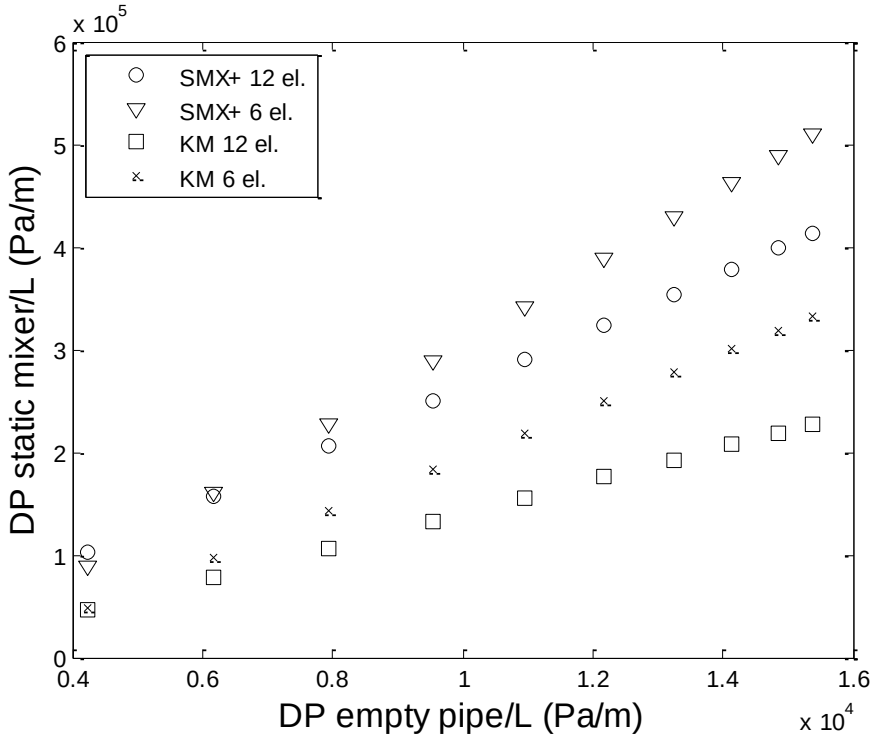

(b)

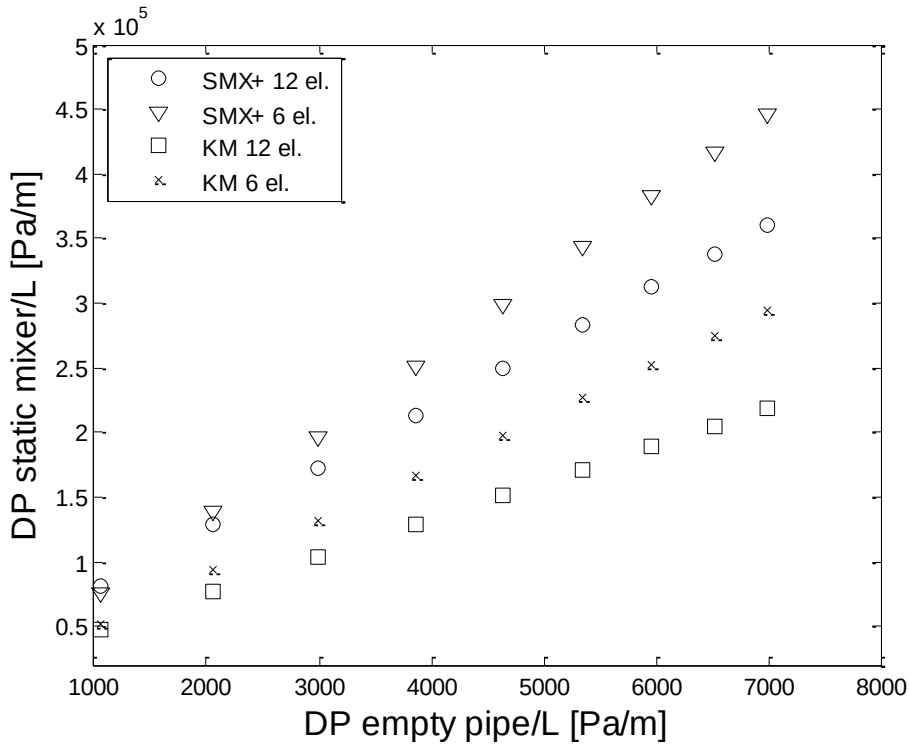

(c)

Figure 4.4 Evaluation of K in the three cases: turbulent (a), laminar (b) and transient (c)

In the plots in Figure 4.4, to combine the empty pipe pressure drop with the static mixer ones a mathematical extrapolation has been done. As specified in the Chapter 2 the fed volumetric flow changes when we pass from the empty pipe rig to the static mixer rig, hence the data have been realigned on the basis of Reynolds number.

Figure 4.4 highlights that the linear correlation predicted by Streiff is a valid model: the coefficient of proportionality between empty pipe and static mixer pressure drop does not change raising the velocity or the pressure drop itself. The calculation of K is immediate in the turbulent, laminar and transient cases. The found and the literature values are shown in the following Table 4.1.

Table 4.1 Experimental and theoretical (Streiff, 1997) K values for the different regimes

Regime		Kenics KM	Sulzer SMX+
Turbulent K_T	Theoretical	150	500(*)
	Experimental	37.8 - 45.32	66.7 – 69.6
Laminar K_L	Theoretical	6.9	37.5(*)
	Experimental	16 – 25.5	28 – 37.8
K for 2100 < Re < 4000	Theoretical	-	-
	Experimental	28.7 - 38.7	47.1 - 62

(*) values for SMX, (there are not available values for SMX+)

In Table 4.1 there are two experimental values, the first comes out from the calculation on the 12 elements and the second is obtained from the 6 elements data. As explained before the values for 6 elements are higher.

The experimental K fits with the literatures derived constants only in the laminar case, while in the turbulent case the overestimation is clearly excessive, accordingly also with the Figure 4.3 (a, b). The values of K for intermediate Reynolds are between the turbulent and laminar ones as expected.

Thakur (Thakur, Vial et al. 2003) reports an overview of the known pressure drop constants in laminar and turbulent cases. Values are widely available for the open, helical inserts Kenics in the laminar regime (Alloca 1982, Pahl and Muschelknautz 1982, Cybulski and Werner 1986, Joshi, Nigam et al. 1995) and K_L ranges from 5 to 8. They are not too far with respect to the experimental value, but most of them have been found out using numerical simulations as Streiff (1997) did. The multilayered SMX design from Koch-Sulzer has been also the subject of literature studies, but reported K_L values are not accurate enough for proper estimation: Pahl and Muschelknautz (1982) reported K_L values between 10 and 60, while Cybulski and Werner (1986) reported values from 10 to 100. The accuracy of the pressure drop parameters K becomes also lower if we move towards a turbulent regime. In this case the CFD simulations are not reliable because of the intrinsic difficulties of representation of the turbulent regime and nevertheless the present values have not been validated and supported by experimental values. There is a substantial lack of experimental data in the literature, that cannot provide us a solid term of comparison. Despite this, the linearity of the last plot and the magnitudes involved allow us to consider reasonable the resulting parameters.

To conclude, in this first experimentation part an energy analysis of the static mixers KMS and SMX+ have been done in order to characterize the performance in terms of pressure drop. Furthermore the energy feed into the system is now known and this information is important in the further analysis.

4.3 Drop size characterization

The multitude of images captured during the PLIF experiments are processed in order to obtain information about the drop size distribution. For each experiment set, 500 pictures have been taken by the camera and saved in the database. The program MATLAB (Mathworks®) potentiated by DIPimage have been used. DIPimage is a MATLAB toolbox for scientific image processing and analysis. In the next subparagraphs the image processing, derived by the previous work of Alberini (Alberini, Simmons et al. 2014), is explained and the results are analysed in detail.

4.3.1 Image processing

As mentioned in the introduction, the images have been processed with the aid of a computer. A series of codes have been created to obtain the data relating to the droplets dimension. Part of these codes have been attached in the Appendix of this thesis.

The pictures present themselves as circular shots of the section of the pipe, in which much of the space is occupied by the fluorescent mixture and has a light grey colour. The other part is occupied by darker spots that represent the dispersed oil droplets. In the Figure 4.5 a typical raw image taken by the camera is shown.

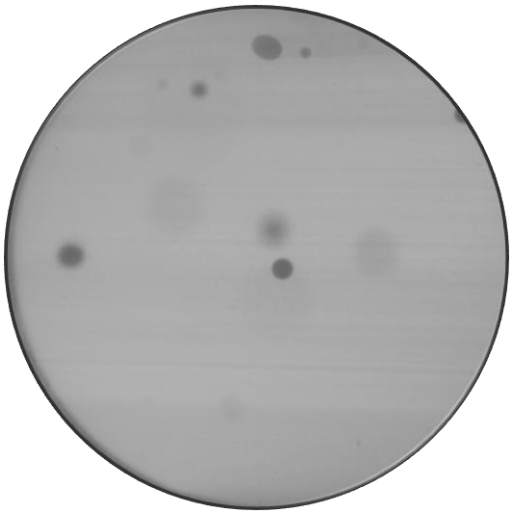

Figure 4.5 A raw image resulted from PLIF experiments

It is evident the presence of an heavy background shading in this image. Trying to process it directly the results are unsatisfactory. Hence, it needs a background correction. It consists of a filtering that removes the background noise while keeping constant the dimension of the droplets. The filter used in all the cases is called "Smooth filter", chosen because it gave the best results in terms of noise abatement. The tuning of the filter is made manually for every run. After this filtering process, the image obtained is shown in the Figure 4.6.

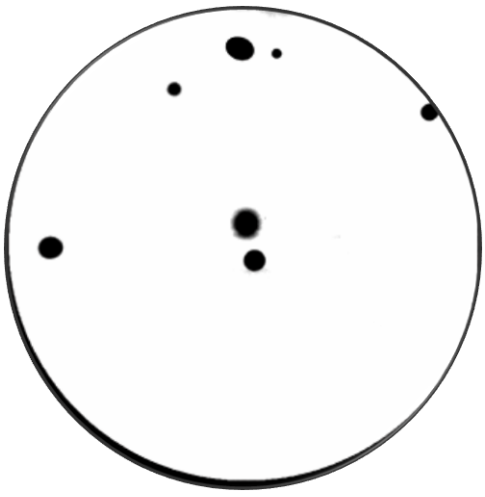

Figure 4.6 A PLIF image after the background correction

Once the image is clearer, the following step is dividing it in two different parts: the black pixels that are the object of interest and the white ones representing the main flow that will be discarded. This step is called segmentation and involves the evaluation of the grey scale.

Noting that the images are 12 bit images, hence the grey values are 4096, an analysis based on the grey scale has been done. This analysis consists of evaluating the number of pixels that have the same grey value for each value of the grey scale. The Figure 4.7 is an histograms plot in which the two peaks represent the objects and the background (it is shown only the interesting part of the chart).

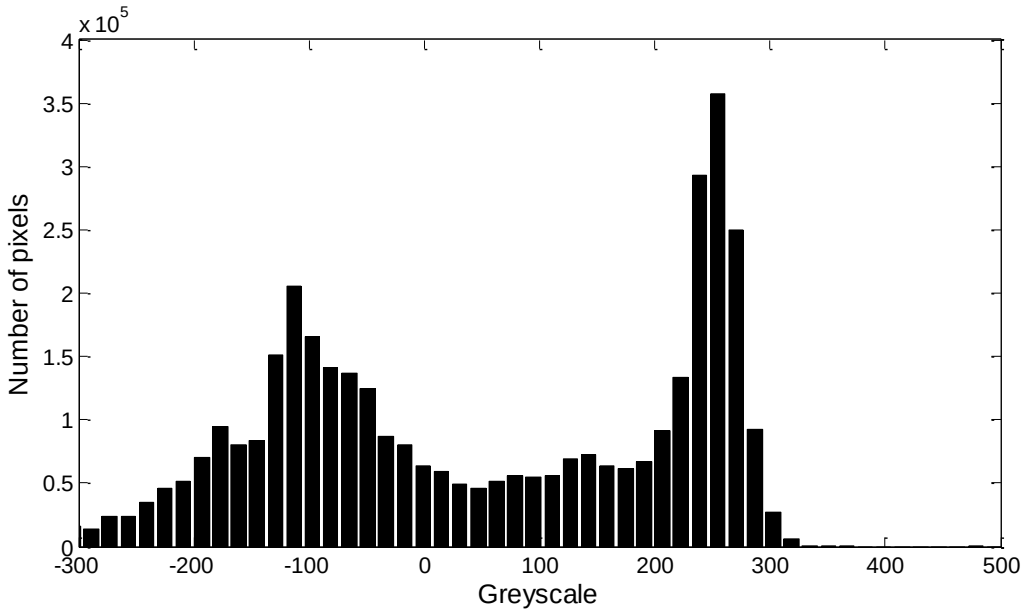

Figure 4.7 Example of greyscale histograms for the threshold evaluation

The representation offered by the program displays negative values that correspond to the dark pixels and positive values that represent lighter colours.

From the plot in Figure 4.7 one needs to choose a value for separating the black values that represent the dark spots (the droplets) from the white pixels that

correspond to the water flow. After the choice of this parameter, all the pixels with a lower grey value will be considered as part of the oil phase, while the lighter will be considered as part of the water phase.

In general, for all the images, the threshold has been found to be close to a value of 100. The segmentation result is a binary image (logical image, containing values of "true" and "false", coded as 1 and 0), with ones at the pixels that belong to the oil phase. This image is displayed in red and black to emphasize that it is a binary image rather than a grey-value image with only two different grey values (Figure 4.8).

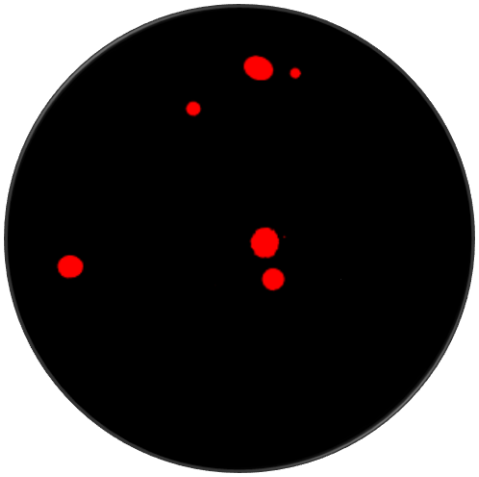

Figure 4.8 Binary image after the segmentation

In this transition, the drops in contact with the wall are discarded, because they could affect the final measurement seen the difficulty to distinguish their border that confuses with the wall. In the reported example it is possible to notice that in the Figure 4.6 the drop on the top-right corner is absent in the Figure 4.8.

The final step, before the actual measurements, it is labelling the drops. Each drop is recognized and named one by one. The labelled final image is displayed in the Figure 4.9.

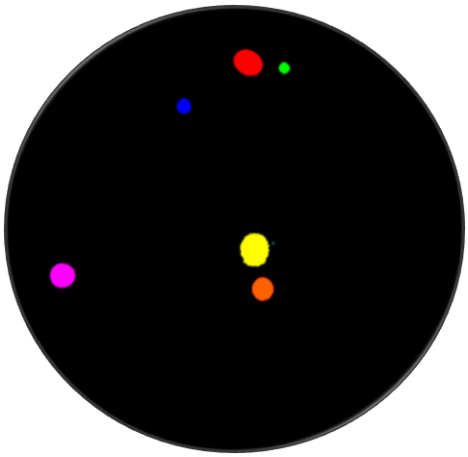

Figure 4.9 Labelled image

Once the drops are selected, the system calculates for each one the main dimensions: perimeter, area and diameter. In this work the last parameter has been taken in consideration.

The high number of images and droplets posed the problem of saving the data: saving every diameter one by one would have required a great deal of memory. This problem has been solved dividing the range of possible dimensions (10 μm – 3 mm) in a number (26 in the present case) of discrete intervals. Thus, the result of the analysis was a matrix that counted how many drops diameter were included in each interval.

In the Figure 4.10 a recapitulation of the processing steps.

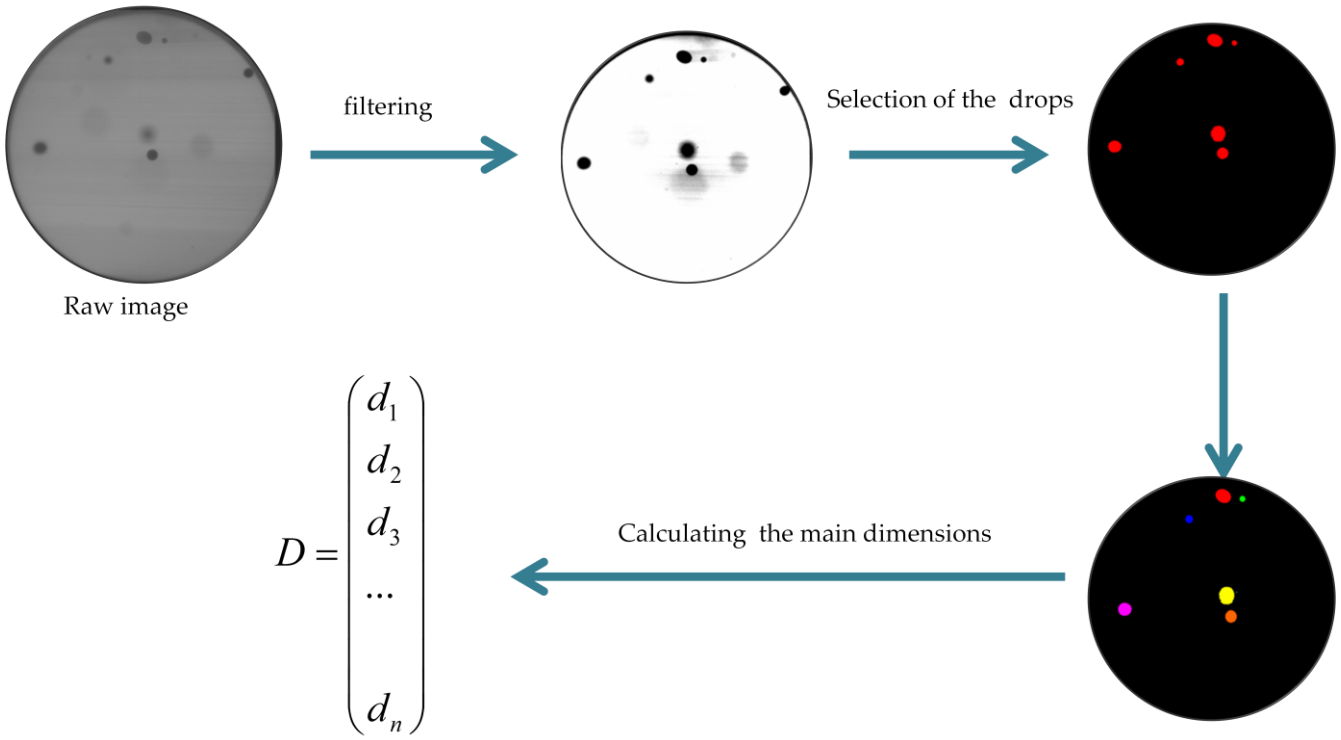

Figure 4.10 Summary of the Image processing

This analysis was repeated for 500 images for 7-10 different velocity and 5 configurations (6-12 SMX+ and KM and the empty pipe). A fast calculation states that 20000-25000 images are processed in total. In the Figure 4.11 images for different runs are shown.

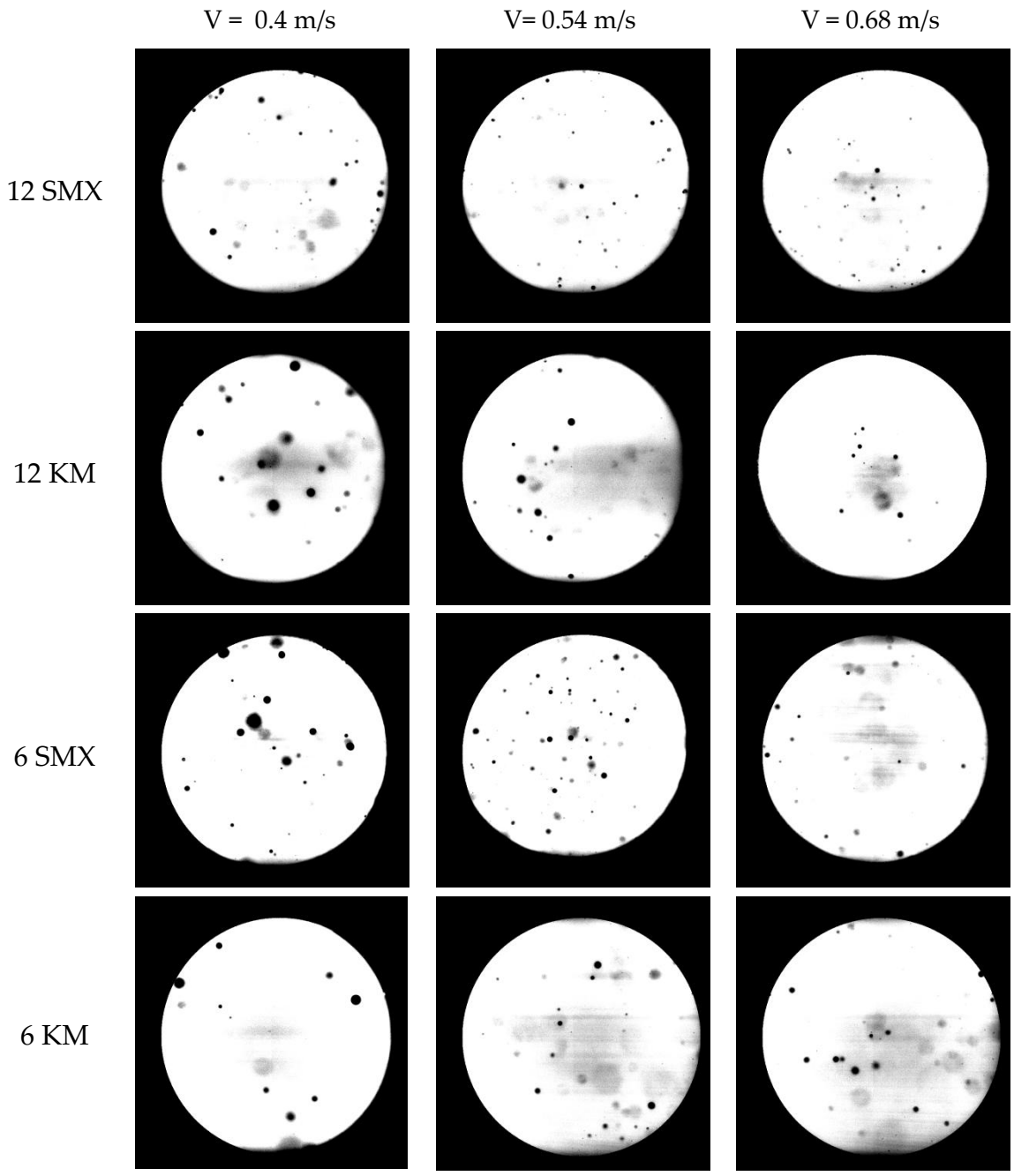

Figure 4.11 Filtered images for different runs

The processing phase has been conducted trying to find the best parameter for each run, but the quality of the final image has been found to be directly connected to the experimental shot. It is fundamental to make the focus plan of the camera coincide with the incidence plan of the laser sheet. This shrewdness

guarantees the quality of the images. A limit of the method is due to the shadows caused by the first drops hit by the laser sheet. Since the laser ray comes from the left side of the images, it is possible to notice in some pictures in the figure above, that some images have grey zones on the right part of the section. This problem has been overcome in this case thanks to the histograms greyscale tools, but it could be difficult to avoid it if the dispersed volume fraction is raised and the density of the droplets increase.

In the present case the reliability of the results has been verified as explained in the next paragraph.

4.3.2 Drop Size Distribution (DSD)

The matrixes resulting from the image processing have been processed accordingly to Equation 2-21 to obtain the DSD in terms of volume frequency. A typical plot is displayed in Figure 4.12.

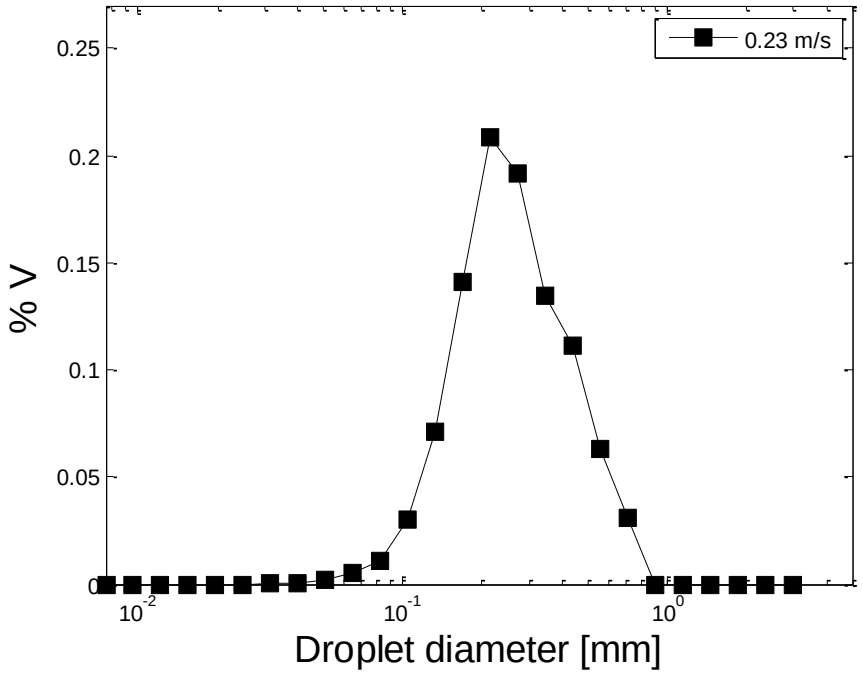

Figure 4.12 DSD for Sulzer SMX+ 12 elements and superficial velocity of 0.23 m/s

To evaluate the repeatability and the consistence of the method, in the next Figure 4.13 a series of DSD plots are displayed. These plots represent the DSD, changing the number of images processed: 100, 200, 300 and 500. Different velocities and configurations have been taken as examples, but it has been noticed that the same behaviour results for every run.

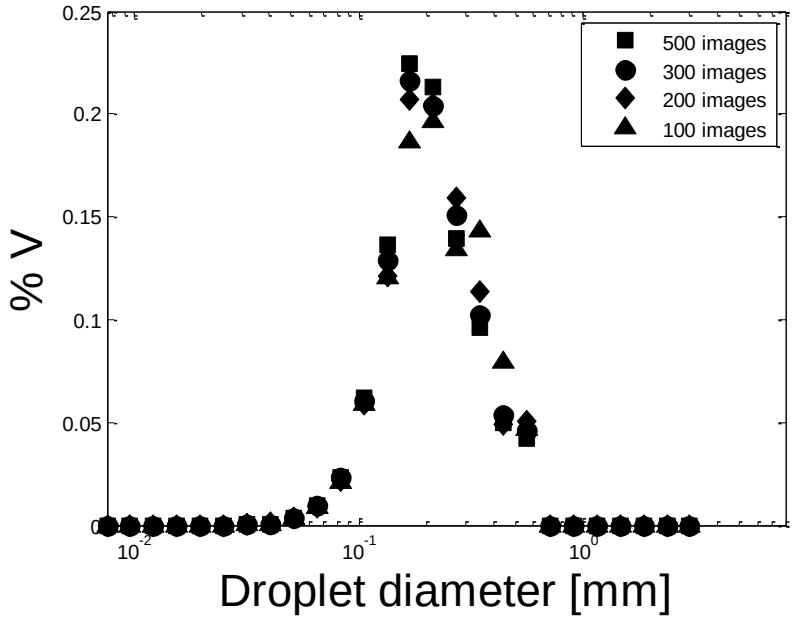

(a)

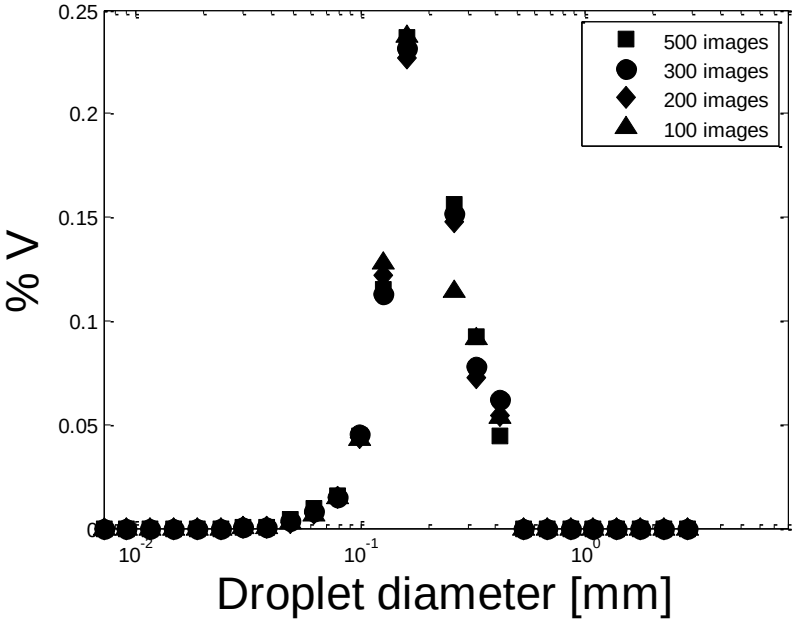

(b)

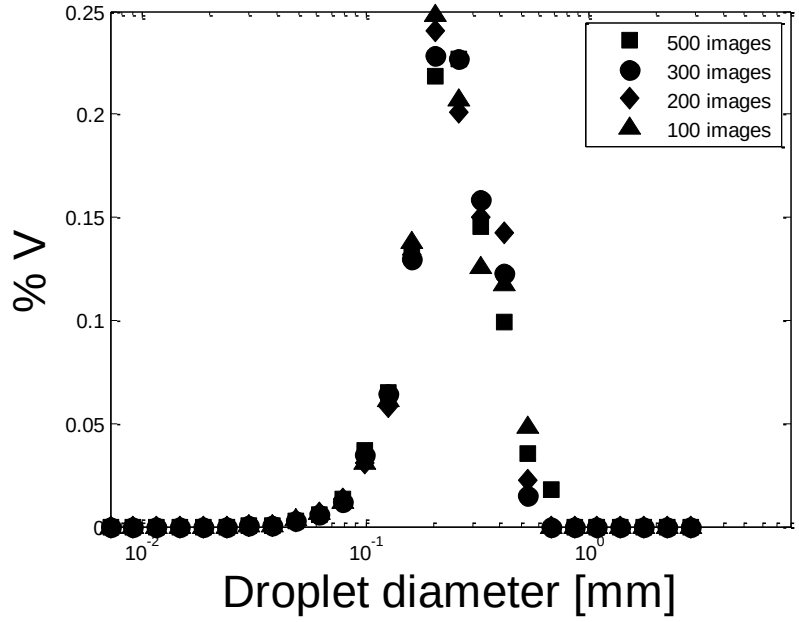

(c)

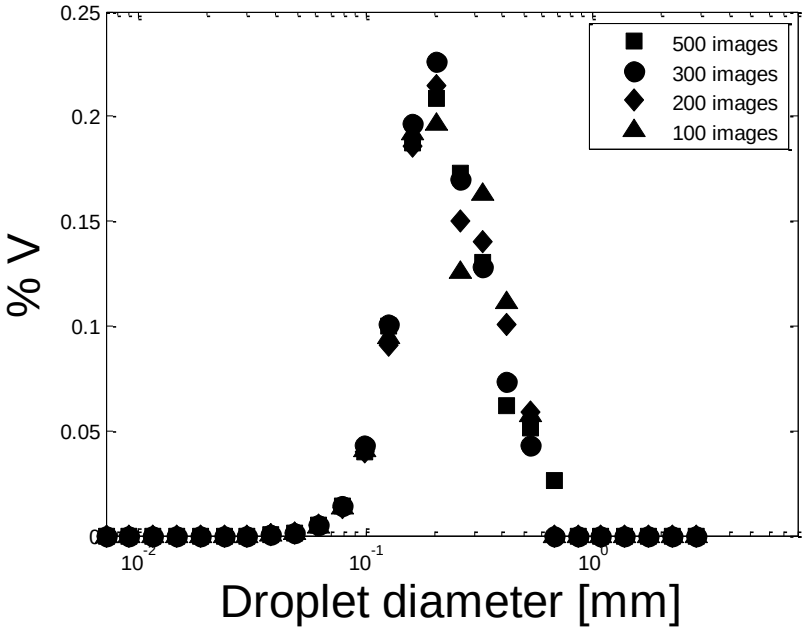

(d)

Figure 4.13 Drop Size Distribution changing the number of processed images for different static mixers and velocities: (a) SMX+ 12 el. v=0.46 m/s; (b) KM 12 el. v= 0.54 m/s; (c) SMX+ 6 el. v= 0.4 m/s; (d) KM 6 el. v=0.62 m/s

Since the shape of the curve does not change much raising the number of pictures processed, it is allowed to assume that the method is reliable and that

the threshold has been reached already with 200 images. However in the following analysis all the images have been processed to have a greater statistical relevance.

The abundance of data available allows us to compare the performance of the static mixer. The literature (Paul 2003) states that in dispersing immiscible liquids the SMX+ has better performance than the KM model. In the next plot (Figure 4.14) the DSD for the four analysed rigs are compared while keeping constant the velocity.

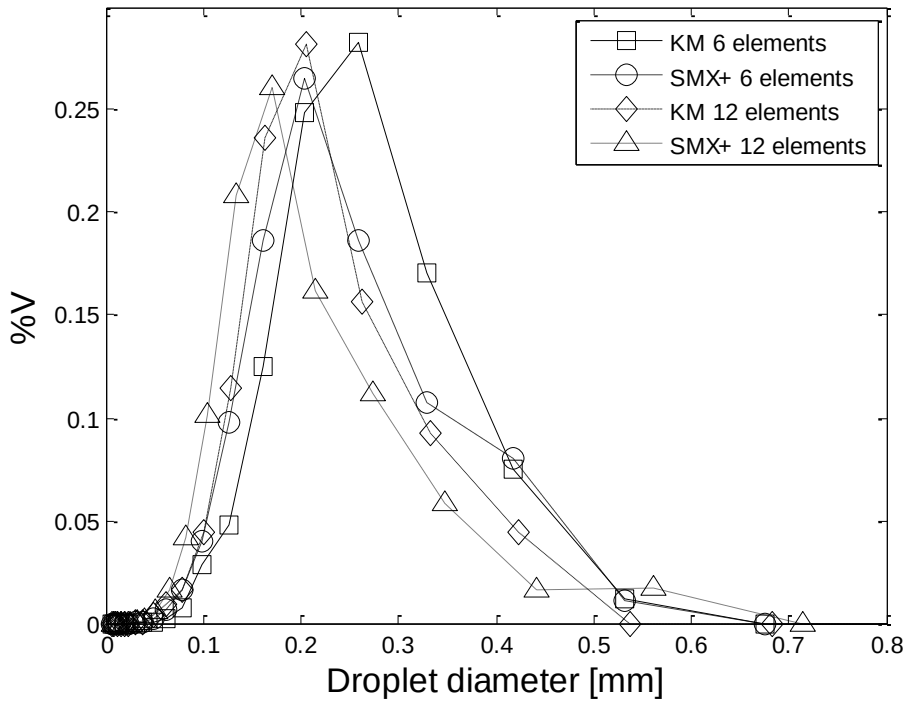

Figure 4.14 Drop size distribution for different sets of Static Mixer for v= 0.46 m/s

As expected, the SMX+ performs better than KM at the same number of elements, and of course raising the number of elements the DSD moves towards smaller diameters. To be aware of the effect that the static mixers give to the emulsification process, enhancing the breakup, it is interesting to illustrate (in

Figure 4.15) the same latter DSD adding the distribution that correspond to the empty pipe without any mixing device within it. (NOTE: it has been necessary to change the axis scale to show the empty pipe DSD).

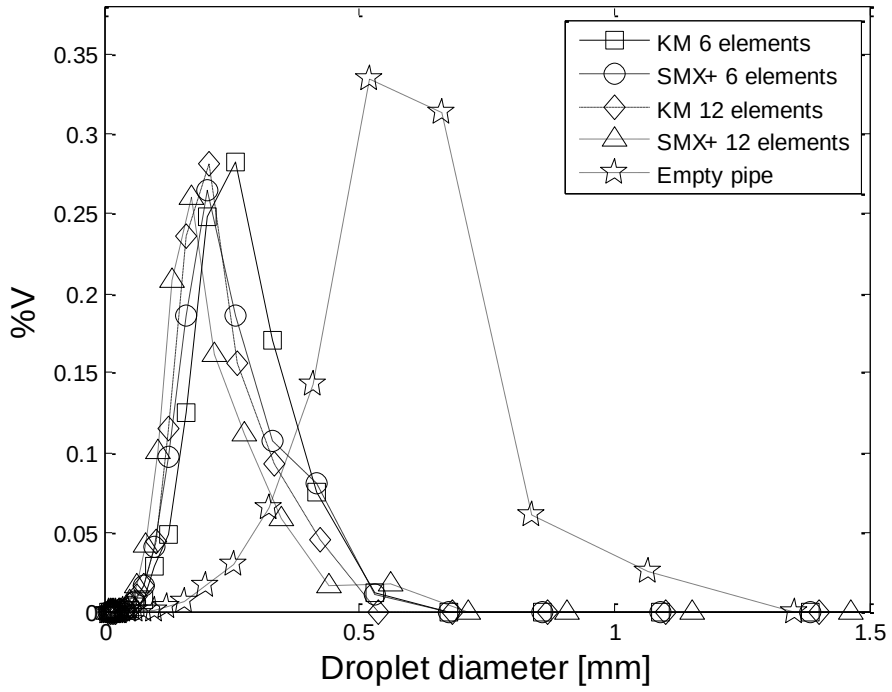

Figure 4.15 Drop size distribution for different sets of Static Mixer and Empty pipe for v= 0.46 m/s

Another parameter to investigate is the performance variation while raising the velocity of the main flow. The system is receiving a bigger amount of energy, so the expectations are about having a improved performance. This is what actually happens in the Figure 4.16 that represents the DSD of the SMX+ with 12 elements, raising the velocity. As explained in the next paragraphs, this statement is true only for low velocities.

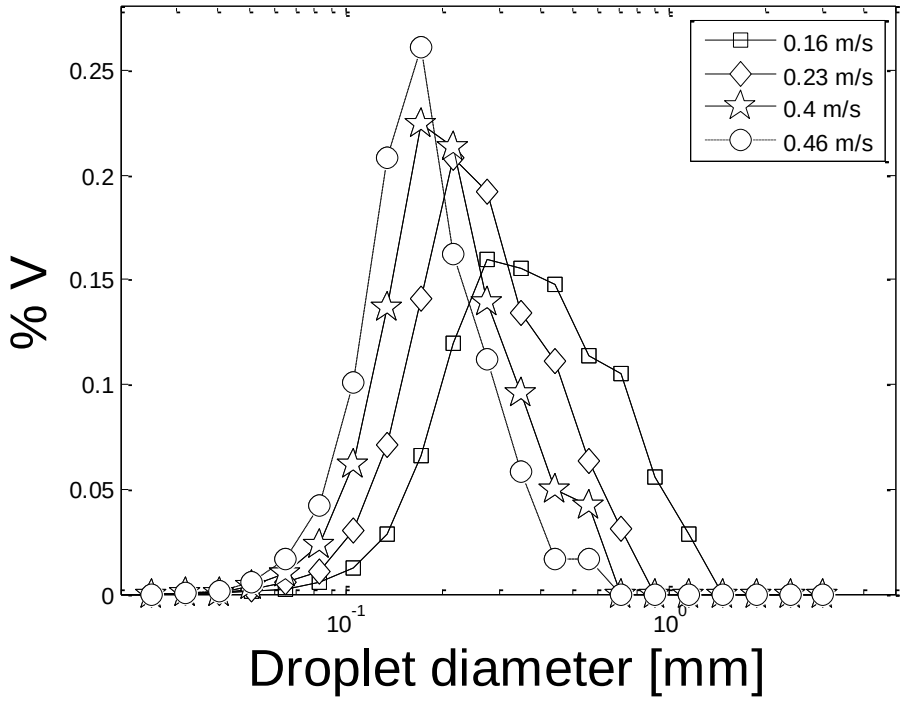

Figure 4.16 Drop size distribution for different superficial velocities using 12 SMX+ elements.

The DSD data can be also approximated and represented with an upper-limit log-normal curve. The parameters necessary for adapting this model to the experimental data are d_{10}, d_{50} and d_{90} as exposed in the Chapter 2 (2-23, 2-24, 2-25 and 2-26). Figure 4.17 shows two examples representing the cumulative drop size distributions, F_v.

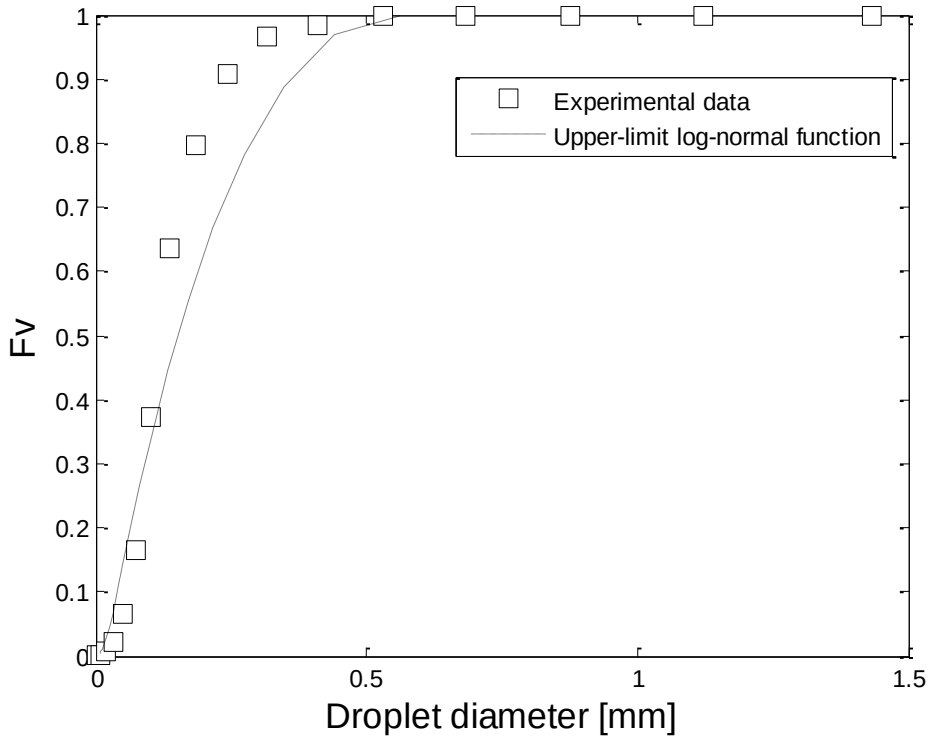

(a)

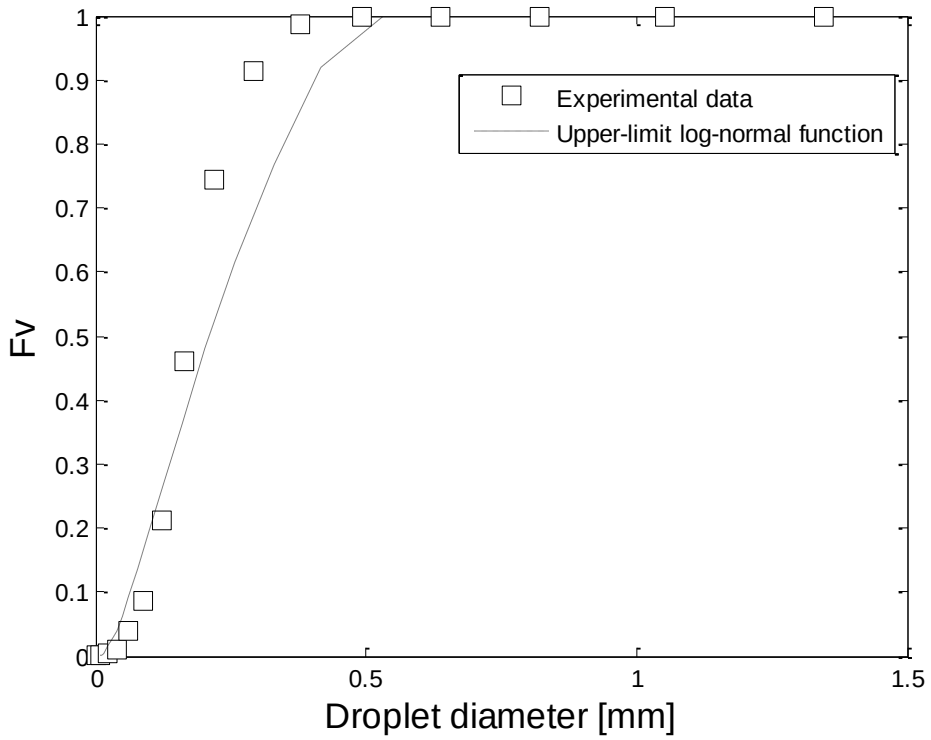

(b)

Figure 4.17 Cumulative volume fraction, comparison between the model and the experimental data, for SMX+ 12 el. and v = 0.23 m/s (a) and 6 KM 6 el. and v = 0.46 m/s

The literature model manages to represent the cumulative volume fraction with a good grade of approximation especially at low velocities, while loses precision at velocities next to 1 m/s. The visible error between the experimental data and the model can be due also to the image processing structure, that does not save each single diameter, but it categorizes the values in discrete intervals (as explained above). For completeness, in Table 4.2 the characteristic diameter necessary for building the curves (in Figure 4.17) are reported.

Table 4.2 Characteristic diameters for calculating the upper limit log-normal distribution curves in Figure 4.16

Case	d_{10} (mm)	d_{50} (mm)	d_{90} (mm)
(a)	0.126	0.225	0.437
(b)	0.130	0.212	0.324

The DSD is often summarized by a single parameter, the Sauter mean diameter (Eq. 2-18). The d_{32} for the different sets and velocity is plotted in the Figure 4.18.

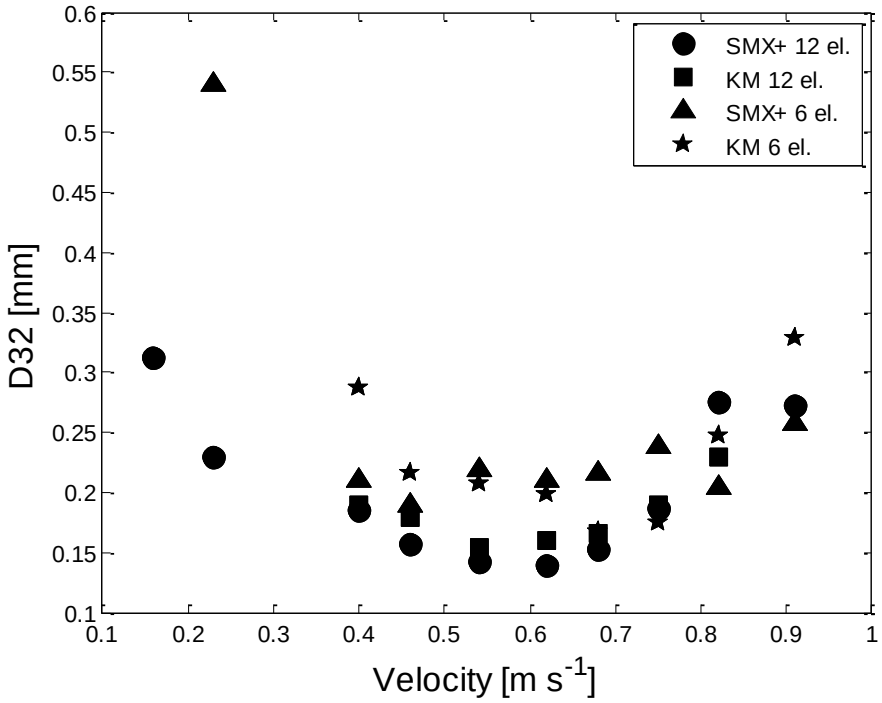

Figure 4.18 Sauter Mean diameter d_{32} for different velocity and sets of static mixer

In this figure it is pointed out once more the better performance of the SMX+ respect to the KM. An unexpected behaviour is also distinguishable for velocity higher than 0.65 m/s. In fact, the Sauter diameter starts to increase despite of the theoretical predictions. This phenomenon is also appreciable in Figure 4.19 where the maximum diameter is plotted versus the average energy dissipation rate in the turbulent flow, accordingly to Equation 2-11. This plot is drawn in logarithmic axis accordingly to literature references.

The average dissipation rate has been calculated for each configuration as:

$$\bar{\varepsilon} = \frac{v \cdot \Delta P}{4 \cdot \rho_w \cdot L_{sm}} \tag{4-1}$$

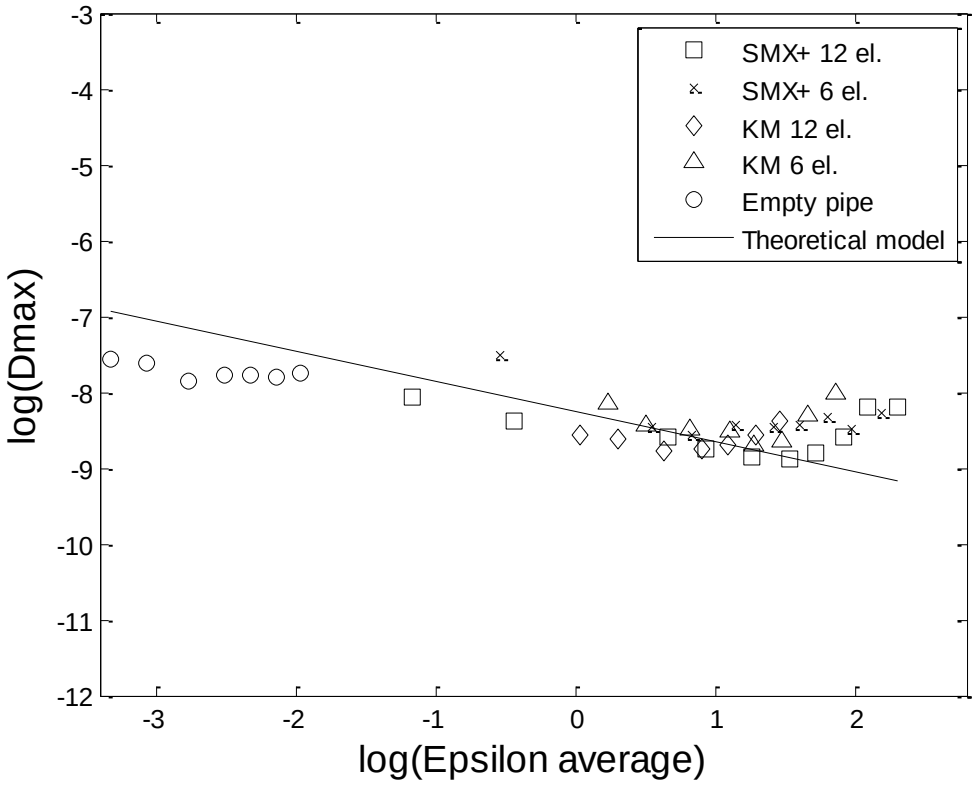

Figure 4.19 Comparison between experimental and theoretical maximum droplets diameter

This last plot is explanatory, the performance of static mixer in blending the two liquids are good and follow the theoretical expectation until a point. After this point, the raise of the turbulence into the systems causes a critical mechanism that affects the performance. The perfect fitting in the left part of the plot is significant but it is also evident the unexpected but gradual deviation of the experimental maximum diameter in the right part of the plot. This phenomenon is resumed and deeper investigated thereafter.

The d_{32} can be also plotted with the initial diameter to appreciate the decrease of the droplets size compared to the initial dimension. The latter foresight is necessary since the initial droplet diameter changes as a function of the main flow velocity, as shown in the Figure 3.7.

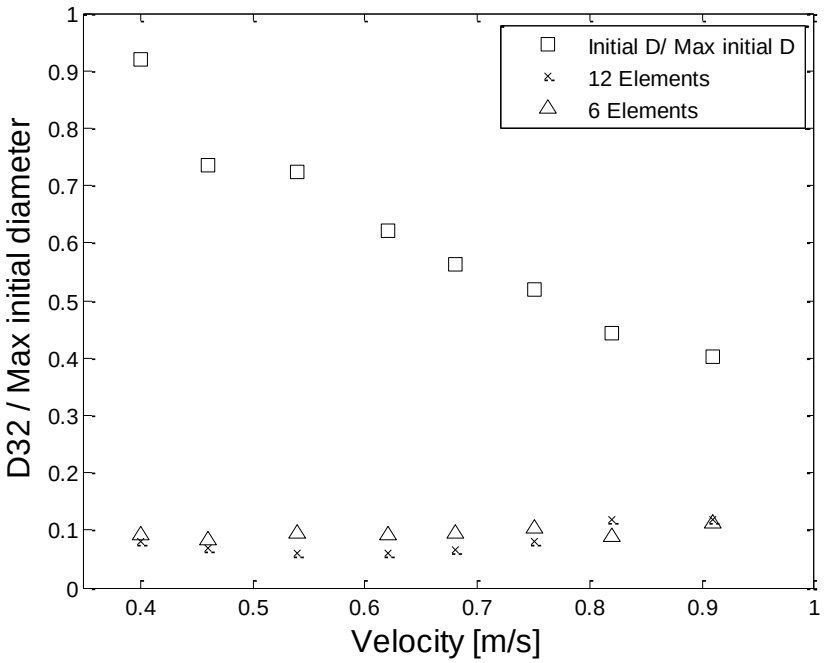

(a)

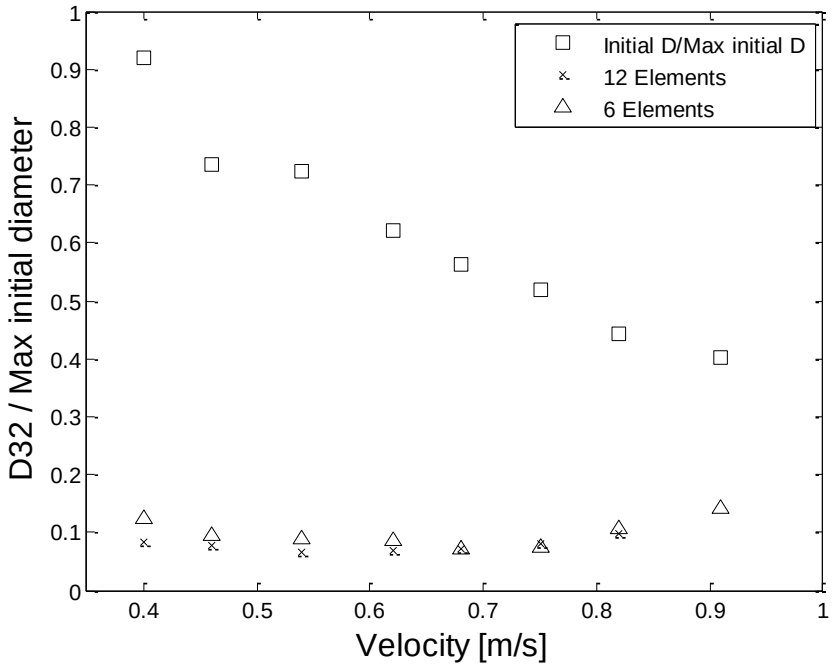

(b)

Figure 4.20 Comparison of d_{32} and initial diameter at different velocities for SMX+ (a) and KM (b)

The data have been normalized dividing by the maximum initial diameter for a more significant representation. The decrease of the initial diameter is appreciable and it is due to the increasing of the turbulence in the main flow. Despite this, the resulting d_{32} seems to not be influenced by this parameter. It is natural to notice that the 12 elements points are always below the 6 elements ones. Of course, they have more mixing elements and the breakup is more efficient even if, to double the elements does not bring even remotely to double the performance.

4.3.3 Instability detection

Two important parameters that are often brought up in these cases are: Weber and Capillary numbers. Both express the relation between the viscous forces and the surface forces:

$$We = \frac{\rho_{oil} \cdot v^2 \cdot d_{32}}{\sigma} \tag{4-2}$$

$$Ca = \frac{\mu_{oil} \cdot v}{\sigma} \tag{4-3}$$

They are usually plotted together in graphs like in Figure 4.21 (Saylor 2012).

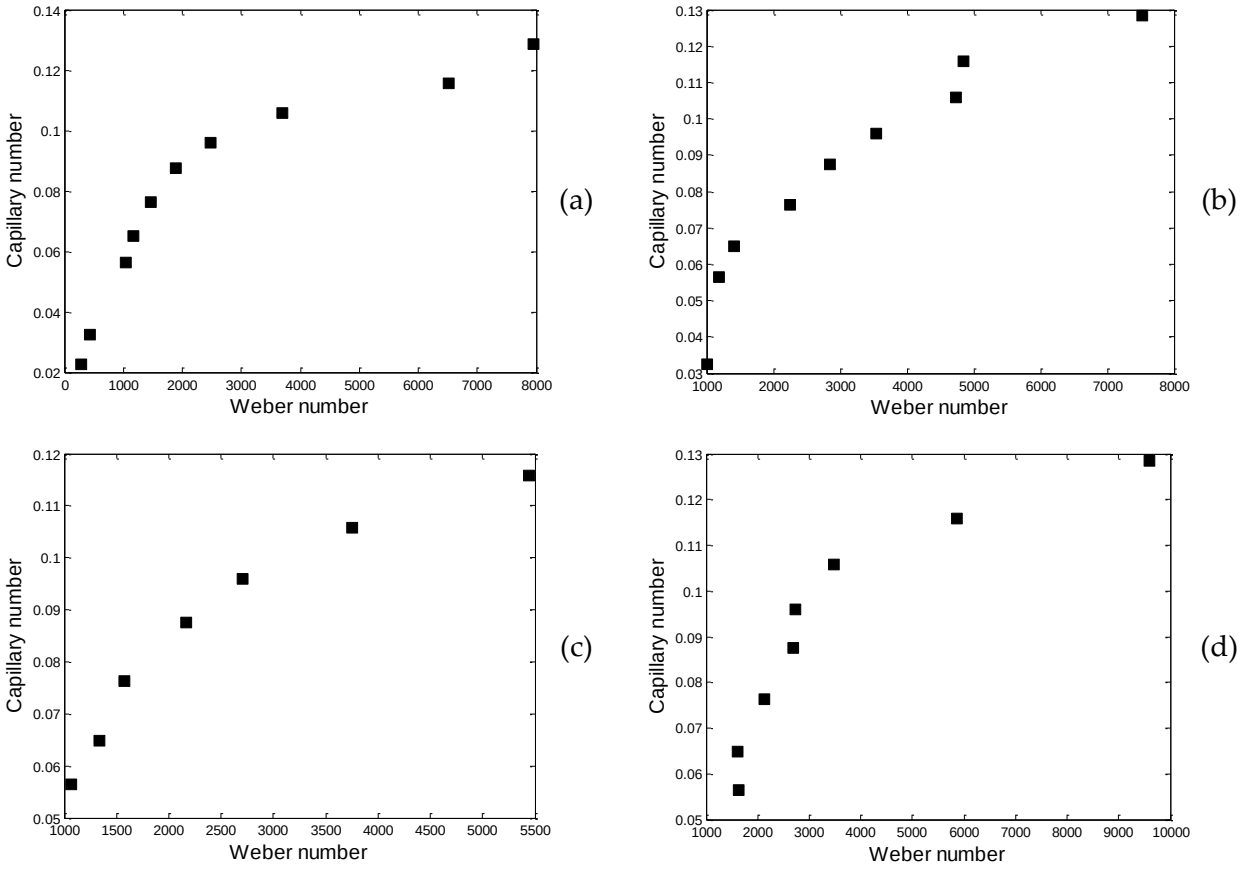

Figure 4.21 Capillary vs. Weber number for SMX+ 12 el. (a), KM 12 el. (b), SMX+ 6 el. (c) and KM 6 el.

The plots in this case are not helpful in detecting the instability mentioned above. It is only visible that increasing the Weber number also the Capillary number increases that it was well-known before considering that those two parameters contains the velocity that is the only variable changing.

Before going deeply into the discussion about the noticed instability for high primary flow rates it is useful briefly analyzing the following Figure 4.22. It compares the DSD at different velocities of the primary flow, for the various settings.

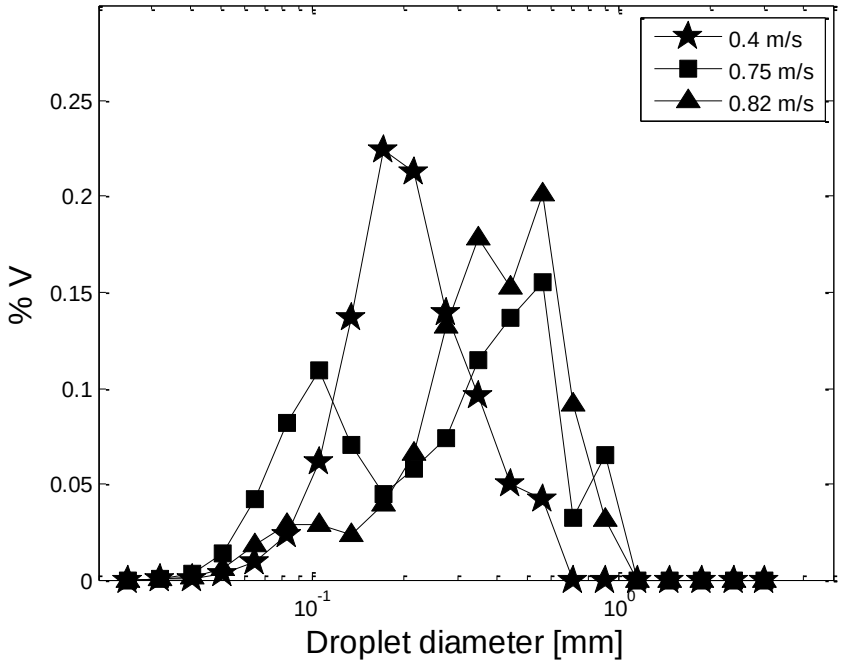

(a)

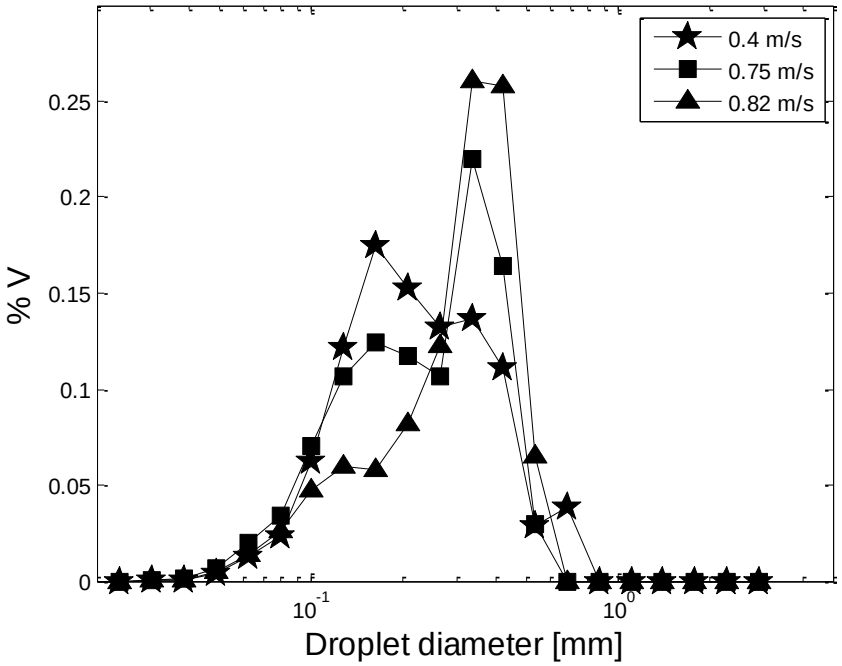

(b)

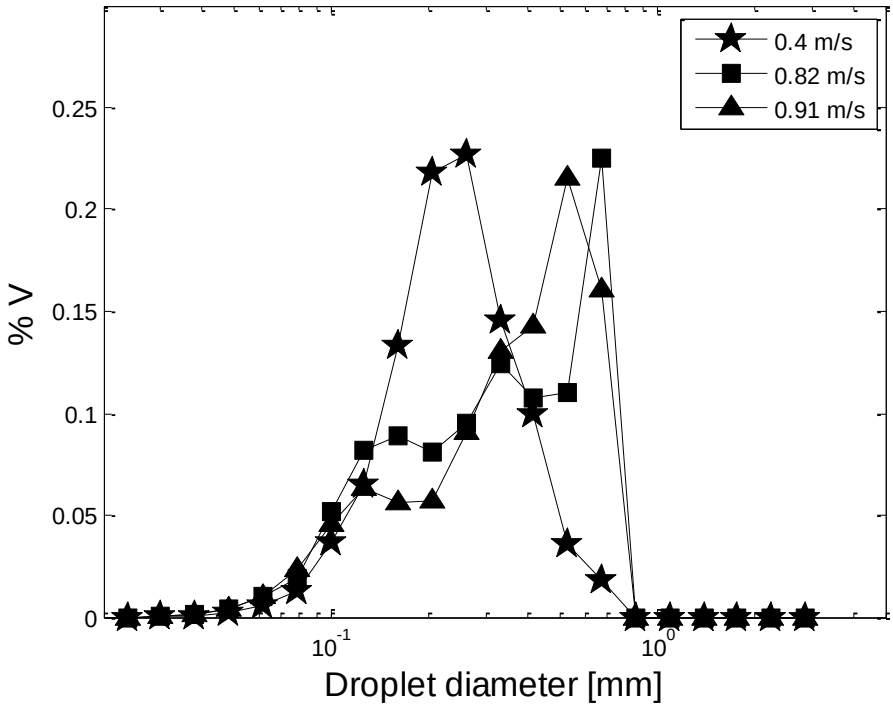

(c)

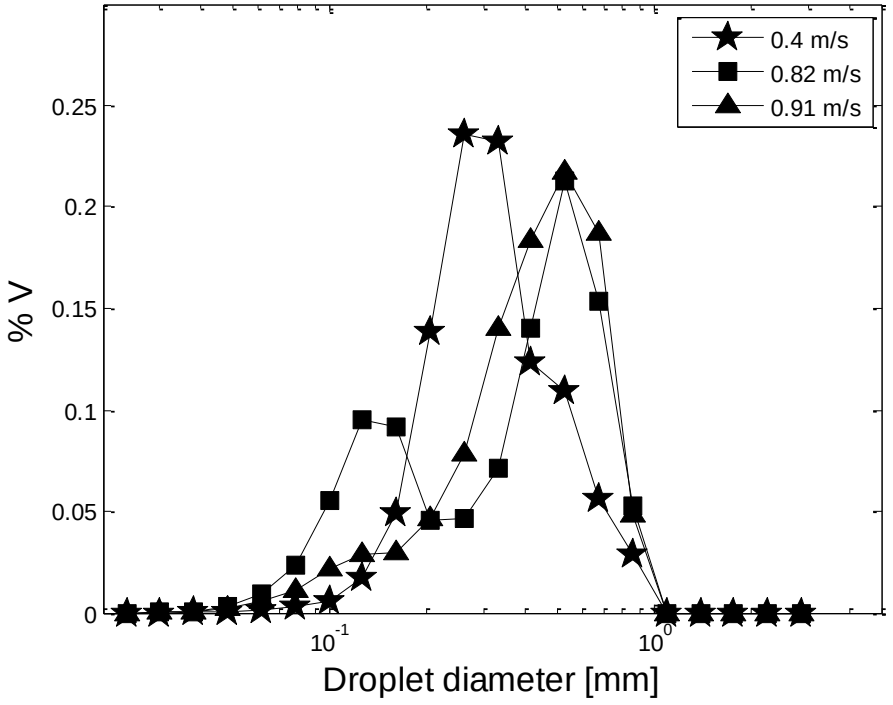

(d)

Figure 4.22 DSD comparison at low and high velocities for SMX+ 12 el. (a), KM 12 el. (b), SMX+ 6 el. (c) and KM 6 el.

The affection of the performance is clearly visible in the four charts. As explained in the beginning of the paragraph the expectation was to see the DSD moving towards the left (smaller size) raising the velocity. This happens for certain range of velocities as shown in the Figure 4.15, but after a critical value the above mentioned instability reveals. As a consequence, the DSD shape changes from a Gaussian to a bimodal curve. This curve has two different peaks: one positioned in correspondence of the expected equilibrium value and one in the right part of the chart. The first peak is the one that in thermodynamic equilibrium condition should be achieved, in fact as suggested by the Equation 2-12 and 2-13 the increase of turbulence brings to smaller drop size. But it has been noticed that the instability is too high and a certain number of the drops does not break up properly, not reaching the equilibrium condition and creating the second peak. This one is the unforeseen one and it is positioned between the initial droplet size and the equilibrium peak. The velocity raise makes the latter peak appears and the higher is the velocity, the higher becomes the peak, while the one on the left gradually becomes flat (Figure 4.23).

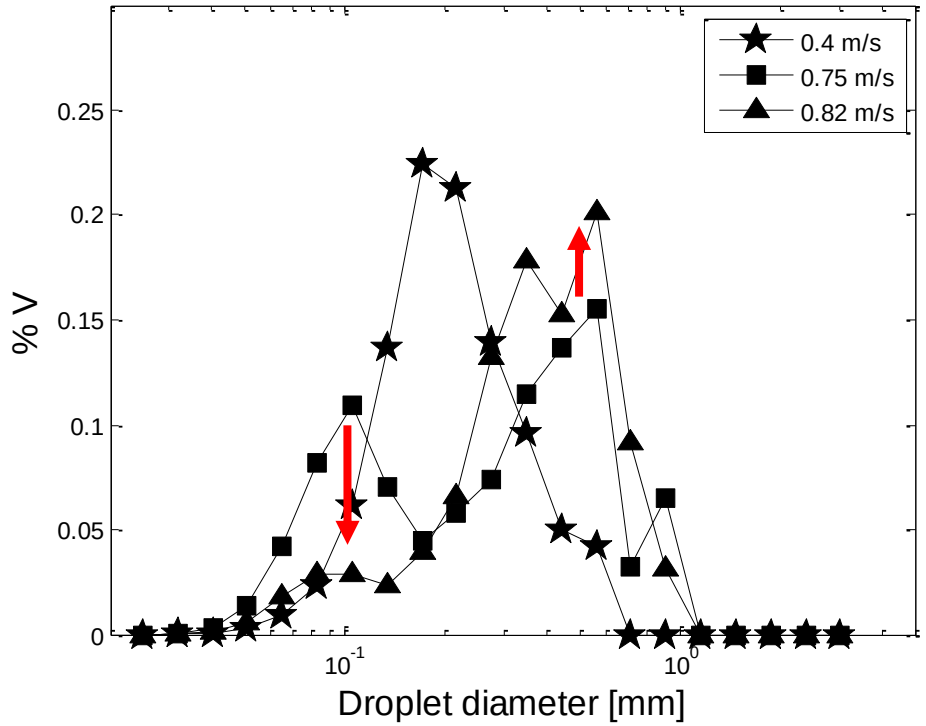

Figure 4.23 DSD for 12 SMX+: peaks modifications caused by the velocity raise

This behaviour has not been reported in the literature before and it has been possible to detect thanks to the applied online *in situ* measurement.

Seen the process gradual revealing, it can be hypothesised that the velocity raise causes a critical event within the system.

Two different motivations can be proposed for explaining the observed phenomenon:

1- The increase of the velocity causes consequently a diminution of the average resident time of the drops in passing across the mixing equipment. The resident time is not the same for every drop because each drop follows a different trajectory so it is more appropriate speaking about a resident time distribution. This distribution is sensitive to change of velocities: when the flow is slow a large number of drops

has a sufficient resident time to reach the equilibrium; but increasing the turbulence the resident time distribution moves towards smaller values and an increasing number of drops has not enough time to achieve the thermodynamic stability.

2- Some droplets bypass the static mixers elements avoiding the mechanical impact on the metal of the static mixers. The drop size corresponding to the instability peak are agreeable with the interstices dimensions of the SMX+ for example and the density ratio between the dispersed and the continuous phase (oil is less dense than water) can justify a less inertia attributable to oil that can slip away avoiding the metal. On the other hand is well-known that the break-up mechanism is caused mostly by the turbulence created by the mixing elements and not by the impacts on them.

Supporting the two possible qualitative explanation, Figure 4.24 shows the empty pipe DSD at high velocity compared with the instable DSD of static mixers, at the same velocity, proposed above. It is interesting to notice that there is a correspondence between the instable peak and the empty pipe Gaussian curve peak. It could be said that for that group of drops the static mixer presence has no effects.

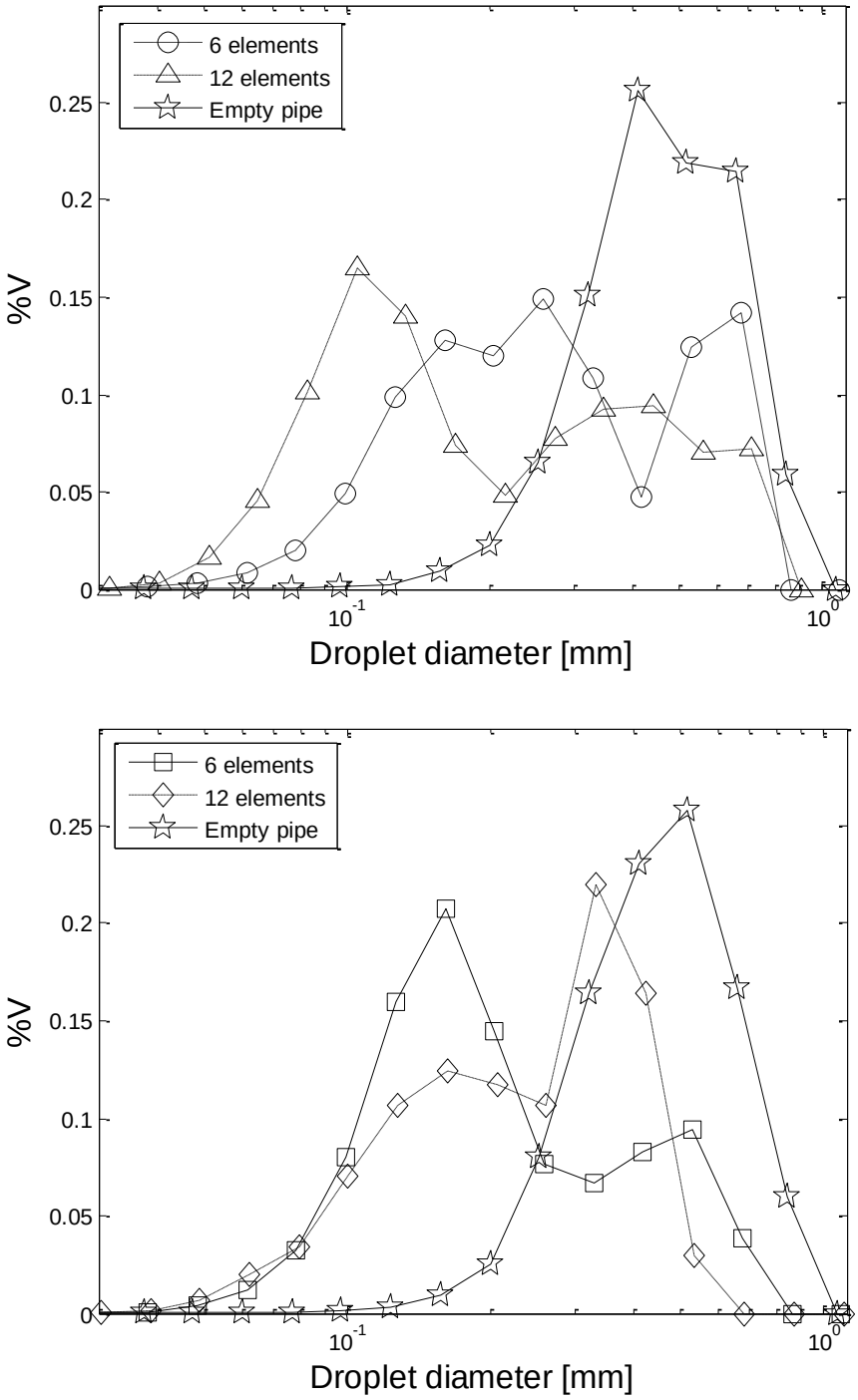

Figure 4.24 Comparison between Static Mixer and Empty Pipe DSD for: SMX+ at v=0.68 m/s (a), KM at v=0.75 m/s (b)

For a better understanding of the phenomena involved in this mechanism, a computational fluid dynamic (CFD) simulation occurs, as well as further experimentations even inverting the dispersed with the continuous phase.

In the next paragraph a study based on the energy input into the system has been developed. The DSD is related to the pumping power input in order to find the optimum and avoiding wastes of energy. In fact, raising the turbulence above a critical point has been noticed to do not improve the mixing performance. This represents clearly a waste of energy and, consequently, an increase in costs of the mixing process.

4.4 Energy model

Facing the problem from an energy point of view requires the recall of the surface energy for a single drop described by Equation 2-13. This energy can be seen as a potential energy enclosed on the surface of the drop: the bigger is the droplet, the higher is the surface energy. Basically it means that a droplet with a big diameter has more energy available for the breakup mechanism, hence it is easier to break a drop with a diameter of 2 mm than a drop with a diameter of 2 μm.

With this assumption, we can look at the mixing equipment with a black box approach, considering the inlet drop and the outlet daughter drops. The initial inlet droplet has a known diameter thanks to the High Speed Camera detections shown in Figure 3.7. Consequently it has a certain initial surface energy. For calculating the outlet drops surface energy one needs to involve the volume fraction $f_v(d_i)$:

$$E_{\text{sup}}^{outlet} = \sum_{n}^{i=1} E_{\text{sup}}(d_i) \cdot f_v(d_i) \tag{4-1}$$

where $f_v(d_i)$ and $E_{\text{sup}}(d_i)$ are, respectively, the volume fraction and the surface energy corresponding to the diameter d_i after the mixing process. In Figure 4.25 a scheme of the black box approach is reported, in terms of mass and energy.

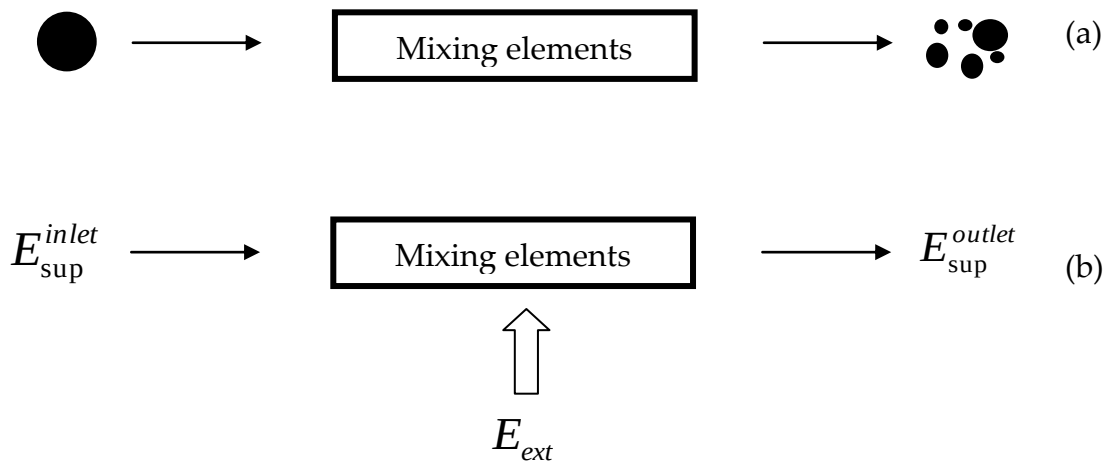

Figure 4.25 Scheme of the balance of mass (a) and energy (b)

In the latter Figure 4.25 (b), apart from the above mentioned surface energy, there is another term, an external energy E_{ext} that corresponds to the energy used by the pump and lost within the system. This pumping energy per unit of mass is calculated as follows:

$$E_{ext} = \frac{\Delta P_{sm}}{\rho} \tag{4-2}$$

Where ΔP_{sm} is the pressure drop within the static mixer and ρ the density of the main flow (water).

As explained in the previous paragraphs, the objective of this work is to correlate the mixing performance with the energy expenditure. The goodness of mixing can be summarised by the Sauter diameter d_{32}, previously introduced. Figure 4.26 puts together this latter parameter with the external energy input per unit of mass.

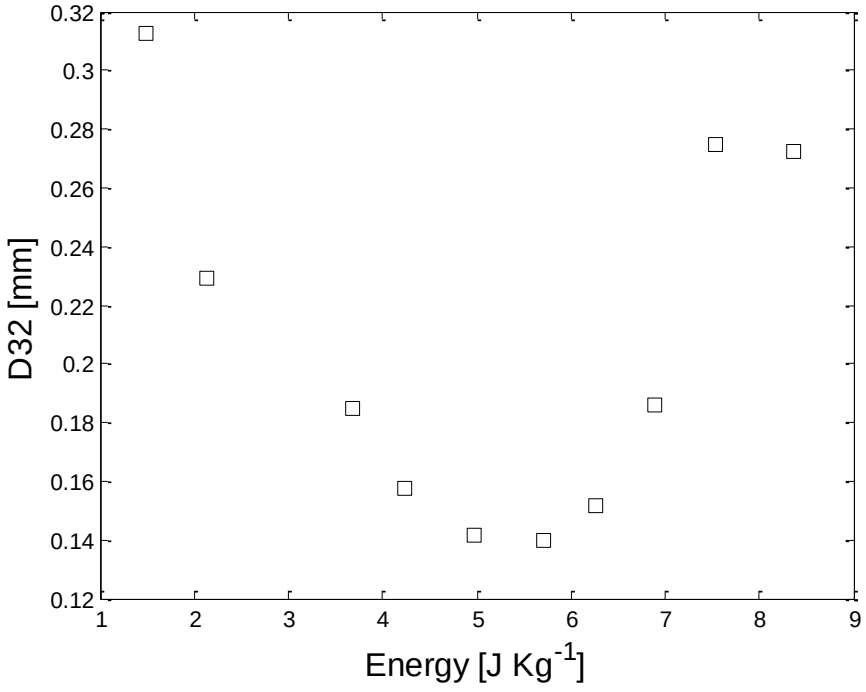

(a)

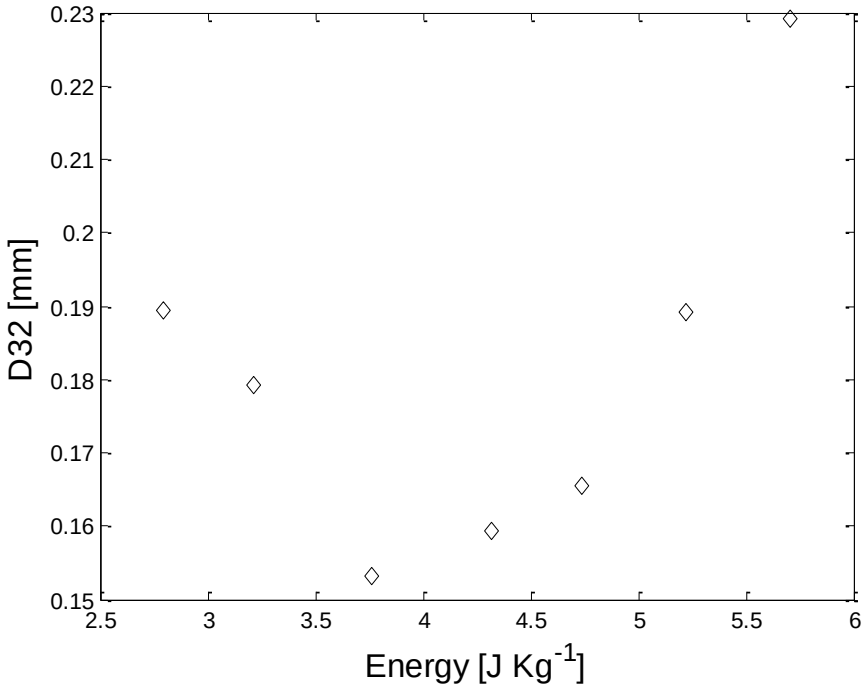
D32 [mm]
Energy [J Kg-1]
0.23
0.22
0.21
0.2
0.19
0.18
0.17
0.16
0.15
2.5
3
3.5
4
4.5
5
5.5
6

(b)

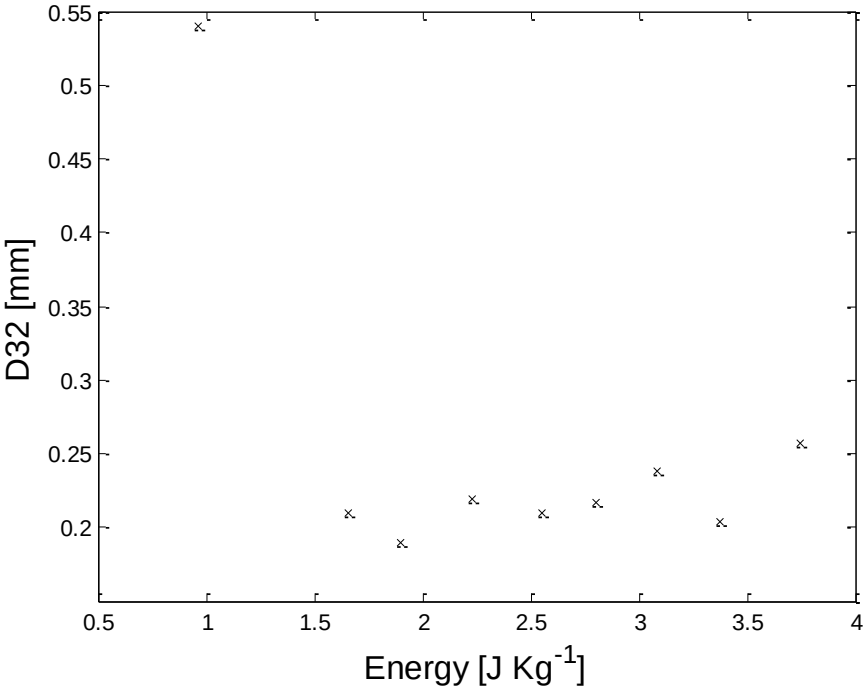
D32 [mm]
Energy [J Kg-1]
0.55
0.5
0.45
0.4
0.35
0.3
0.25
0.2
0.5
1
1.5
2
2.5
3
3.5
4

(c)

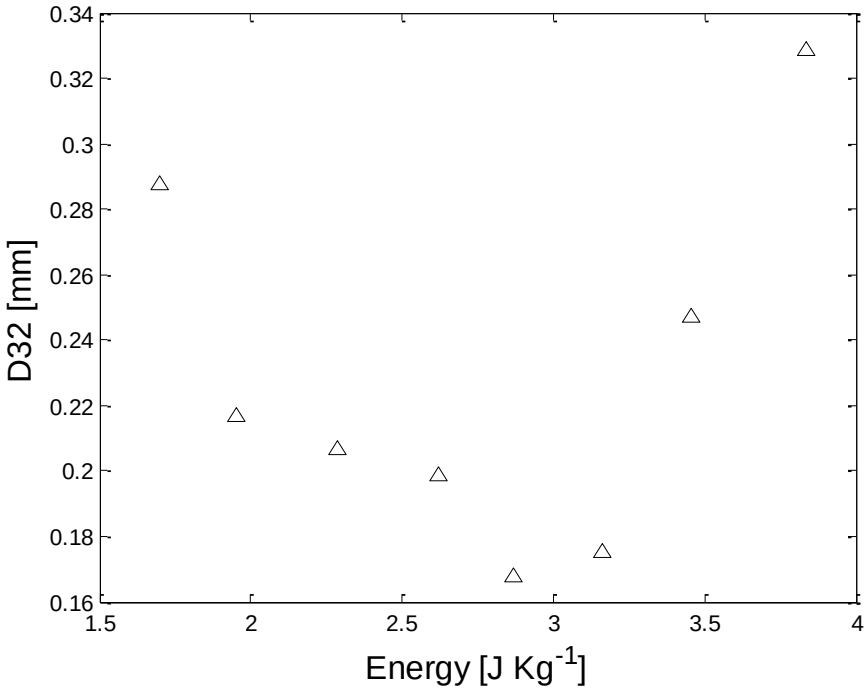

(d)

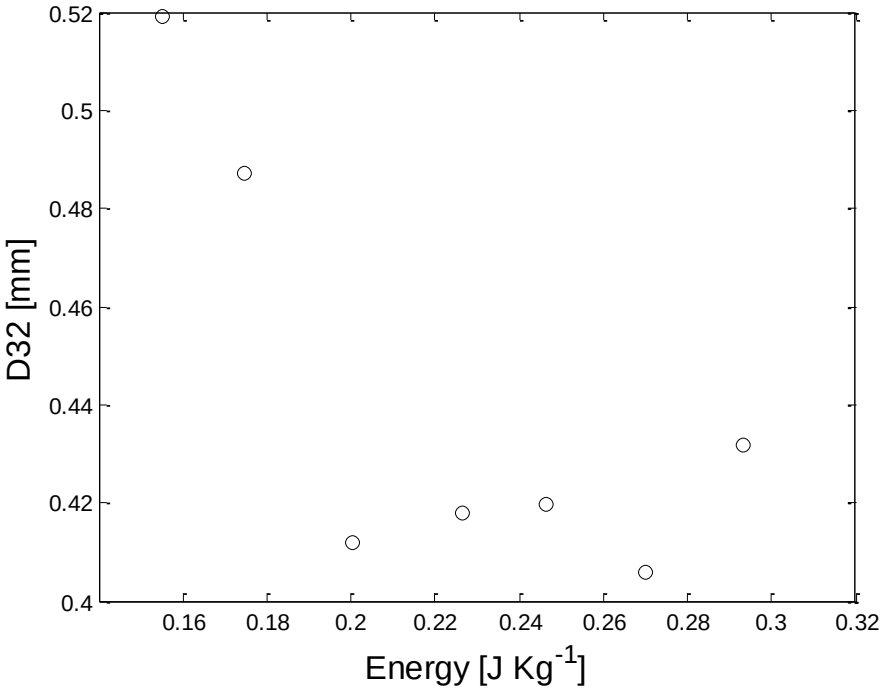

(e)

Figure 4.26 d_{32} trend in relation with the energy input into the system for 12 el. SMX+ (a), 12 el. KM (b), 6 el. SMX+ (c), 6 el. KM (d) and empty pipe (e)

These curves trace the same trend observed in the Figure 4.17 where the d_{32} was plotted versus the velocity of the main flow. This is obvious, seen that the pressure drop and the superficial velocity are proportional with a factor of 1,75. It is important to underline that the d_{32} is a parameter that does not give the right relevance to the bimodal distribution. In fact, the d_{32} is a typical characterizing factor for describing Gaussian curves. Noting this, for a qualitative analysis these plots can anyway give an idea of the critical event that is happening inside the static mixer.

Continuing in this qualitative discussion, even more important than the energy, in this case, is the power input. In fact, the time, in which the energy is dissipated, is a crucial factor, because it is directly related to the resident time that the fluids spend in crossing the elements. The power input per unit of mass has been widely used in the next charts and it is defined as:

$$P = \frac{\Delta P_{sm} \cdot v}{\rho \cdot L_{sm}} \tag{4-3}$$

Where, ΔP_{sm} is the pressure drop within the static mixer, ρ the density of the main flow (water), v is the superficial velocity and L_{sm} the characteristic length of the static mixers reported in Table 3.1.

In Figure 4.27 the d_{32} vs. the power input into the system.

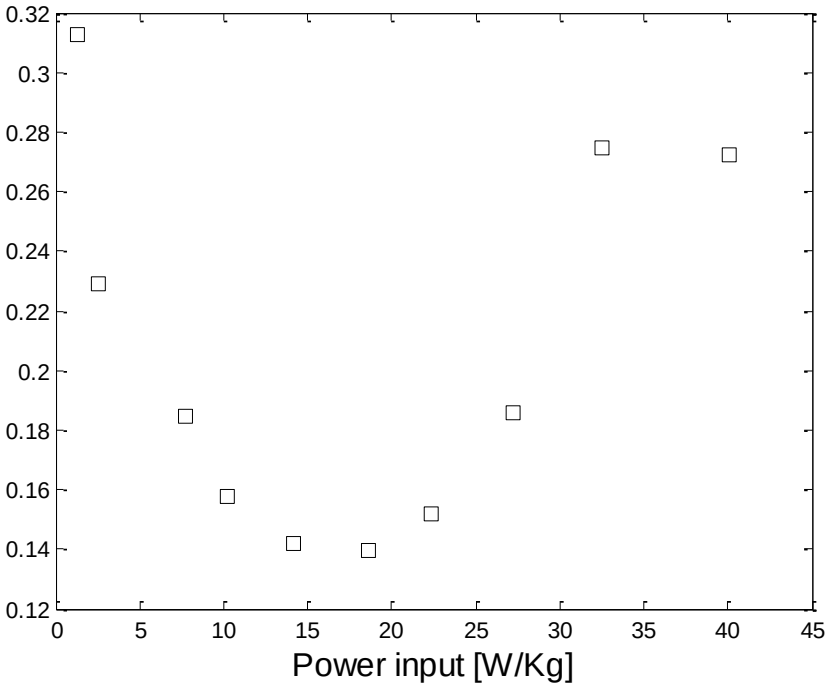
0.32
0.3
0.28
0.26
0.24
0.22
0.2
0.18
0.16
0.14
0.12
0
5
10
15
20
25
30
35
40
45
Power input [W/Kg]

(a)

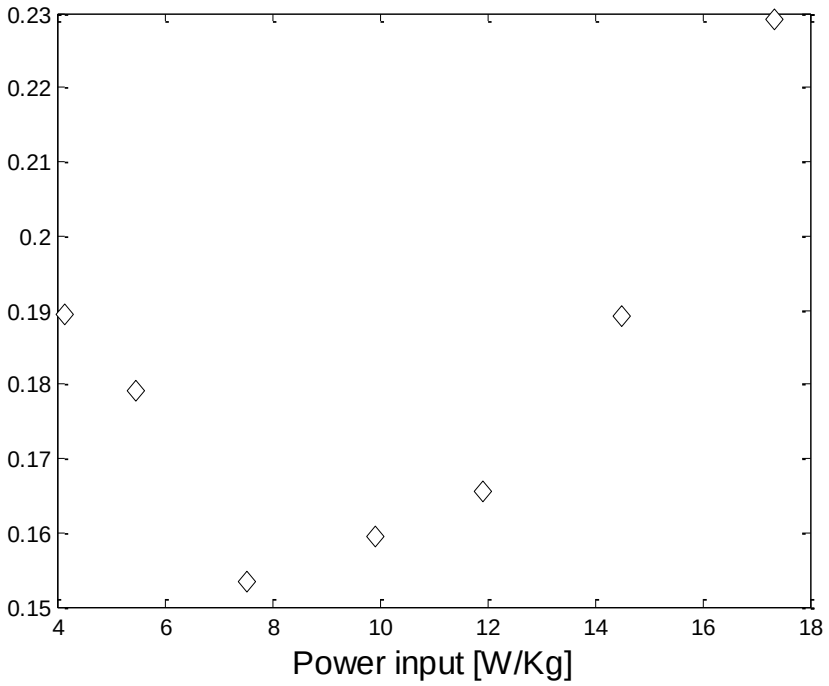
0.23
0.22
0.21
0.2
0.19
0.18
0.17
0.16
0.15
4
6
8
10
12
14
16
18
Power input [W/Kg]

(b)

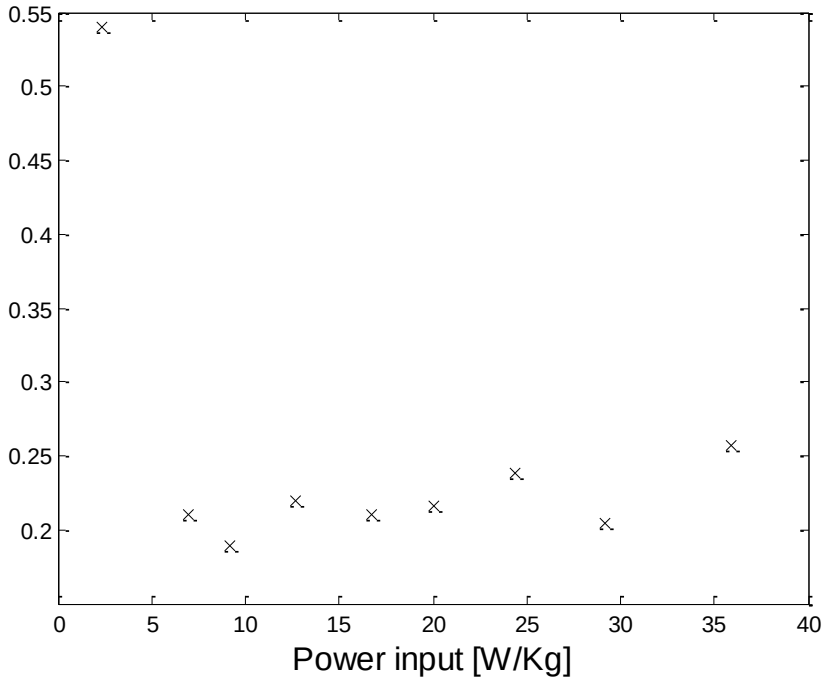
0.55
0.5
0.45
0.4
0.35
0.3
0.25
0.2
0
5
10
15
20
25
30
35
40
Power input [W/Kg]

(c)

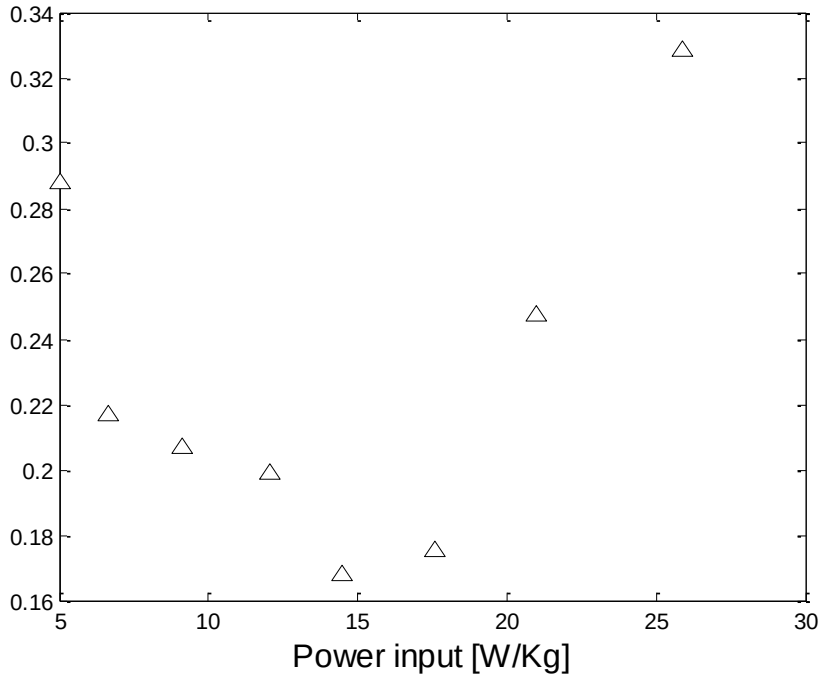
0.34
0.32
0.3
0.28
0.26
0.24
0.22
0.2
0.18
0.16
5
10
15
20
25
30
Power input [W/Kg]

(d)

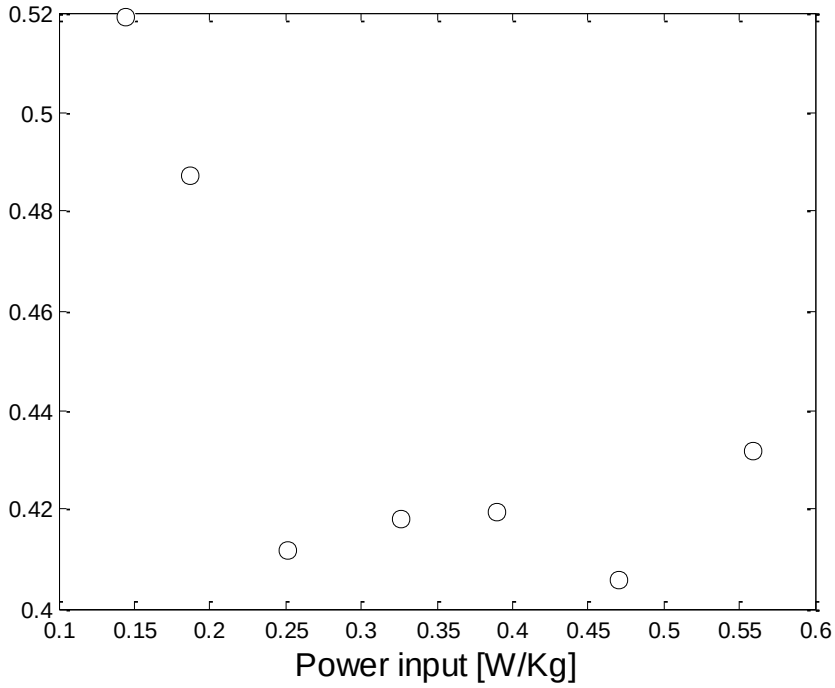

(e)

Figure 4.27 d_{32} trend in relation with the Power input into the system for 12 el. SMX+ (a), 12 el. KM (b), 6 el. SMX+ (c), 6 el. KM (d) and empty pipe (e)

Plotting d_{32} as a function of the power input it results to have the same shape of the charts in Figure 4.26. These latter plots does not give a real and reliable d_{32}, but they can be useful to individuate the breaking point meant as the critical point after which the behaviour of the system starts to deviate from the theoretical model.

More interesting it is involving, in the analysis, the surface energy of the droplets introduced at the beginning of this paragraph. Using this parameter the mixing performance can be seen from an energy point of view. When the initial droplet enters in the first element it has a high initial surface energy, this energy is available for the break-up process. In the following plots (Figure 4.28) it is reported the difference between the inlet surface energy and the outlet surface energy $\Delta E = E_{\text{sup}}^{inlet} - E_{\text{sup}}^{outlet}$ vs. the power input. The idea is

understanding how much of this energy is dissipated and comparing the different configurations at the same superficial velocity. Seen that the velocity influences the initial drops dimension, keeping constant the velocity allows us to consider the initial condition equal for every setting.

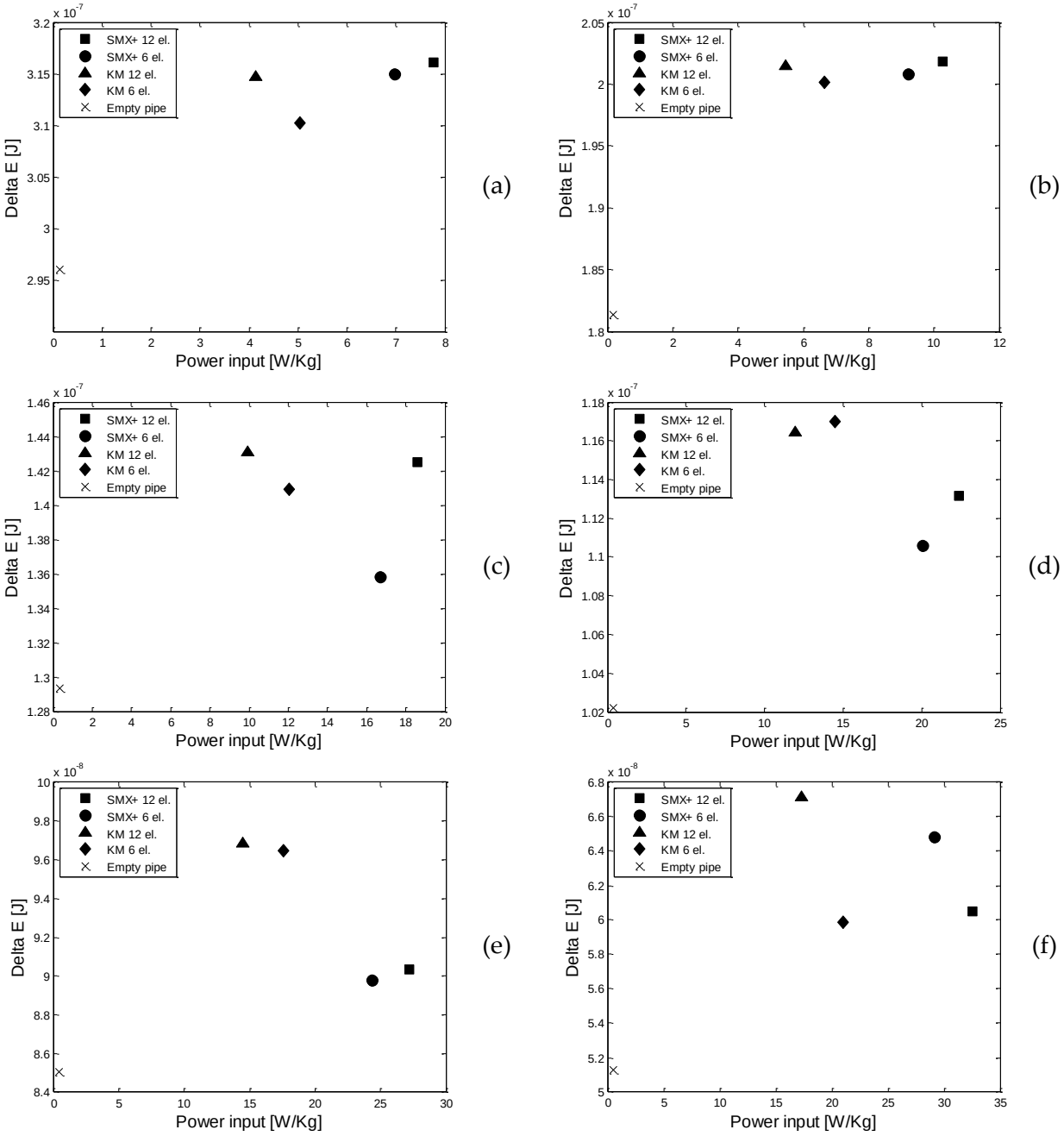

Figure 4.28 Surface energy conversion as a function of the power input for the different static mixer at several superficial velocity: 0.4 m/s (a), 0.46 m/s (b), 0.62 m/s (c), 0.68 m/s (d), 0.75 (e), 0.82 m/s (f)

The range of power involved in the above plots changes and is not possible the use of the same axis without losing accuracy in resolution. The first three charts reproduce expected trends: the 12 elements static mixers result to have higher surface energy conversions than the correspondent 6 elements. At the velocity of 0.68 m/s, and for higher velocities, the energy conversion does not follow the theoretical behaviour anymore and it is impossible to find a predictive model. Figure 4.28 suggests that the critical velocity is between 0.62 and 0.68 m/s.

The surface energy has been found to be a promising variable to investigate. Discussing about it, it is possible to state that, if the emulsification process is happening with high efficiency, the outlet surface energy of the daughters droplets should be low, almost negligible compared to the initial one (reminding that $E_{\sup} \propto d^2$). For this analysis it is useful to introduce a parameter, a kind of yield for evaluating the mixing performance:

$$Y = \frac{E_{surf}^{inlet} - E_{surf}^{outlet}}{E_{surf}^{inlet}} \tag{4-3}$$

The success of the mixing process is high when Y is close to 1. This parameter is defined for taking into account the variation of the initial surface energy E_{surf}^{inlet} with the velocity. In fact, raising the velocity the initial droplet has a lower dimension and consequently a lower E_{surf}^{inlet}; it is important considering this effect to prevent the production of misleading data in output. Y is a significant parameter that can replace the use of d_{32} that as explained before loses meaning when the distribution becomes bimodal. Contrariwise Y takes into

account the distribution and gives meaningful information about droplets breakup.

In Figure 4.29 Y is plotted versus the power input. In each plot a critical power is individuated by the dashed vertical line corresponding to Y = 0.95, an arbitrary value chosen for the comparisons because it corresponds in most of the cases to the critical point. Under this value the DSD deviates from the Gaussian curve.

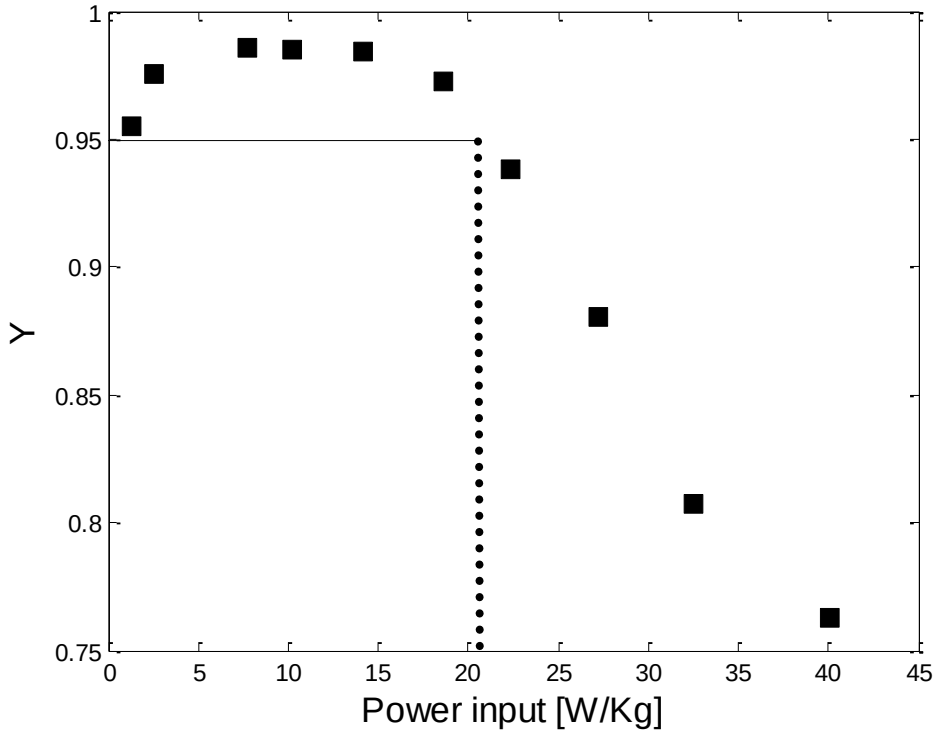

(a)

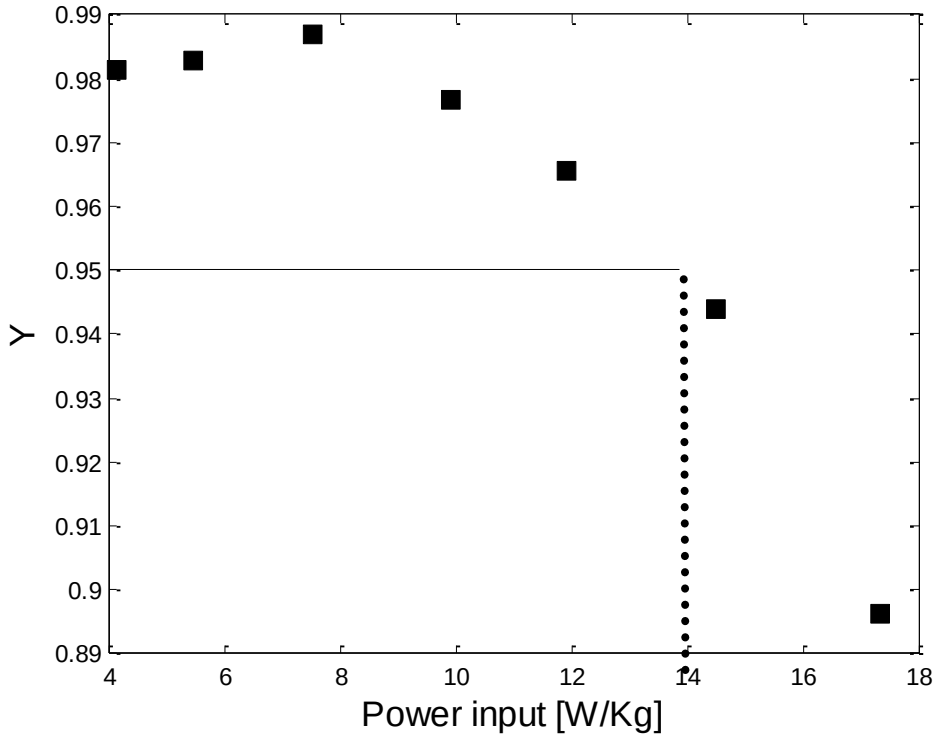
0.99
0.98
0.97
0.96
0.95
0.94
0.93
0.92
0.91
0.9
0.89
Y
4
6
8
10
12
14
16
18
Power input [W/Kg]

(b)

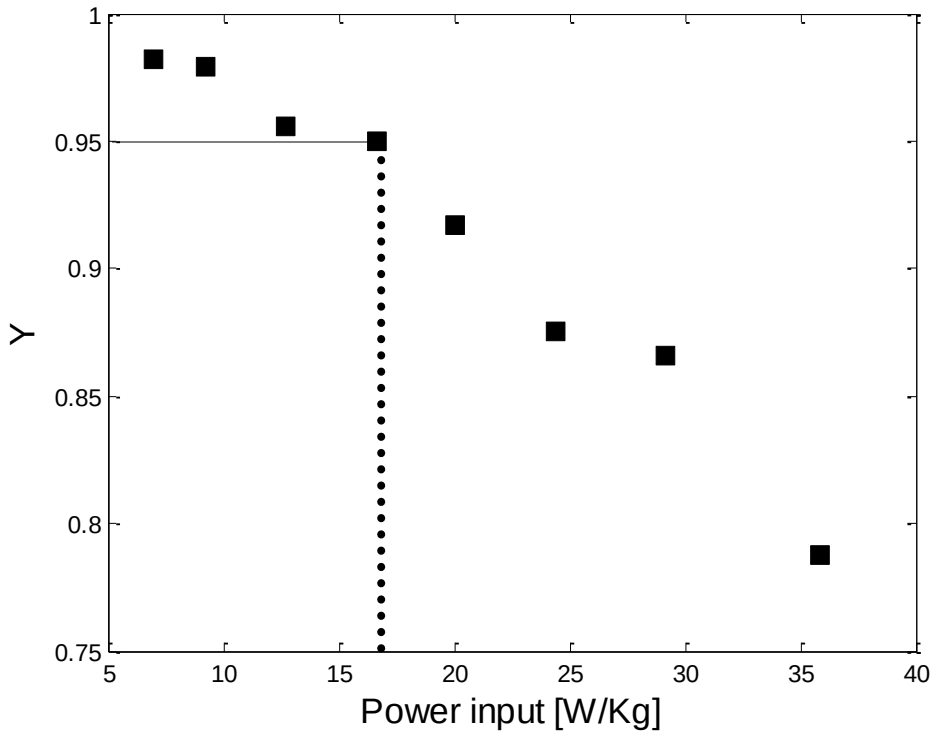
1
0.95
0.9
0.85
0.8
0.75
Y
5
10
15
20
25
30
35
40
Power input [W/Kg]

(c)

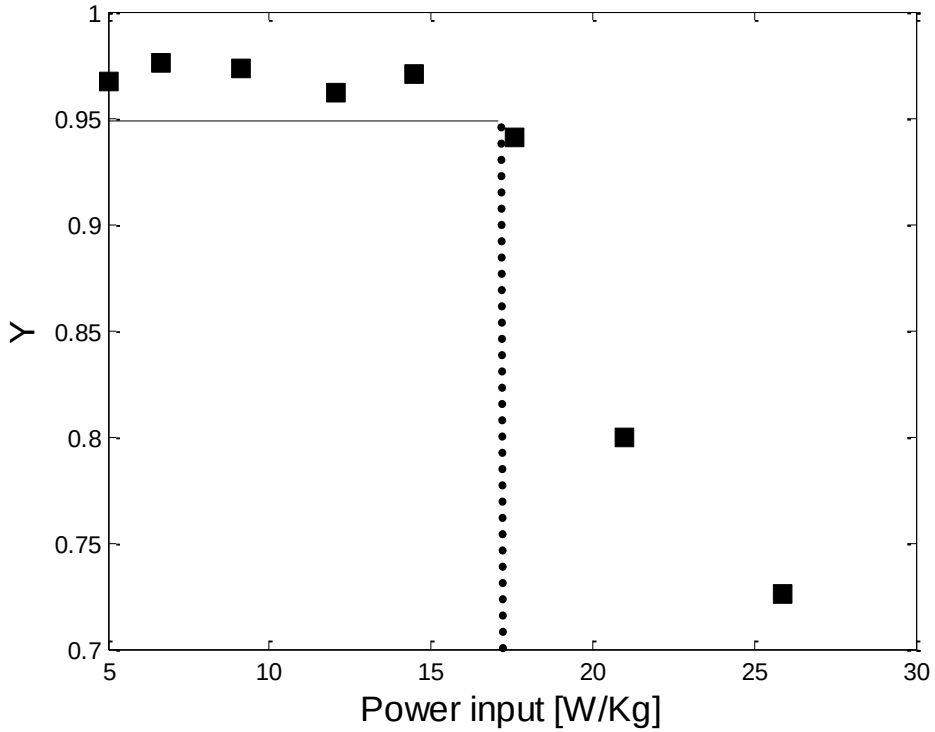

(d)

Figure 4.29 Yield trend as a function of the power input for: SMX+ 12 el. (a), KM 12 el. (b), SMX+ 6 el. (c), KM 6 el. (d)

It is clearly visible in the latter Figure 4.29 that, in each chart, two different zones can be individuated. On the left, Y is close to 1 and this means that the process is happening with high efficiency and the droplets are breaking down properly, reaching very small dimensions as predicted by the correlations in literature. Contrariwise, the right part of the charts shows a decrease of the yield that goes below 0.95 reaching in some cases values of 0.75. The number itself has no high relevance, but this trend, the same for each configuration can provide a useful information: the critical power.

In the plots, the vertical dashed line divides the two zones: the high efficient one on the left and the low efficient one on the right. This parameter can be useful to predict the static mixer performance during the design phase of the process. In particular, it is possible to predict if the fluids can reasonably reach

the equilibrium conditions within the equipment, hence if the final drop size distribution would be in line with the results suggested by the theoretical model. The equilibrium condition is intended as the condition in which the final DSD and d_{32} follow the theoretical model.

Using all the information obtained so far, and particularly the critical power observed in the last figure, a mapping of the process has been drawn. It is shown in the Figure 4.30 and it correlates the power input, the energy input that express the pumping expenditure and the Sauter mean diameter d_{32} and Y that evaluate the mixing process.

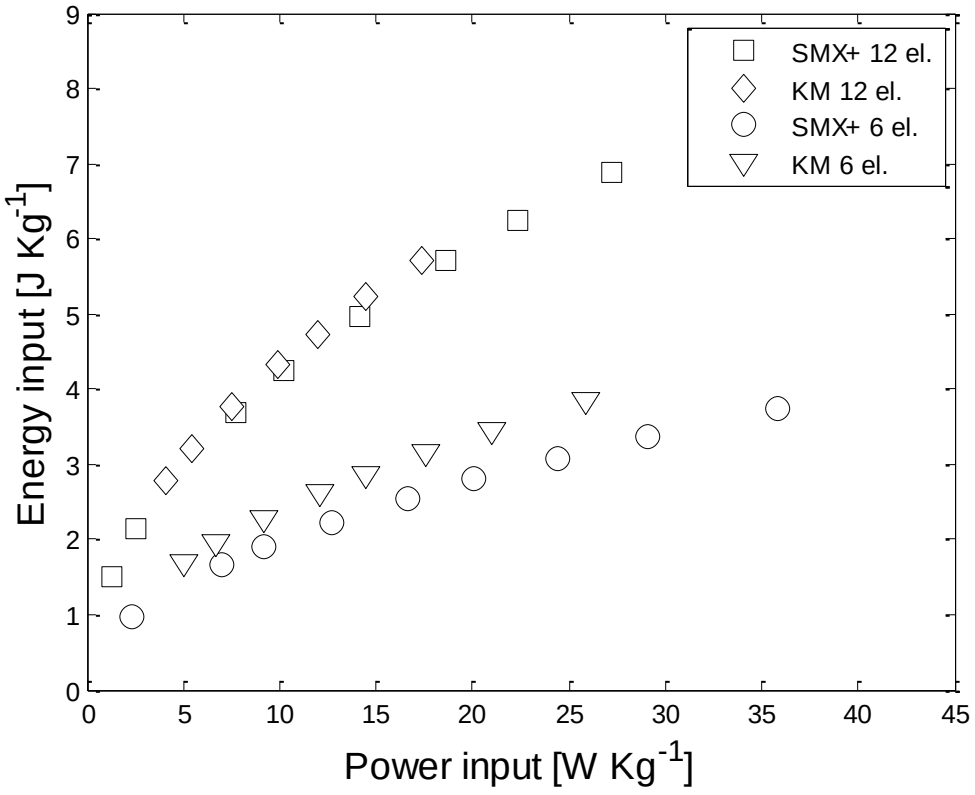

Figure 4.30 Mapping of the mixing process for the different configurations of static mixer

In this chart, one wants to compare the performance of the static mixer with a particular focus on the energy and power consumption, that are key parameters in the mixing process, since they are directly connected to the operating costs. For each experimental point on the plot there are a correspondent d_{32} and Y that have been previously determined. The power and the energy input are both calculated from the pressure drop data, they have been plotted together to give relevance also to the resident time. In fact, in the charts the average resident time is the derivative in each point: when the curves become flat the resident time becomes smaller, almost close to tend to zero. The objective of this plot is giving instructions about the number of elements and the power that are necessary for the success of the process.

Knowing for each setting the critical power, a dashed line can be drawn on the plot for distinguish the equilibrium and the instability zones of work. In the Figure 4.31 these lines (in green) can be observed. For a better understanding of the utility of this mapping a couple of examples can be discussed.

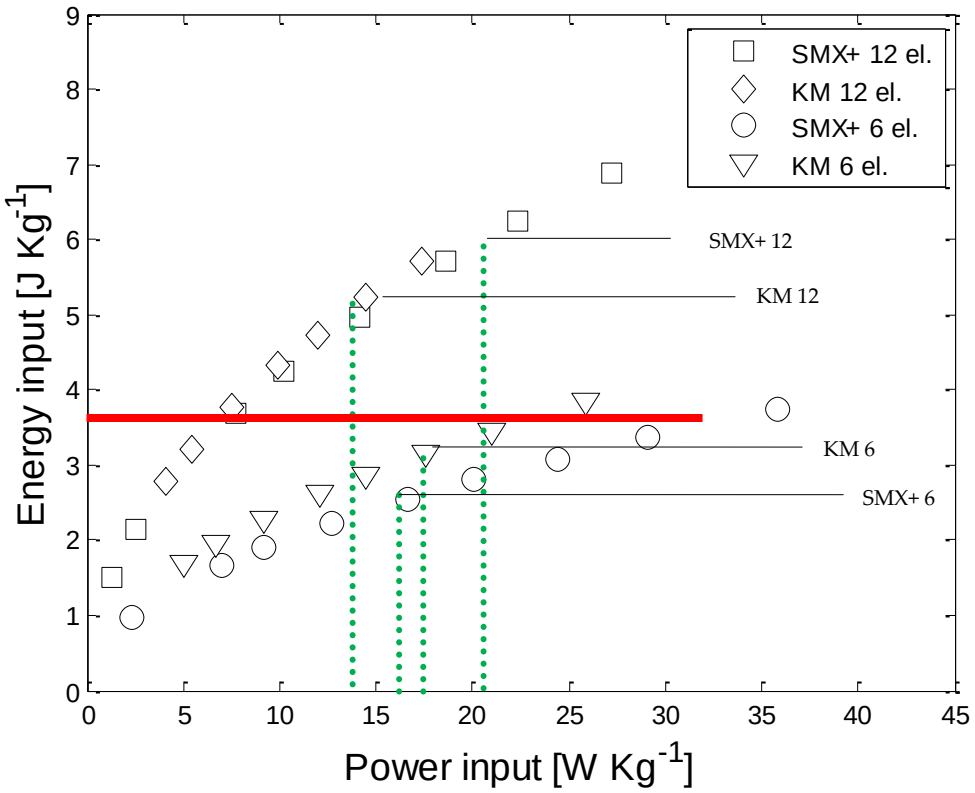

Figure 4.31 Mapping of the mixing process for the different configurations of static mixer with critical power lines (Example 1)

Referring to Figure 4.31, we imagine in Example 1 to fix a determined energy input that we want to spend into the process, for instance 3.6 J/Kg indicated by the horizontal red line. It could be reasonable to think that putting into the system the same amount of energy would bring the system at the same equilibrium droplets size, but this is far from the truth. In fact the operating point, (that is the intersection between the red horizontal line and the characteristic curve of the static mixer) is situated on the right respect of the critical power line in the cases of 6 elements. While for the 12 elements, both SMX+ and KM have the operating point on the left of the green critical power line.

Accordingly to the previous statements, this situation clearly suggests that the 12 elements settings will reach the equilibrium condition and so they will ensure good performance, while in the 6 elements case the final DSD would be affected by the instability. The following Table 4.3 confirms this hypothesis.

Table 4.3 Summary of d_{32} and Y for the different settings of Static mixer (Example 1)

Configuration	SMX+ 12 el.	KM 12 el.	SMX+ 6 el.	KM 6 el.
d_{32} [mm]	0.165	0.168	0.227	0.247
Y	0.986	0.987	0.80	0.82

Hence the data from Table 4.3 suggest the 12 elements as better operating choice. In the next Example 2 the red line is moved down in order to position the four operating points all on the right of the respective critical power line. Again, the objective is to understand which one is the best choice during the design phase.

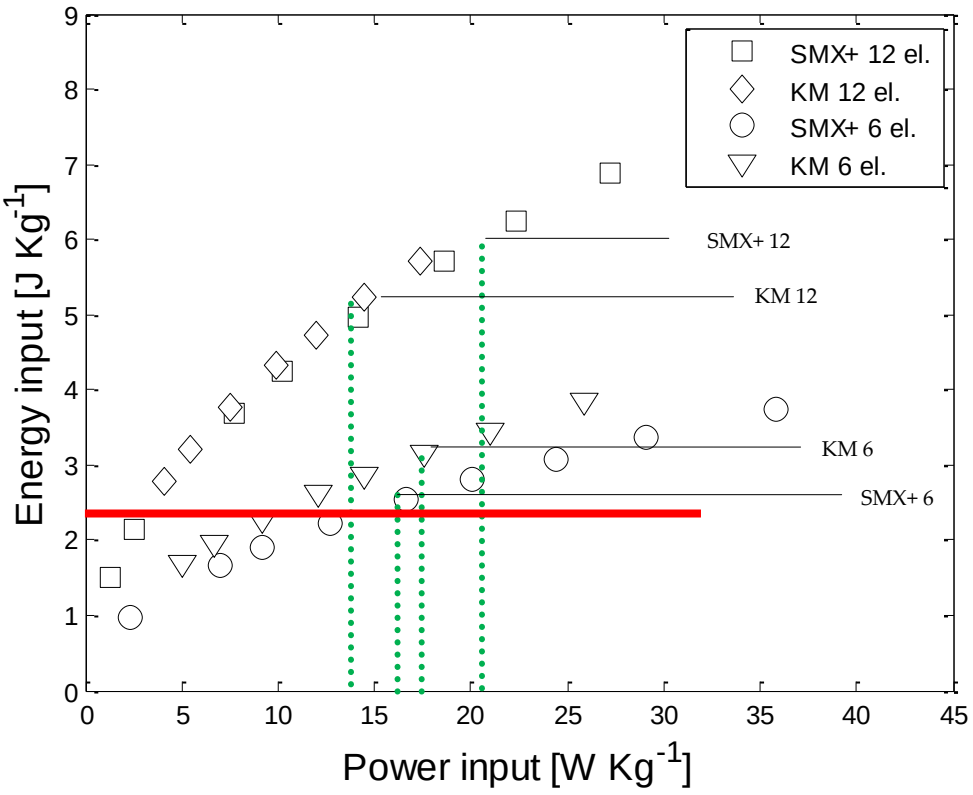

Figure 4.32 Mapping of the mixing process for the different configurations of static mixer with critical power lines (Example 2)

Since the operating point are in the equilibrium part of the chart (on the left), it is reasonable that this time the mixing performance would be high for every setting.

Table 4.4 Summary of d_{32} and Y for different settings of Static mixer (Example 2)

Configuration	SMX+ 12 el.	KM 12 el.	SMX+ 6 el.	KM 6 el.
d_{32} [mm]	0.19	-	0.21	0.2
Y	0.976	-	0.95	0.973

Although the data are extrapolated from the d_{32} curve in Figure 4.27 and Y from Figure 4.29, it is clear that in the current example the drops sizes are

comparable and both 6 and 12 elements arrangements can be examined and employed in the mixing process (unfortunately we are out of range for the KM 12 elements, but the closest points correspond for d_{32} to a value of 0.188 mm and for Y case to 0.98).

In this case the difference in the design choice would be in the pumping power spent, in fact, for feeding the same energy per unit of mass in a 6 elements configuration it would need a higher main flow velocity and consequently a higher pumping cost than in the 12 elements configuration. On the other hand it would need a higher investment cost for providing the necessary static mixer elements to the process in the 12 elements setting.

Imagining to extend this analysis, increasing the number of elements and models involved, this mapping of the process could be used as an help to the designer in projecting the continuous mixing process. The results of this work could be seen also from an energy saving point of view. In fact, it has been found that the increase of the turbulence and consequently the increase of the energy input into the system does not necessarily bring to better performance. On the contrary this can affect the performance and with higher operating costs; in this sense the process mapping can be a useful tool for finding the optimum condition of the process.

Chapter 5

Conclusions

In this work static mixer performance in mixing of immiscible fluids has been investigated. Several experimentations have been executed during this research work. Static mixers have been tested both in terms of energy and mixing performance in dispersing immiscible liquids.

In the first experimental part, described in Paragraph 4.1, the collection of pressure drops data has allowed the extrapolation of characteristic parameters that describe the energy lost by the flow in crossing the mixing elements. The main findings are key parameters (K_L and K_T), determined for the investigated static mixer models (Kenics® KM Chemineer™ and Sulzer™ SMX plus); they have been compared with the values available in literature. These data have been also used for modelling the mixing performance of the examined devices.

In Paragraph 4.2 the evaluation of the mixing performance has been discussed. The PLIF technique, developed as a visualization method, has provided information for characterizing the drop size distribution of the O/W emulsion employed. The number of elements and the superficial velocity have been investigated as variables, revealing an interesting instability above a critical velocity. In this range of velocities the time spent by the drops within the mixing equipment seems to do not be enough for completing the breakup

mechanism. It has been noticed that the static mixer is “bypassed” by a certain number of drops (a number that increases raising the velocity), hence they behave as if the pipe was empty, as shown in Figure 4.24. This observed instability affects the mixing performance and requires further investigation for a deeper and proper understanding.

The obtained information has been used for the comparison of the different static mixer models in dispersing the emulsion. A model for predicting mixing performance has been proposed and found to be an useful tool for the choice of the necessary number of mixing elements and the optimization of the mixing costs in the design phase of the mixing process.

5.1 Future work

Further experimentations could enhance the consistence of the model and integrate it. It would be useful repeating the experiments raising the number of elements and the range of the viscosities involved. It would be even more interesting conduct a deeper investigation about the instability detected for high velocities, for enhancing the understanding in the breakup mechanism. For this intent a CFD simulation could give more information about the turbulent dissipation rate within the fluid in crossing the motionless mixer and clarify the dynamic interactions between the two phases.

Appendix A

Image processing Matlab code

```
% File name definition

    f1='G:\giuseppe';
    f2='812 Water100 05oil 12 kenics\RawData';%name folder
    f3='812 Water100 05oil 12 kenics';%name file

%Matriz initialization

    colonne = 500;
    righe = 26;
    Perim = zeros(righe,colonne);
    Area = zeros(righe,colonne);
    Diam= zeros(righe,colonne);

%Maximum definition and creation of the ranges

    maxp=1000;
    maxa=50000;
    espmaxd=3;
    espmaxp=3.8;
    espmaxa=5;

    val = logspace(0,espmaxp,righe);
    vala = logspace(1,espmaxa,righe);
    vald = logspace(0,espmaxd,righe);

% Centre for images

        xc=1010;
        yc=1012;
        r=860;

% Cycle for image uploading and processing

    for k=1:500;
        if k<10

            fname=[f1,'\',f2,'\',f3,'00000',num2str(k),'.T000.D000.P00
            0.H000.LA.tif']
        elseif k < 100
```

```
    fname=[f1,'\',f2,'\',f3,'0000',num2str(k),'.T000.D000.P000
    .H000.LA.tif'];
  elseif k < 1000

    fname=[f1,'\',f2,'\',f3,'000',num2str(k),'.T000.D000.P000.
    H000.LA.tif'];
else

    fname=[f1,'\',f2,'\',f3,'00',num2str(k),'.T000.D000.P000.H
    000.LA.tif'];
end
k1=k;

    A = imread(fname);
    image = dip_image(A,'sfloat');

%Filter and background removal

    b = smooth(image,430,'ft');
    C = A-b;
    C=double(C);
    y=C;
    Aa=y;
    sizeA=size(A);

%Round cut
    imgCutci = zeros(sizeA(1,1),sizeA(1,1));
    for i=1:sizeA(1,1);
        for j= 1: sizeA(1,1);
            tmp = (i-xc)*(i-xc)+(j-yc)*(j-yc);
            if (tmp<=r*r)
                imgCutci(i,j)=Aa(i,j);
            else
                imgCutci(i,j)=0;
            end
        end
    end

image = dip_image(imgCutci,'sfloat');

%Segmentation and labelling

    b = image<80;
    b = brmedgeobjs(b,2);
    lab = label(b,2,15,50000);
    if lab==0
         disp('no drop')
    else

%Measurement and saving of the size

        data = measure(lab,[],{'size','perimeter','feret'});
        perimeter = data.perimeter;
        sz = data.size;
        diam=data.feret(1,:);
        elemperim = numel(perimeter);
```

```
                for i=1: elemperim
                    for j=1:righe
                        if perimeter(i) < val(j+1)
                            Perim(j,k1)= Perim(j,k1)+1;
                            break
                        end
                    end
                    for j=1:righe
                        if sz(i) < vala(j+1)
                            Area(j,k1)= Area(j,k1)+1;
                            break
                        end
                    end
                    for j=1:righe
                        if diam(i) < vald(j+1)
                            Diam(j,k1)= Diam(j,k1)+1;
                            break
                        end
                    end
                end
            end
    end

%Final saving of the resulting matrixes

    f3A=['Area',f3];
    save(f3A,'Area')

    f3P=['Perimeter',f3];
    save(f3P,'Perim')

    f3D=['Diameter',f3];
    save(f3D,'Diam')
```

References

Alberini, F., M. J. H. Simmons, A. Ingram and E. H. Stitt (2014). "Assessment of different methods of analysis to characterise the mixing of shear-thinning fluids in a Kenics KM static mixer using PLIF." Chemical Engineering Science **112**: 152-169.

Alloca, P. T. (1982). "Mixing efficiency of static mixing units in laminar flow." Fiber Prod 8: 12-18.

Anxionnaz, Z., M. Cabassud, C. Gourdon and P. Tochon (2008). "Heat exchanger/reactors (HEX reactors): Concepts, technologies: State-of-the-art." Chemical Engineering and Processing: Process Intensification **47**(12): 2029-2050.

Arai, K., Konno, M., Matunada,Y., Saito, S. (1977). "Effect of the dispersed-phase viscosity on the maximum stable drop size for breakup in turbulent flo." Chem Engng Japan **10**: 325-330.

Arratia, P. E. and F. J. Muzzio (2004). "Planar laser-induced fluorescence method for analysis of mixing in Laminar flows." Industrial & Engineering Chemistry Research **43**(20): 6557-6568.

Aubin, J., I. Naude, J. Bertrand and C. Xuereb (2000). "Blending of Newtonian and Shear-Thinning Fluids in a Tank Stirred with a Helical Screw Agitator." Chemical Engineering Research and Design **78**(8): 1105-1114.

Baldyga, J. (2001). "Applications of Computational Fluid Mechanics (CFD) in chemical and process engineering." Inzynieria Chemiczna I Procesowa **22**: 3-14.

Bałdyga, J. and J. R. Bourne (1999). Turbulent mixing and chemical reactions, Wiley.

Berkman, P. D. and R. V. Calabrese (1988). "Dispersion of viscous liquids by turbulent flow in a static mixer." AlChe Journal **34**: 602-609.

Cabaret, F., C. Rivera, L. Fradette, M. Heniche and P. A. Tanguy (2007). "Hydrodynamics Performance of a Dual Shaft Mixer with Viscous Newtonian Liquids." Chemical Engineering Research and Design **85**(5): 583-590.

Calabrese, R. V., Chang, T.P.K., Dang, P. T. (1986a). "Drop breakup in turbulent stirred-tank contactors. Part 1: Effect of dispersed phase viscosity." AlChe Journal **32**: 657-666.

Calabrese, R. V., C. Y. Wang and N. P. Bryner (1986b). "Drop breakup in turbulent stirred-tank contactors. Part 3 : Correlation for mean size and drop size distribution." AlChe Journal **32**: 677-681.

Capek, I. (2004). "Degradation of kinetically-stable o/w emulsions." Advances in Colloid and Interface Science **107**(2-3): 125-155.

Coulaloglou, C. A. and L. L. Tavlarides (1977). "Description of interaction processes in agitated liquid-liquid dispersions." Chem. Engng Sci. **32**: 1289-1297.

Cramer, C., P. Fischer and E. J. Windhab (2004). "Drop formation in a co-flowing ambient fluid." Chemical Engineering Science **59**(15): 3045-3058.

Cybulski, A. and K. Werner (1986). "Static mixers-criteria for applications and selection." Int Chem Eng 26(1): 171-180.

Dahm, W. J. A., K. B. Southerland and K. A. Buch (1991). "Direct, High resolution, Four-dimensional Measurements of the Fine Scale Structure of Sc>>1 Molecular Mixing in Turbulent Flows." Phys. Fluids A **3**: 1115.

Das, P. K., J. Legrand, P. Morancais and G. Carnelle (2005). "Drop breakage model in static mixers at low and intermediate Reynolds number." Chemical Engineering Science **60**(1): 231-238.

Davies, J. T. (1985). "Drop sizes of emulsions related to turbulent energy dissipation rates." Chemical Engineering Science **40**(5): 839-842.

Dickinson, E. (2003). "Hydrocolloids at interfaces and the influence on the properties of dispersed systems." Food Hydrocolloids **17**(1): 25-39.

Dickinson, E., Stainsby, G. (1982). "Colloids in Foods." Applied Science: London.

Eastwood, C. D., L. Armi and J. C. Lasheras (2004). "The breakup of immiscible fluids in turbulent flows." Journal of Fluid Mechanics **502**: 309-333.

Ferrouillat, S., P. Tochon, C. Garnier and H. Peerhossaini (2006). "Intensification of heat-transfer and mixing in multifunctional heat exchangers by artificially generated streamwise vorticity." Applied Thermal Engineering **26**(16): 1820-1829.

Fischer, P. and P. Erni (2007). "Emulsion drops in external flow fields — The role of liquid interfaces." Current Opinion in Colloid & Interface Science **12**(4–5): 196-205.

Fournier, M. C., L. Falk and J. Villermaux (1996). "A new parallel competing reaction system for assessing micromixing efficiency—Experimental approach." Chemical Engineering Science **51**(22): 5053-5064.

Ghanem, A., T. Lemenand, D. Della Valle and H. Peerhossaini (2014). "Static mixers: Mechanisms, applications, and characterization methods - A review." Chemical Engineering Research & Design **92**(2): 205-228.

Grace, H. P. (1982). "Dispersion phenomena in high-viscosity immiscible fluid systems and application of static mixer as dispersion devices in such systems." Chemical Engineering Communications **4**(225-277).

Hall, S., M. Cooke, A. W. Pacek, A. J. Kowalski and D. Rothman (2011). "SCALING UP OF SILVERSON ROTOR-STATOR MIXERS." Canadian Journal of Chemical Engineering **89**(5): 1040-1050.

Hesketh, R. P., A. W. Etchells and T. W. F. Russell (1991). "Bubble breakage in pipeline flow." Chem Engng Sci. **46**: 1-9.

Hinze, J. O. (1955). "FUNDAMENTALS OF THE HYDRODYNAMIC MECHANISM OF SPLITTING IN DISPERSION PROCESSES." Aiche Journal **1**(3): 289-295.

Joshi, P., K. D. P. Nigam and E. B. Nauman (1995). "The Kenics static mixer, new data and proposed correlations." Chem Eng Journal 59: 265-271.

Karasso, P. S. and M. G. Mungal (1996). "Scalar Mixing and Reaction in Plane Liquid Shear Layers." J. Fluid Mech. **323**: 23.

Kiss, N., G. Brenn, H. Pucher, J. Wieser, S. Scheler, H. Jennewein, D. Suzzi and J. Khinast (2011). "Formation of O/W emulsions by static mixers for pharmaceutical applications." Chemical Engineering Science **66**(21): 5084-5094.

Kolmogorov, A. N. (1949). "On the breakage of drops in a turbulent flo." Dokl. Akad. nauk. SSSR **66**: 825-828.

Konno, M., Y. Matsunaga, K. Arai and S. Saito (1980). "Simulations model for breakup process in an agitated tank." Chem Engng Japan **13**: 67-73.

Kukukova, A., J. Aubin and S. M. Kresta (2009). "A new definition of mixing and segregation: Three dimensions of a key process variable." Chemical Engineering Research & Design **87**(4A): 633-647.

Legrand, J., P. Morancais and G. Carnelle (2001). "Liquid-liquid dispersion in an SMX-Sulzer static mixer." Chemical Engineering Research & Design **79**(A8): 949-956.

Lemenand, T., C. Habchi, D. Della Valle, J. Bellettre and H. Peerhossaini (2014). "Mass transfer and emulsification by chaotic advection." International Journal of Heat and Mass Transfer **71**: 228-235.

Lobo, L. and A. Svereika (2003). "Coalescence during emulsification: 2. Role of small molecule surfactants." Journal of Colloid and Interface Science **261**(2): 498-507.

Lobry, E., F. Theron, C. Gourdon, N. Le Sauze, C. Xuereb and T. Lasuye (2011). "Turbulent liquid-liquid dispersion in SMV static mixer at high dispersed phase concentration." Chemical Engineering Science **66**(23): 5762-5774.

Luo, H. and F. Svendsen (1996). "Theoretical model for drop and bubble breakup in turbulent dispersions." AlChe Journal **42**: 1255-1233.

Lynn, R. S. (1958). "Turbulator." US Patent 2,852,042, The Garrett Corporation.

Maa, Y. F. and C. C. Hsu (1997). "Effect of primary emulsions on microsphere size and protein-loading in the double emulsion process." Journal of Microencapsulation **14**(2): 225-241.

McClements, D. J. (1996). "Principles of ultrasonic droplet size determination in emulsions." Langmuir **12**(14): 3454-3461.

Meijer, H. E. H., M. K. Singh and P. D. Anderson (2012). "On the performance of static mixers: A quantitative comparison." Progress in Polymer Science **37**(10): 1333-1349.

Middleman, S. (1979). "Drop size distributions produced by turbulent pipe flow of immiscible fluids through a static mixer." Ind. Eng. Chem. Process Des. Dev. **13**: 78-83.

Nienow, A. W., Edwards, M.F., Harnby, N. (1997). "Mixing in the process industries." Oxford: Butterworth-Heinemann.

Oldshue, J. Y. (1983). "Fluid mixing technology." New York: McGraw-Hill.

Pacek, A. W., C. C. Man and A. W. Nienow (1998). "On the Sauter mean diameter and size distributions in turbulent liquid/liquid dispersions in a stirred vessel." Chemical Engineering Science **53**(11): 2005-2011.

Pahl, M. H. and E. Muschelknautz (1982). "Static mixers and their applications." Int Chem Eng 22: 197-205.

Pan, G. and H. Meng (2001). "Experimental study of turbulent mixing in a tee mixer using PIV and PLIF." AIChE Journal **47**(12): 2653-2665.

Paul, E. L., Atiemo-Obeng, V.A., Kresta, S.M. (2003). "Handbook of industrial mixing: science and practice, vol.1." Hoboken NJ: Wiley-Interscience.

Prince, M. J. and H. W. Blanch (1990). "Bubble coalescence and breakup in air-sparged bubble columns." AlChe Journal **36**: 1485-1499.

Rao, J. J. and D. J. McClements (2010). "Stabilization of Phase Inversion Temperature Nanoemulsions by Surfactant Displacement." Journal of Agricultural and Food Chemistry **58**(11): 7059-7066.

Rueger, P. E. and R. V. Calabrese (2013). "Dispersion of water into oil in a rotor-stator mixer. Part 1: Drop breakup in dilute systems." Chemical Engineering Research & Design **91**(11): 2122-2133.

Saylor, J. R., Bounds, G. D. (2012). "Experimental Study of the Role of the Weber and Capillary Numbers on Mesler Entrainment." Wiley Online Library.

Schramm, L. (2005). "Emulsions, Foams and Suspensions Fundamentals and Applications." Wiley-VCH Verlag GmbH & Co. KGaA.

Shinnar, R. (1961). "On the behaviour of liquid dispesions in mixing vessels." Fluid Mech. **10**: 259-275.

Simmons, M. J. H. (2014). "Notes of Liquid mixing in industrial system." School of Chemical Engineering, University of Birmingham.

Simmons, M. J. H. and B. J. Azzopardi (2001). "Drop size distributions in dispersed liquid-liquid pipe flow." International Journal of Multiphase Flow **27**(5): 843-859.

Sleicher, K. S. (1962). "Maximum stable drop size in turbulent flow." AlChe Journal **8**: 471-477.

Soderman, O., Lonnqvist, I., Balinov, B. (1992). "Emulsions-A Fundamental and Practical Approach." Kluwer Academic Publishers: Dordrecht: 239.

Streiff, F. A., Mathys,P.,Fischer,T.U. (1997). "New fundamentals for liquid-liquid dispersion using static mixers." Réc. Prog. Gén. Proc. **11**: 307-314.

Sutherland, W. S. (1874). "Improvement in apparatus for preparing gaseous fuel." UK Patent 1874.

©Sulzer. "SMX™ plus Static Mixer." from http://www.sulzer.com/it/-/media/Documents/ProductsAndServices/Agitators_Mixers_Dispensers/Static_Mixers/Brochures/Flyer_SMX_plus_d.pdf.

Tadros, T., P. Izquierdo, J. Esquena and C. Solans (2004). "Formation and stability of nano-emulsions." Advances in Colloid and Interface Science **108–109**(0): 303-318.

Tadros, T. F. (2013). "Emulsion Formation, Stability, and Rheology." Wiley-VCH Verlag GmbH & Co. KGaA.

Taylor, P. (1998). "Ostwald ripening in emulsions." Advances in Colloid and Interface Science **75**: 107-163.

Tcholakova, S., N. D. Denkov and T. Danner (2004). "Role of surfactant type and concentration for the mean drop size during emulsification in turbulent flow." Langmuir **20**(18): 7444-7458.

Tesch, S., C. Gerhards and H. Schubert (2002). "Stabilization of emulsions by OSA starches." Journal of Food Engineering **54**(2): 167-174.

Thakur, R. K., C. Vial, K. D. P. Nigam, E. B. Nauman and G. Djelveh (2003). "Static Mixers in the Process Industries—A Review." Chemical Engineering Research and Design **81**(7): 787-826.

Theron, F. and N. Le Sauze (2011). "Comparison between three static mixers for emulsification in turbulent flow." International Journal of Multiphase Flow 37(5): 488-500.

Thomson, W. (1871). "Hydrokinetic solutions and observations." Philosophical Magazine **42**: 362-377.

Tsouris, C. and L. L. Tavlarides (1994). "Breakage and coalescence models for drops in turbulent dispersions." AlChe Journal **40**: 395-406.

Unger, D. R. and F. J. Muzino (1999). "Laser-Induced Fluorescence Technique for the Quantification of Mixing in Impinging Jets." AlChe Journal **45**: 2477.

Wadley, R. and M. K. Dawson (2005). "LIF measurements of blending in static mixers in the turbulent and transitional flow regimes." Chemical Engineering Science **60**(8-9): 2469-2478.

Walstra, P. (1993). "Principles of emulsion formation." Chemical Engineering Science **48**(2): 333-349.

Wang, C. Y. and R. V. Calabrese (1986b). "Drop breakup in turbulent stirred-tank contactors. Part2: Relative influence of viscosity and interfacial tension." AlChe Journal **32**: 667-676.

Ringraziamenti

Alla fine di un percorso lungo e bello come questo sono tante le persone che vorrei ringraziare per avermi aiutato nel mio percorso, in maniera conscia e non, a crescere e a credere in quello che facevo.

In primo luogo mi sento in dovere di ringraziare la mia relatrice la prof. Brunazzi per avermi aiutato nella stesura di questa tesi e dato la possibilità di svolgere il tirocinio all'estero presso l'Università di Birmingham, dove sono stato accolto a braccia aperte nel gruppo del prof. Simmons al quale vanno altri ringraziamenti per le possibilità che mi ha concesso di sviluppare questa ricerca e di continuare la mia carriera accademica.

Questo lavoro non avrebbe visto luce senza l'aiuto del mio supervisore a Birmingham, Federico che oltre ad aiutarmi e guidarmi nel lavoro si è rivelato amico sincero e perché no ottimo partner di biliardino. Ringrazio anche le fantastiche persone che ho conosciuto durante la mia esperienza Erasmus.

Prima di poter iniziare a buttar giù questa tesi è stato necessario impilare uno dopo l'altro tutti quei mattoni, (alcuni non in senso figurativo) chiamati esami, e per questo un Grazie va ai miei colleghi e amici Bruno, Marina e Giacomo con cui ho lavorato gomito a gomito in questi anni.

A Pisa ho avuto la fortuna di incontrare delle persone che hanno reso questa esperienza universitaria indimenticabile, e sono state e saranno la mia seconda famiglia: Luigi, Flavio, Davide, Gianluca, Gianluca, Carmelo, Dario e tutti gli amici che ho avuto l'onore di conoscere qui. Non sarebbe stato lo stesso senza di voi, Grazie.

Ringrazio poi Piazzale Genova, i "Malati proprio", le "Ballerine Volanti" e tutti i miei compagni di squadra di questi anni, è stato un onore esserne il loro capitano.

Ringrazio la mia guida da sempre Andrea per la sua amicizia e il suo sostegno, le chiacchierate e i consigli che mi hanno accompagnato. Ringrazio gli amici di

sempre, con cui la lontananza non è mai stato un problema, ma al contrario un collante: Cosimo, Angela, Valentina, Roberta, Alessandro; i miei cugini, i nonni e i miei zii per aver creduto sempre in me e per l'affetto che mi avrebbero dato anche se non ce l'avessi fatta.

Un Grazie speciale va a Giovanna che mi ha supportato e sopportato in tutte le difficoltà con pazienza e comprensione; per tutti i sacrifici che abbiamo fatto insieme, questo traguardo è anche suo.

Dulcis in fundo, coloro che hanno fatto sì che arrivassi fin qui, i miei genitori e Gabriella, li ringrazio immensamente per il sostegno, l'aiuto e la stima, ma soprattutto per l'esempio che mi hanno dato giorno dopo giorno e da cui non smetto di imparare.